2009

Platforms and Protocols for the Multidimensional Microchip Electrophoretic Analysis of Complex Proteomes

John K. Osiri
Louisiana State University and Agricultural and Mechanical College, josiri1@tigers.lsu.edu

PLATFORMS AND PROTOCOLS FOR THE MULTIDIMENSIONAL MICROCHIP ELECTROPHORETIC ANALYSIS OF COMPLEX PROTEOMES

A Dissertation
Submitted to the Graduate Faculty of the
Louisiana State University and
Agricultural and Mechanical College
in partial fulfillment of the
requirements for the degree of
Doctor of Philosophy
in
The Department of Chemistry

by
John Kalu Osiri
B.S., Grambling State University, 2005
May, 2010

Dedication

This work is dedicated to my uncle and guardian, Professor Igwe E. Udeh, my advisor, Professor Steven A. Soper, my loving mother, Madam Ngozi Osiri and my late father, Prince Dr. John K. Osiri, Sr.

Acknowledgements

I thank God for strength, wisdom and guidance throughout my Ph.D. work. I also thank all my spiritual mentors for their prayers and support, including Bishop B. C. Edohasim, Mr. Tony and Mrs. Grace Nze, Pastor Jerry Baldwin, and Pastor Larry Stockstill.

I thank my wonderful uncle, Prof. Igwe E. Udeh, who saw it fit to take me under his wings when I came to America. He refused to give me fish; instead, he taught me how to fish. Now, I am so good at fishing that I am teaching others what he taught me. He is an open-minded man of principles with great love and passion for his family and his students. Without him I would not have had the opportunity for a first-rate education in America.

I thank my advisor, Professor Steven A. Soper, for his terrific mentorship. I couldn't ask for anyone better. I simply couldn't! He gave me the opportunity to work in his laboratory, with little research experience, a couple weeks after my undergraduate work (in the fall of 2005). I have a graphic memory of the conversation we had in front of Room 202, Choppin Hall, in the summer of 2005. It ended with him saying something like, "Sure, sure," surely ushering me into the beginnings of my LSU experience. I was so thrilled to begin graduate school that summer in the Super Soper laboratory instead of having to wait till the fall. Let's just say that I have learned from Dr. Soper or at least improved on various aspects of life just by being under his tutelage including, suiting up, presenting talks, writing, dealing with people, approaching research, and conducting business in general. Dr. Soper inspires! He comes down to your level to teach you while requiring nothing but excellence from you at the same. His mentorship is superb, and I am grateful for getting my doctorate under him. I greatly admire him and I have soaked up some of his ways that I have earned the title of "Soper, Jr." among my peers in the department.

I am very grateful to the Louisiana Board of Regents, the National Science Foundation and the National Institute of Health. These entities provided funding for my projects.

I thank my mother, Madam Ngozi Osiri, for all her encouragements and tender love. She always called me up from afar to tell me she was praying for me, and then she would instruct me to stay focused. She made it a point to let me know that she was proud that I was pursuing an advance degree, especially since she only acquired an elementary education. I also thank my awesome siblings, Nina "anini", Emile "Mbumbu", Nnene "fine girl", and Kate "sister Katie" for counting on me and hanging in there with me through thick and thin.

I thank my father, Prince Dr. John K. Osiri, Sr., who passed in his birth month of March in 2008, and in the middle of my doctoral program. I wish he had lived to see the day I walked the stage on my graduation. I was my father's prince. He gave me solid support and taught me to be a man. There is no way I would have done this without the impact he made in my life. He raised me believing I didn't have an option, but to get an advanced degree. He demonstrated his level of confidence in me when he told me multiple times that "not only are you going to purse a doctorate, but that you would also get a masters in business administration and a law degree," and he was serous about it. He indoctrinated into me that "everybody is the architect of his own fortune," and imparted to me the I-CAN-DO spirit with an unquenchable desire to always reach higher. My father left indelible lessons with me. I am working on a memoir that comprises what he has taught me, his ways and his personal and community life. He was a great man. Daddy, I know you are looking down from above with a nod and a smile. I hope I am making you proud. I miss you dearly.

Okay! There is no way I can do a paragraph for everyone that has made this dissertation possible because there are so many of them, and I would most likely forget to mention some names. Please "pardon my infinite ignorance" if I didn't mention your name. I borrowed the last clause in quotation from Mr. Robert Zinn, the computer guru of LSU chemistry. He saved and serviced my laptops on numerous occasions. I am very grateful to have met him and to have him as a great friend. Thanks Bob! Thanks to LSU's editor, Susanna Collins Dixon, for proofreading this dissertation. She

made sure that I produced a high quality dissertation document for publication. I thank Dr. Hamed Shadpour, whose work I continued upon his graduation from LSU. He was more or less a long-distance advisor and suffice it to say that we have stayed connected from his graduation till date. We have built a strong friendship and together are in the initial stages of launching a biotech/research company. I thank other Soper group members, past and present, including Dr. Shawn Llopis, my first graduate student mentor, Dr. Maggie, Dr. Andre, Dr. Ron, Dr. Julie, how could I forget Dr. Jason, and my boy Udara, Samuel, Dr. Matt and Dr. Hong. Together, Dr. Akira and I built a two-color laser-induced fluorescence system in a matter of weeks! I thank Katrina and Mike (Mikey-like-it) who recently joined the group and have worked with me on the future directions of this project already. My sincere gratitude also goes to Mrs. Terri Johnson, Dr. Soper's assistant. I had so much fun working in the Soper Group. Thanks to the entire Soper Research Group for all the support system they provided me, for the laughs and the moments we shared together.

Thanks to Mr. Don Peterson for providing his expertise in electronics. Thanks to the Electronic Shop, particularly to Mr. Marcus Nauman and Mr. Brad Ellison, for their technical support in software development and instrumentation. I am grateful to Mr. George Gascon and the Machine Shop crew for chip cutting. To the folk at CAMD, especially to Dr. Jost Goettert, Dr. Datta, Dr. Varshni, Fareed, my boy Johannes, whose has gone back to Germany, Shaloma, and Dawit, I say, "thank you!"

I thank my dissertation committee members and the many LSU professors that taught, inspired and/or encouraged me, including Professors Graca Vicente, Steven Watkins, George Stanley, Isaiah Warner, Robert Cook, and Doug Gilman. In the same vein, I also thank Grambling State professors, especially Professors Walter Davis, Felix Ifeanyi, Ben Nwokolo (Endowed Professor of Construction Engineering), Parashu Sharma, Arun K. Agarwal, Benjamin Martin, Allen Miles, Connie Walton, Danny Hubbard, Frank Ohene, Hoffman Chen, Bobby Burkes and Pia R. Alburquerque.

Previously, and in this paragraph, I used unique words or phrases as a form of endearment for the people associated with the words or phrases. I have also used certain Igbo words in the Abiriba dialect in certain cases. I have been fortunate to have crossed paths with friends, colleagues and peers that have inspired and/or encouraged me as well. I thank Nicole Sanowar, who worked late nights in the lab with me on many occasions, Brandy Snowden, Sunjung "Sunny" Park and the Chen Group in the LSU plant pathology department, Dr. "The Real Theo" Udeigwe, Chris Akudo, Dr. Edem Okudzeto, Jerimiah Forsythe and other peers at LSU Chemistry, the Thomas and Millican family, Simone Phipps, Brother Alvin Cavalier and the Xi Nu Lambda chapter of the Alpha Phi Alpha in Baton Rouge, Leon C. Prieto, Chris Jackson (#5), Fedly Bonneau (#7), my line brothers and the Lumbar Yard village, including dwellers, Calvin Williams, Nigel Lewis, Adonis Ducre and Antar Khan. I also thank Chiemerie Nmezi, Nnamdi Owen, Gift Joe, and the rest of the SAAS boys, the Essien family in Calabar for my late friend, Dominic, O. J. Patrick, Thomas Isidahomen, John Otuaga, Big brother Ijoma of Warri, and the rest of the PTI men, and Daniel Onuoha "Odaniedokwe", Chucks Achomadu, Charles Okoroafor, Kelechukwu Uwoma "Captain Mefor" who represent the Aba people. I thank my Facebook friends who have also encouraged me along the way. I also thank umu nne and umu nna from Abiriba, including the Enachioken, Nde now Otisi, Nde Osiri, Nde Ezema, Nde Mbeku, Nde Ako and Nde Opie, particularly, Ete Opie Okeke, Ete Okeke Opie, Ete Okafor Opie, and Nde Umueso. Lastly, but not the least, I thank Anisha V. Williams for all her support and encouragement.

Table of Contents

List of Tables

List of Figures

List of Commonly Used Abbreviations and Acronyms

µ-CE	Microchip CE
µ-CZE	Micro-capillary zone electrophoresis
μ_{eof}	Electroosmotic mobility
μ_{ep}	Electrophoretic mobility
µ–TAS	Micro-total analysis system
1-D	One-dimensional
2-D	Two-dimensional
4σ	Peak width
A	Area
BSA	Bovine serum albumin
C	Concentration
CE	Capillary electrophoresis
CEC	Capillary electrochromatography
CGE	Capillary gel electrophoresis
Cmc	Critical micelle concentration
COC	Cyclic olefin copolymer
CPC	Conductive polymer composite
CSE	Capillary sieving electrophoresis
CZE	Capillary zone electrophoresis
D	Diffusion coefficient
Da	Dalton
DIGE	Differential gel electrophoresis
DNA	Deoxyribonucleic acid
E	Electric field

EDC	1-ethyl-3-[3-dimethylaminopropyl] carbodiimide hydrochloride
EOF	Electroosmotic flow
ESI	Electrospray ionization
G	Conductivity
GC	Gas chromatography
H	Plate height
H_D	Height equivalent of a theoretical plate for longitudinal diffusion
H_{inj}	Plate height contribution from injection
H_{TOT}	Total plate height
IEF	Isoelectric focusing
IMAC	Immobilized metal affinity chromatography
J	Joule heating
K	Cell constant
L	Length (distance)
LC	Liquid chromatography
L_{eff}	Effective separation length
LIF	Laser-induced fluorescence
LiGA	Lithography, electroplating, and molding (a German word)
L_{inj}	Injection length
LOD	Limit of detection
L_{tot}	Total separation length
MALDI TOF	Matrix-assisted laser desorption/ionization time-of-flight
MEEKC	Microemulsion Electrokinetic Chromatography
MEKC	Micellar electrokinetic chromatography
MHEC	Methyl hydroxyl ethyl cellulose

mRNA	Messenger RNA
MS	Mass spectrometry
MS/MS	Tandem mass spectrometry
MT	Migration time
MW (or Mw)	Molecular weight
N	Separation efficiency or Plate number
O	Orthogonality
P	Peak capacity
PBS	Phosphate buffered saline
PC	Polycarbonate
PCR	Polymerase chain reaction
PDMS	Poly(dimethylsiloxane)
pI	Isoelectric point
PMMA	Poly(methyl methacrylate)
PTM	Post-translational modification
R	Resistance
R	Correlation coefficient
RNA	Ribonucleic acid
RP-LC	Reverse-phase liquid chromatography
R_s	Resolution
SDS	Sodium dodecyl sulfate
SDS μ-CGE	Sodium dodecyl sulfate micro-capillary gel electrophoresis
SDS PAGE	Sodium dodecyl sulfate polyacrylamide gel electrophoresis
SNR	Signal-to-noise ratios
SPE	Solid phase extraction

SPRI	Solid phase reversible immobilization
T	Time
T	Absolute temperature
TCEP	Ttris(2-carboxyethyl)phosphine
TTE	TRIS TAPS EDTA
T_g	Glass transition temperature
tRNA	Transfer RNA
λ_+ and λ_-	Limiting ionic conductances
2-DE	Two-dimensional Electrophoresis

Abstract

The need for rapid, portable and high-throughput systems in proteomics is now prevalent because of demands for generating new protein-based disease biomarkers. However, 2-D protein profile patterns are lending themselves as potential diagnostic tools for biomarker discovery. It is difficult to identify protein biomarkers which are low abundant in the presence of highly abundant proteins, especially in complex biological samples like serum. Protein profiles from 2-D separation of the protein content of cells or body fluids, which are unique to certain physiological or pathological states, are currently available on internet databases. In this work, we demonstrate the ability to separate a complex biological sample using low cost, disposable, polymer-based microchips suitable for a multidimensional techniques that employed sodium dodecyl sulfate micro-capillary gel electrophoresis (SDS μ-CGE) in the 1st dimension and micellar electrokinetic capillary chromatography (MEKC) or microemulsion electrokinetic capillary chromatography (MEEKC) in the 2nd dimension. The peak capacity generated by this microchip technique was about 3-fold greater compared to conventional 2-D separation methods and the complete separation time was 60X faster. To minimize electroosmotic flow effects, we dynamically coated the channels with methylhydroxyethyl cellulose. Proteins were detected by laser-induced fluorescence following their labeling with dyes. To mitigate challenges posed by labeling the proteins, we investigated the use of a label-free technique that relied upon conductivity measurements. Preliminary data are presented on the fabrication of on-chip electrodes using a conductive SU-8 polymer via lithography.

1 Integrated Multifunctional Microfluidics for Automated Proteome Analyses

1.1 Proteins and Their Roles in Cell Functioning

1.1.1 Proteins and Their Synthesis

Proteins are biopolymers that have a variety of important functions, including transport of small molecules to and from the cells, maintaining the structure of the cells, immune response, catalyze numerous biological processes – just to mention a few. They are composed of amino acids, whose sequences are coded by genes. Proteins are diverse and complex. For instance, millions of different proteins are present in humans [1] and the functions of many are yet to be determined. Sometimes, proteins only function when working in concert or as complex with other proteins or some other biomolecule such as a lipid, carbohydrate or nucleic acid.

The synthesis of proteins is a two step process that begins with deoxyribonucleic acid (DNA) being transcribed into a messenger ribonucleic acid (mRNA). During transcription, RNA polymerase first synthesizes an mRNA using a single stranded DNA (ssDNA) as template within the cell's nucleus. The mRNA, endowed with a mobility system, migrates to the cytoplasm where only the coding mRNA sequence is recognized in groups of three nucleotides together called a codon. The second step is the translation process, which begins when the ribosome binds to the mRNA at the start codon (adenine, uracine, guanine; AUG), which is recognized by the initiator transfer RNA (tRNA). The tRNA is responsible for transferring particular amino acids based on the codon onto a peptide chain until the protein sequence is realized. After the process of translation, proteins can further undergo post-translational modifications, which involve altering the structure of the protein, such as deamidation [2], altering the protein structure, such as the creation of disulfide bonds [3], the addition of functional groups such as acylation [4], or even the addition of a peptide or another protein [5].

1.1.2 Protein Structure, Localization and Function

To carry out their functions in biological systems, proteins must maintain a specific structure.

They can fold into various conformations, which are held in place by both covalent and noncovalent bonds, such as disulfide bridges and hydrogen bonds, respectively. For instance, certain cell membrane proteins that aid in the transport of ions or metabolites form a cylindrical channel to facilitate transport of molecules to and/or from the cytoplasm and the extracellular environment. Channel proteins form an aqueous pore that passively allows the passage of specific molecules when they are opened [6].

The localization of a protein can also determine the protein's function. Proteins possess highly specialized functions depending on their localization within the organism or within the cell [6]. Therefore, we would expect for membrane proteins, as an example, to have roles different from cytosolic proteins. In the same vein, different membrane proteins would have different functions. For example, myelin membrane proteins comprise only 18% of the membrane mass because the main role of the membrane is electrical insulation, whereas mitochondrial membrane proteins comprise 75% of the membrane composition because that membrane is actively involved in metabolism and energy production [7]. Certain cellular proteins are involved in host-pathogen interaction processes because these types of interactions result in protein expression changes within both the host and the pathogen [8]. For example, in response to viral infections, the IFN-induced double-stranded PKR protein, the mammalian serine-threonine kinase, phosphorylates the elF2alpha translation initiation factor, which in turn halts the translation of both the cellular and viral mRNA thus inhibiting the replication of the virus [9].

The serum protein catalogue is very comprehensive, diverse and large with $>10^7$ different proteins [1]. There are various sources of proteins in the human serum. Classical proteins, such as albumin produced by the liver, are specifically produced to carry out various functions in the blood tissue. Tissue leakages, which are indeed targeted as protein markers, are secreted from both normal and diseased cells and interleukins function as patrol antibodies aiding in immune system response. It is virtually impossible to discuss all protein functions within the serum matrix because they are so

numerous, but as an example, the albumin protein maintains the colloidal osmotic pressure of the blood, hence they are highly abundant and account for about 55% of the total human serum proteome. They are also important in transporting ions, molecules, and drugs from one site to another using the blood as a carrier fluid [10].

1.2 The Study of Proteins

1.2.1 The Proteome and Proteomics

The word "proteome" was first used in 1994 at the Two-dimensional Electrophoresis (2-DE) meeting in Siena to imply the total protein complement in a cell, tissue or body fluid at a given time [11]. It is possible to elucidate the entire proteome of an organism, but this task becomes more daunting and extremely challenging as the study goes from looking at a unicellular organism, such as *E. coli*, to a complex organism such as the human species. For instance, the proteome for *E. coli* K12 W110 strain [12], whose genome has been sequenced with a total of 4,226 proteins predicted for the entire proteome [13], is less than half what is expected within one average human cell [14, 15]. Proteomics is the study of the entire repertoire of proteins in a given organism, whereas the proteome is a catalogue of the proteins in a specific organism that are coded by the genome. Proteomics is concerned with the determination of structures, expressions, interactions, and functions, which includes activities and roles and localizations of proteins in an organism. The original definition of the proteome views the proteome as the protein complement of the genome, thereby not accounting for the numerous post-translational modifications and the ever-changing state of proteins [16, 17]. Proteomics can therefore be defined as the comprehensive analysis, including the determination of structure, modifications, expression levels, localization and protein-protein interactions, within a given organism, tissue, cell, or biological fluid at a specified time. This definition is congruent with that offered by Schramm *et al.* [18], where the authors defined proteomics as a "functional analysis of the full set of proteins by high-throughput technologies in a given system," which suggests that proteomics goes

beyond protein identification and that protein analysis requires advanced technologies, such as high-throughput processing techniques. Based on the foregoing, proteomics therefore attempts to tackle three main areas of interest, namely; (1) protein expression; (2) protein structure; and (3) protein function. Most of the discoveries and studies on proteins have centered on protein expression because it is approachable at a general level, whereas protein structure and function are far from being understood at a systemic level [19].

1.2.2 Challenges in Proteomics

Because higher biological functions are not performed by the genome but by the varying population of proteins, proteomics has thus become an important tool for the scientist. Proteomics is paramount in drug discovery because most drugs inhibit or alter the function of particular proteins. Unfortunately, proteomics is fraught with numerous challenges that impede its goals. The challenges can be categorized under; (a) the nature of the sample; (b) inadequacy of available techniques; and (c) data analysis.

1.2.2.1 The Nature of Sample

The complexity of a proteome is simply overwhelming. For example, the human genome is composed of only about 3×10^4 genes [20, 21] compared to $>10^7$ different protein constituents estimated for the human serum proteome. Furthermore, proteins are very diverse; proteins sizes can range from a few tens of amino acids (e.g., toxins) to several MDa (e.g., human titin is composed of 26, 926 amino acids); pI range is as wide as 3 to 11; and proteins can be hydrophilic or extremely hydrophobic to the point where they are almost irrecoverable from aqueous media [22]. Membrane proteins, for example, are very hydrophobic proteins and are difficult to analyze. The complexity of the human serum proteome is further compounded by the large dynamic range of $\sim10^{10}$ with albumins making up nearly 55% by weight, even though the dynamic range of proteins within a cell spans six orders of magnitude [1]. Many proteins abound in a given proteome due to gene and protein splicing,

post-translational modifications and other processes that alter the mature, gene-coded protein. To further buttress the point about the challenge posed by the sample complexity, let us assume that a protein has just one copy within a cell and that about 10 fmol of a peptide generated from the proteolytic digestion of a protein is needed to produce a mass spectrum for fingerprinting, then approximately 6 x 10^{10} cells or approximately 600 g of tissue are required for the analysis [23].

1.2.2.2 Inadequacy of Available Techniques

Considering all of the "omics," including genomics, transcriptomics and even metabolomics, proteomics is the most challenging. In proteomics, technology drives biology and not necessarily vice versa because as new technologies emerge, scientists find applications for them in proteomics just as the advent of the mass spectrometer opened new doors and championed the field of protein analysis [19]. Proteomics attempts to determine simultaneously the identities and quantities of proteins; meanwhile data obtained from experimental trials may not correspond to expected results based upon developed standards and controls [24].

Furthermore, proteomics is posed with a level of complexity that has never been attempted before. Unfortunately, typical analytical tools can quantitatively analyze less than fifty analytes, which pales compared to the complex mixture of proteins present in one sample [24]. Sodium dodecyl sulfate polyacrylamide gel electrophoresis (SDS PAGE), affording a dynamic range of $10^2 – 10^4$ and a limit-of-dection (LOD)_ molar concentration of 10^{-6} M can routinely resolve ~2,000 spots per gel, which is well below the >10,550,000 proteins present in a serum proteome. Moreover, it requires well-trained personnel, it is time consuming and it has limited automation potential [25].

Mass spectrometry on the other hand provides better LOD (~10^{-15} mole for peptides) and high specificity, but it also has a limited dynamic range [26]. Furthermore, there is no amplification technique in proteomics such as PCR in genomics, therefore, proteins must be analyzed in their native concentrations.

1.2.2.3 Data Analysis

The number of measurable parameters is enormous in proteomics, but the number of biological and methodological replicates has not increased, and due to the limited number of test subjects, problems pertaining to statistics and bias are prevalent in proteomics [24]. Bias in protein data analysis is so pervasive that it is viewed as a threat to the validity of protein biomarkers for cancer diagnostics where results have been disputed or not reproduced [27, 28]. This issue is apparent when dealing with large data sets, such as those presented in proteomic analyses. It is inherently easier to find a correlation irrespective of real cause and effect due to false positive probably outnumbering true positives [24]. According to Lay *et al*. [24], "the failure of many proteomic studies probably correlates with the failure to consider the analytical need to define quality standards, including method validation and standardization." Unfortunately, due to lack of quality standards across the board, it is difficult to compare results generated from various laboratories.

1.3 Approaches to Protein Analysis

Ideally, a proteomic platform should quantitatively analyze the entire proteome in a high-throughput fashion and at high sensitivity [29]. Two approaches to protein identification are recognized, namely bottom-up and top-down strategies. In the former, typically, a protein mixture is separated; resolved or separated proteins are enzymatically broken into peptides before the peptides are fed into a mass spectrometer for mass analyses. This strategy is also called the "gel approach" because it heavily relies on the use of two-dimensional (2-D) IEF/SDS PAGE to separate the proteins prior to proteolytic digestion of the proteins after excising the protein spots from the gel. In the latter, the intact protein mixture is directly subjected a proteolytic digestion without protein separation followed by separation of the peptides with the isolated peptides submitted for mass analysis. A variation of the top-down approach is called "shotgun proteomics" or multidimensional protein identification technology (MudPIT) because it is typically based upon early digestion of a protein mixture followed

by a multidimensional chromatographic separation of the peptides coupled to a mass spectrometer for peptide mass determination. The only difference is that in shotgun proteomics, a non-separated protein mixture instead of an isolated individual protein is digested.

1.3.1 Top-down and Shotgun Strategies

In the top-down or shotgun strategy, an individual protein or a protein mixture, respectively, is digested thereby generating peptides, which are more uniform and easier to analyze compared to a complex protein sample that contains a mixture of very small, very large, very hydrophobic and very acidic/basic proteins. These extreme properties tend to yield poor 2-D IEF/SDS PAGE results [19]. In terms of ionization source, electrospray ionization (ESI) is commonly used for top-down or shotgun strategies, especially because liquid chromatography (LC), used in the separation of the peptides, couples naturally to ESI due to the ability of continuous sample infusion into the ES ion source [30]. However, this continuous infusion of sample only tends to overwhelm the mass spectrometer and as such more complex peptide mass spectra are generated. Suffice it to say that, the top-down and bottom-up strategies are complementary to each other in terms of proteomic coverage [19].

1.3.2 Bottom-up Strategy

There are several advantages for using the bottom-up strategy. Firstly, proteins can be visualized immediately after SDS PAGE separation (i.e., before protein digestion). Therefore, the researcher can gain information lost when employing a top-down proteomic strategy, such as post-translational modifications. Secondly, because a gel separation is required, protein profiles of the sample can be generated. Thirdly, purifying the proteins via 2-D IEF/SDS PAGE reduces the complexity of the sample so that ideally only one resolved protein spot is digested at a time, which means that fewer peptides are fed into the MS resulting in simple peptide mass spectra compared to the MS spectra obtained from a shotgun analysis. However, the entire process is time consuming, laborious and limited to automation.

To minimize these disadvantages, scientists have looked towards using microchip-based proteomic analysis [31]. Microchip-based proteomics strategies have appeared in the literature. Li *et al.* [32] identified proteins from membrane-bound protein extracts of *Haemophilus influenzae* by first separating the membrane proteome fraction by a 1-D SDS PAGE, and tryptic digesting excised protein spots and finally introducing the peptides into an integrated microchip capillary electrophoresis (CE)/nanoelectrospray system. The authors reported a concentration LOD of 3.2 – 43.5 nM for different peptides and a migration time and peak area reproducibility (*i.e.*, RSD) of 3.1% and 6-13%, respectively. The mass analyzer was a quadrupole time-of-flight (Q-TOF) MS system. Mellors *et al.* [33] reported a microchip CE device that performed electrospray MS directly from the corner of a glass chip without the need for an external tip. The CE-MS analysis of peptides and proteins using this device resulted in efficiencies of over 2×10^5 theoretical plates (or 10^6 plates/m). Also, Musyimi *et al.* [34] developed a poly (methyl methacrylate), PMMA, CE chip that directly coupled to a rotating ball for a MALDI-TOF MS analysis of protein digests. While it is easier to couple CE to ESI [35], MALDI offered the advantage of higher tolerance to impurities in the protein sample.

1.4 Principles of Microchip Proteomics

Besides the well-established technologies, such as 2-D IEF/SDS PAGE used in the analysis of proteomes, new tools are evolving for analyzing proteins that are based on the use of microfluidics [36, 37]. The term "microfluidics" refers to analytical tools where fluids can be driven in microstructured channels and reservoirs. The first successful marriage between microchip technology and chemistry is certainly to be found in the field of genomics, where two types of devices are now included in the chemist/biologist toolbox, namely microarrays and CE microchips. The concept of a microarray, simultaneously introduced by several teams [38-41], relies on the parallelization of hundreds to thousands of recognition reactions with immobilized probes. Microarrays found their most successful application in genomics, because a binding reaction directly gives sequence information. DNA surface

chemistry allows either on-chip synthesis of short oligonucleotides or post-synthesis immobilization of PCR products. The other successful alliance of microchip technology was the development of CE microchips for DNA sizing [42]. In this case, the success does not rely solely on parallelization, but on separation efficiency due to micro-dimensions, integration of sample preparation, labeling, gel loading, and detection [43, 44]. From these examples, it should be noted that key success factors for microfluidics are the high degree of parallelization they offer for several similar functions on the same chip due to micrometer dimensions and integration of different functions [45]. While genomics has been the primary driver for micro-analytical tools developments, new efforts are now being forged to provide valuable microfluidic systems for the analysis of proteomes.

1.4.1 Why Microsystems?

There are several advantages toward using microsystems for proteomic analysis. Firstly, the microsystems require small sample volumes. Secondly, high surface-to-volume ratios as afforded by miniaturized platforms are preferable for protein extraction where the analyte-wall interaction is required, especially for analyte extraction onto a solid support. Thirdly, short analysis times can be achieved due to reduced length scales, which reduces analyte diffusion and thus, more efficient separations. Also, improved mass transport is advantageous for protein extraction or protein digestion purposes.

1.4.2 The Proteomic Processing Pipeline

The most basic task of proteomics is the detection and identification of proteins from a biological sample. One approach, as mentioned above, for this analysis follows the bottom-up strategy, which begins with the separation of proteins by 2-D IEF/SDS PAGE according to isoelectric point and molecular weight after protein extraction/preparation of the proteins from cells or biological fluids, followed by fragmentation of the proteins excised from the gel and mass analysis typically by matrix-assisted laser desorption ionization time-of-flight mass spectrometry (MALDI-TOF MS). Identification

of proteins can be achieved by comparing the mass/charge-ratios of these peptides to respective databases [22]. The proteomic workflow is broadly comprised of sample preparation, protein separation, protein digestion and identification of proteins by MS analysis.

1.4.2.1 Protein Preparation

Sample preparation entails extracting the proteins of interest from the biological matrix as well as ridding the sample of salts and other impurities. Sample preparation could involve, but not limited to, cell lysis and protein extraction, pre-concentration, denaturing, and labeling. Proteins are commonly extracted on-chip from the biological matrix by solid-phase extraction techniques. Other methods include liquid-liquid extraction and microdialysis [22]. When dealing with intact cells, unlike serum, protein extraction is preceded by cell lysis. Li and Harrison [46] were they first to report on-chip cell lysis accomplished by a combination of a chemical method using SDS and electrokinetic cell movement. Since then, other on-chip lysis methods have surfaced in the literature including mechanical [47], thermal [48], ultrasonic [49], and electroporetic cell lysis [50, 51].

In solid-phase extraction, analytes are retained on a stationary phase by hydrophobic, electrostatic and/or affinity interactions. For example, Kutter *et al.* [52] modified a glass surface to create a C_{18} phase, which was used to extract neutral dyes. They estimated the gain in concentration due to the enrichment to be 80-fold and the elution of the isolated material could occur in less than 4 min. Besides on-chip wall modification, integrating polymeric membranes or monoliths are other ways to produce high surface-area solid-phase extraction phases, which can be done on-chip. Simply modifying the surface can only result in a surface-to-volume ratio area of 230 – 781 mm^{-1} [53] compared to 1500 mm^{-1} that is obtainable from polymeric membranes, such as polyvinylidene difluoride (PVDF), which could be placed at the inlet of a polymeric nanospray for protein desalting prior to ESI-MS [54]. Recently, Yang *et al.* [55] reported a PMMA microdevice with monolithic columns on which antibodies were immobilized to selectively purify fluorescently tagged amino acids

from a mixture containing green fluorescent protein (GFP). A 20-fold enrichment and 91% recovery were achieved for the labeled amino acids.

1.4.2.2 Protein Separation

Protein separation involves reducing the complexity of the protein mixture by sorting them into smaller purified protein compartments. The goal is to obtain individual protein plugs or spots, so that each protein can be easily identified without interference from another protein. Separating a complex protein mixture into individual proteins is usually impractical, especially when dealing with a complex proteome that contains numerous proteins. The conventional method of 2-D separation involves a charge-based separation where proteins are separated based on their isoelectric points followed by a size-based separation, where proteins are separated according to their molecular weight. This method has the advantage of routinely resolving up to 2,000 proteins with reports of up to 5,000 [56, 57] and 10,000 when large sized gels are used [58]. But the process is time consuming, laborious and not very reproducible [59, 60].

Microchip separations on the other hand offer fast analysis time, require minimal sample volumes, and can be automated; therefore, using a microchip platform that offers a high peak capacity is a forward looking approach. Numerous groups have reported different microchip 2-D systems for protein separations [61]. Microchip 2-D strategies have been developed to generate high peak capacities of 2,600 and 2,880, which are some of the highest peak capacities recently reported for microchip protein separation [62, 63]. In the former, Osiri *et al.* [62] profiled proteins in mammalian serum sample using a PMMA 2-D microchip employing SDS μ-CGE and MEKC in the first and second dimension, respectively; whereas in the former, Yang and co-workers [63] reported a 2-D IEF/PAGE separation of *E. coli* protein lysate also on a PMMA microchip.

1.4.2.3 Protein Digestion

According to the proteomic processing pipeline, following protein separation is the breaking

down of the individual proteins into peptides prior to mass analysis of the peptides. Traditionally, proteins are excised from the gel and proteolytically digested in a trypsin solution. In microdevices, researchers have taken various approaches. Wang *et al*. [64] incorporated commercially-available trypsin-coated microparticles into microchannels to digest a 3 μL sample of model proteins that were hydrodynamically pumped through the channel within 6 min. Jin *et al*. [65] also digested model proteins using trypsin-coated microparticles, but electrokinetically injected the proteins into the digestion bed. Lee *et al*. [66] reported a trypsin immobilized solid-phase bioreactor within a PMMA channel without any embedded microparticles. Model proteins were pressure-driven through the bioreactor and the reaction time for digesting cytochrome *c* was within 24 s. To increase the trypsin concentration and the reaction time, groups have attempted to improve the surface area for trypsin immobilization by incorporating silane-based sol-gel [67], tetramethoxysilane hydrogel [68], or by immobilizing trypsin on monoliths developed on glass [69]. Krenkova and Foret [70] extensively reviewed various microdevices on which enzymatic reactors were developed.

1.4.2.4 Peptide Separation and Mass Spectrometry Analysis

In order to identify the digested protein, the resulting peptides must be fed into a mass spectrometer. Great progress has been made towards interfacing some type of 1-D microchip separation to a mass spectrometer via a microchip ionization-based interface, especially ESI and MALDI. In many instances, the peptides are first separated prior to mass analysis. For example, Musyimi *et al*. [34] electrophoretically separated cyctochrome *c* digests on PMMA microchips coupled to online MALDI-MS using a rotating ball inlet. Work involving interfacing micro-separations to MS has received great attention and has spawned research efforts across many laboratories resulting in numerous publications [31]. This aspect of proteomics is worth mentioning, but is beyond the scope of this dissertation. For information regarding interfacing microchips to MS, the reader is referred to a recent review article [31].

1.4.3 The Need for Integrated Microsystems for Protein Analysis

According to Freeman J. Dyson, "new directions in science are launched by new tools, much more often than by new concepts [71]." This statement is clearly in agreement with the contributions of microchip technology to proteomics because microchip technology was initially developed for genomics [38-41], particularly, in the area microarray, but also found great use in CE [42] and now proteomics. The integration of various processes, such as sample preparation, labeling, gel loading, and detection [43, 44] for DNA analysis soon became tractable. By integrating various devices into a single chip, dead volumes are minimized and total analysis time is reduced. Furthermore, the goal of integrating proteomic processes onto a chip is to make the technology available to the non-trained user by providing high levels of process automation, especially in clinical settings where the user simply needs to input the sample into the system and then get a readout after a short period of time. As discussed earlier, various units corresponding to the proteomic processing pipelines are currently used in isolation. However, several groups have attempted to integrate two or three processing units onto one microfluidic platform, but integrating all of the processing units onto one chip for a full proteomic analysis is a goal that has not been realized to date.

1.5 Integrated Microfluidic Systems for Protein Analysis

1.5.1 An Ideal Integrated Microfluidic System and Its Components

For the analysis of complex protein samples, which uses non-miniaturized integrated systems, the analysis time is typically several days, the sample volume lies in the µL- mL range and the transfer of the sample from one step of the protocol to the next is a source of material loss and contamination. In this context, it is advantageous to work with a miniaturized and integrated system, because this allows for reduction of the material consumption and analysis time as well as eliminating most sample handling issues. These advantages have been highlighted and reviewed by a number of groups and authors [36,72, 73].

Figure 1.1 shows a schematic of the ideal integrated multifunctional microchip for protein analysis, which consists of several processing units, including a sample preparation unit that ideally should include cell lysis and protein extraction parts (I), a 2-D microchip electrophoresis unit (II), solid-phase proteolytic reactors (III), and a microchip peptide separation unit (IV) with an interface to MS [74, 75].

Not only is integration of all the proteomic steps a goal to be realized within the research community, it is also required for personalized medicine where the user simply inputs the sample and expects a readout [76]. However, there has been no report of a fully integrated multifunctional microfluidic platform for automated protein analysis that follows the outlined proteomic process pipeline. In the next paragraphs, we survey major works that have been performed to achieve the ultimate goal of having a fully integrated microsystem for protein analysis and proteomics.

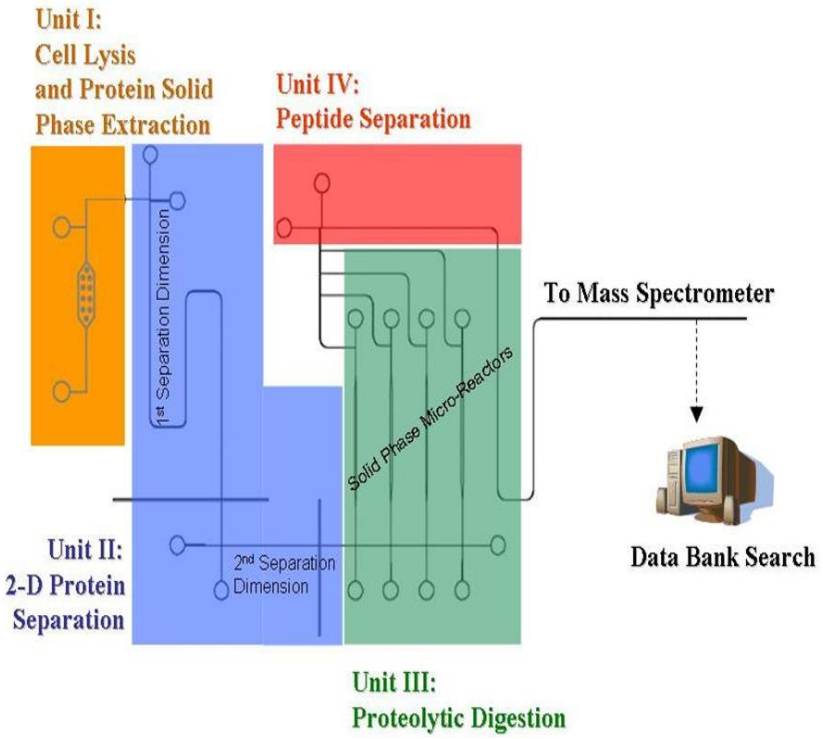

Figure 1.1 Schematic layout of an ideal integrated microchip for full protein analysis. The system should consist of a cell lysis/solid phase extraction unit, 2-D electrophoresis separation unit, solid-phase proteolytic reactors, a microchip peptide separation unit, and an on-line interface to MS, for example using a rotating ball or other interface (see text for details).

Numerous articles and reviews on MS interfaces to microchip protein digestion or peptide separation abound in the literature. We consider efforts in which more than one proteomic unit performing a single processing step was combined with another in a single system. We describe, to best of our knowledge, all of the principal works on developing integrated systems for protein analysis and proteomics. In this review, processes such as on-chip cell lysis, protein extraction, pre-concentration, protein denaturation and/or labeling are included as part of the sample preparation. We considered platform wherein any two or more protein processing devices were combined as being a system and these could have been integrated to an interface for direct mass analysis via MS. Our discussions are primarily focused on the integration of various processing steps prior to MS analysis and we compiled the integrated devices with their various components in Table 1. For example, a protein digestion device that may have been interfaced to a mass spectrometer so was not included in this review. In the same vein, if for example two separate systems comprised of two devices each, and one of the two systems was interfaced with MS and the other was not, both systems were considered in this review and placed under the category of integrated systems with two devices.

1.5.2 A Survey of Integrated Microfluidic Systems

1.5.2.1 Integrated Systems with Two Devices

Foote and co-workers [77] developed a microfabricated device with the ability to electrophoretically concentrate fluorescently labeled proteins prior to a separation unit (see Figure 1.2). They were able to concentrate proteins using a porous silica membrane between adjacent microchannels that allowed for the passage of buffer ions, but excluded larger migrating molecules. Concentrated proteins were then injected into a separation column for analysis. Pre-concentration factors of ~600-fold were achieved using this on-chip format, which was followed by SDS μ-CGE separation of the proteins. Using this microfluidic chip, fluorescently labeled ovalbumin was detected at initial concentrations as low as 100 fM by using a combination of field-

-amplified injection and pre-concentration at a membrane prior to microchip CE (μ-CE).

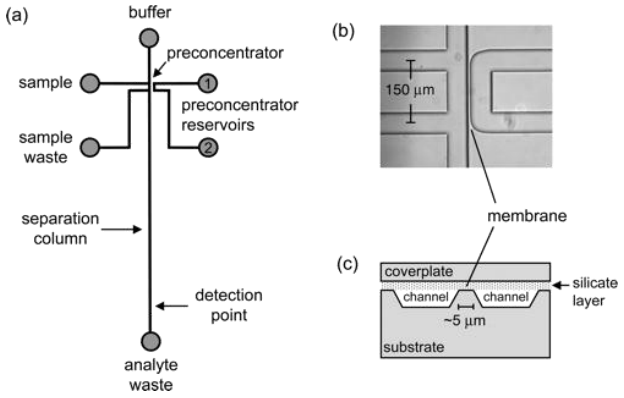

Figure 1.2 (A) Schematic of microchip layout used for preconcentration. (B) Microscopic image of preconcentrator-injector channels. (C) Schematic cross section through injector and preconcentrator channels (Reproduced from Analytical Chemistry 77, 2005, 57-63).

In work performed by Yue *et al*. [78], an integrated glass microfluidic for proteomics, which directly coupled proteolysis with affinity selection, was described (see Figure 1.3). Initial results with standard phosphorpeptide fragments from β-casein in peptide mixtures showed selective capture of the phosphorylated fragments using immobilized metal affinity chromatography (IMAC) beads packed into a microchannel.

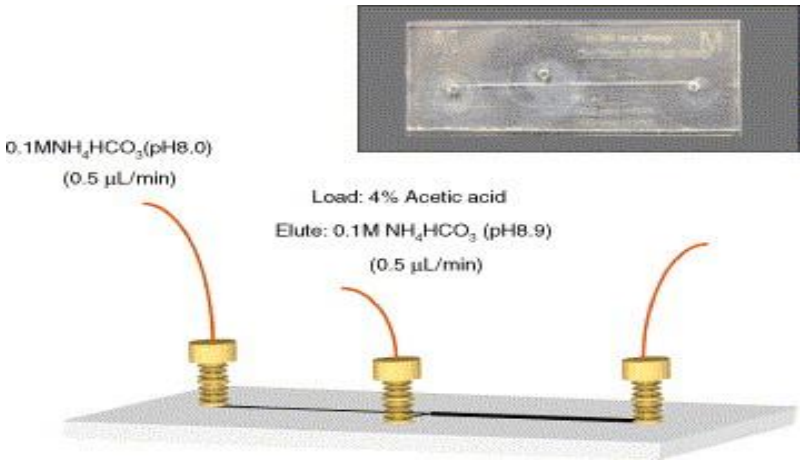

Figure 1.3 Diagram of the integrated trypsin digestion and affinity capture process along with a picture of the actual microdevice (Reproduced from Analytica Chimica Acta 564, 2006, 116-122).

Complete selectivity was seen with angiotensin, with capture of only the phosphorylated forms.

Peterson *et al*. [79] reported a microfluidic device with a dual function containing both a solid phase extractor and an enzymatic microreactor (see Figure 1.4). This device was fabricated from a 25 mm long porous poly (butyl methacrylate-co-ethylene dimethacrylate) monolith prepared within a 50 µm i.d. capillary. This capillary with a pulled 9 – 12 µm needle tip was used as a nanoelectrospray emitter coupling the device to ESI MS. Photografting with irradiation through a mask was then used to selectively functionalize a 20 mm long portion of the monolith, introducing reactive poly (2-vinyl-4,4-dimethylazlactone) chains to enable the subsequent attachment of trypsin, thereby creating an enzymatic microreactor with high proteolytic activity. The other 5 mm of unmodified hydrophobic monolith served as a micro-solid phase extractor. To test system functionality, different volumes of a myoglobin solution ranging from 2 to 20 µL were loaded into the device, and a sequence coverage of ~80% was achieved for the highest loading. The sequence coverage of a protein is the percentage of the protein's amino acid sequence that is detected relative to complete protein's amino acid sequence.

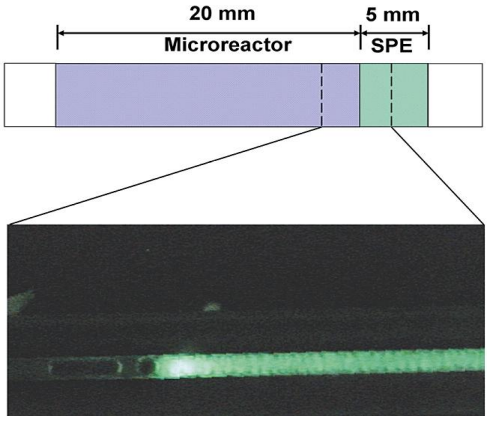

Figure 1.4 Schematic and fluorescence microscopic image of the monolithic dual-function device used for the digestion-SPE isolation for the analysis of labeled proteins and the capture of fluorescent peptides (Reproduced from Analytical Chemistry 75, 2003, 5328-5335).

An integrated poly (dimethylsiloxane), PDMS, microchip for SPE and CE followed by ESI/TOF MS has been developed and evaluated by Dahlin and co-workers [80]. The microchip (see

Figure 1.5) was fabricated in a novel one-step procedure where mixed PDMS was cast over steel wires in a mold. The removed wires defined 50 µm cylindrical channels. Fused-silica capillaries were then successfully inserted into the structure in a tight fit connection. The inner walls of the inserted fused-silica capillaries and the PDMS microchip channels were modified with a positively charged polymer, Poly E-323. In this approach, the chip was fabricated in a two-level cross design. The channel at the lower level was packed with 5 µm hyper-cross-linked polystyrene beads acting as a SPE medium used for desalting. The upper level channel acted as a CE channel and ended in an integrated emitter tip coated with conducting graphite powder to facilitate the electrical contact for ESI. To evaluate the microchip, six-peptide mixtures were dissolved in physiological salt solution, injected, desalted, separated, and sprayed into a MS for analysis with a limit-of-detection in the femtomole regime.

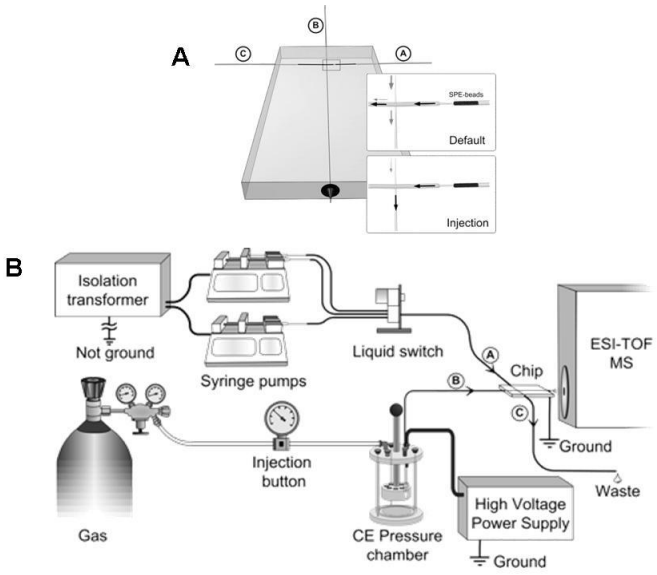

Figure 1.5 (A) Schematic of a PDMS microchip device. Channel A: sample inlet; channel B: CE, channel; C: waste channel. (B) Schematic showing the instrumental setup and the connection of the microchip to the ESI/TOF MS (Reproduced from Analytical Chemistry, 77, 2005, 5356-5363).

In a similar effort to combine preconcentration with electrophoretic separations, Fortier *et al.* [81] investigated the analytical performances of a fabricated microfluidic device, which included an enrichment column, a reversed phase separation channel, and a nanoelectrospray emitter

embedded together in polyimide layers (see Figure 1.6). This configuration minimized transfer lines and connections and reduced post-column peak broadening and dead volumes. The compact microchip was interfaced to both ion trap and TOF MS, and its analytical potentials were evaluated in the context of proteomic applications. Sensitivity measurements were performed on a dilution series of protein digests spiked into rat plasma samples and provided a detection limit of 1 – 5 fmol.

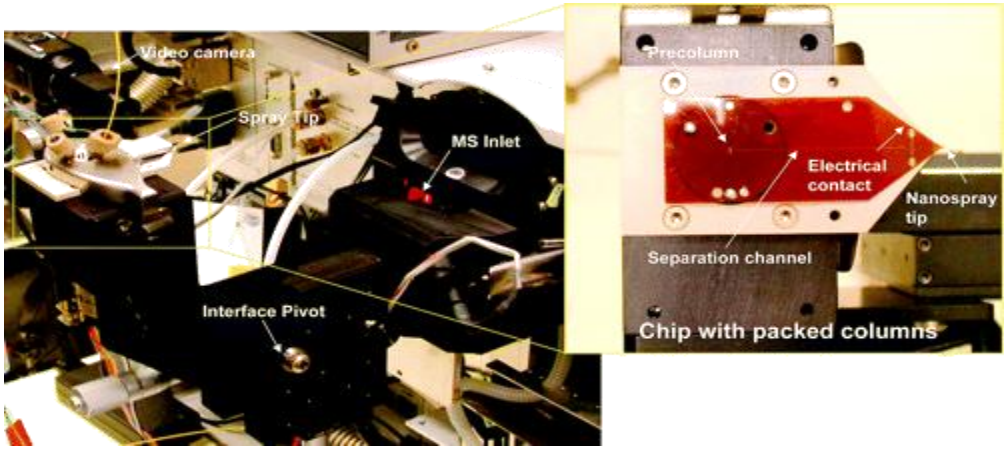

Figure 1.6 Microchip system interfaced to an ion trap MS. The chip was placed on an articulated manifold, which was comprised of a valve rotor with a clamping mechanism ensuring proper port alignment and sealing. A two-way translation stage provided easy positioning of the device in front of the sampling orifice when the manifold was inserted into the MS inlet. The inset shows a close up view of the chip device with the precolumn, separation channel, and nanospray tip (Reproduced from Analytical Chemistry, 77, 2005, 1631-1640).

In another study, Gao and co-workers [82] developed an integrated microchip for rapid and sensitive protein identification by on-line protein digestion and analysis of the digested proteins using ESI MS or transient capillary isotachophoresis/CZE with MS. A miniaturized membrane reactor was constructed by fabricating a PDMS microchip and coupling the microfluidic to a poly (vinylidene fluoride) porous membrane with adsorbed trypsin (see Figure 1.7), which produced a large surface area-to-volume ratio by the porous membrane media with adsorbed trypsin to provide ultrahigh catalytic turnover. The residence time of protein analytes inside the trypsin-adsorbed membrane, the reaction temperature, and the protein concentration controlled the extent of protein digestion.

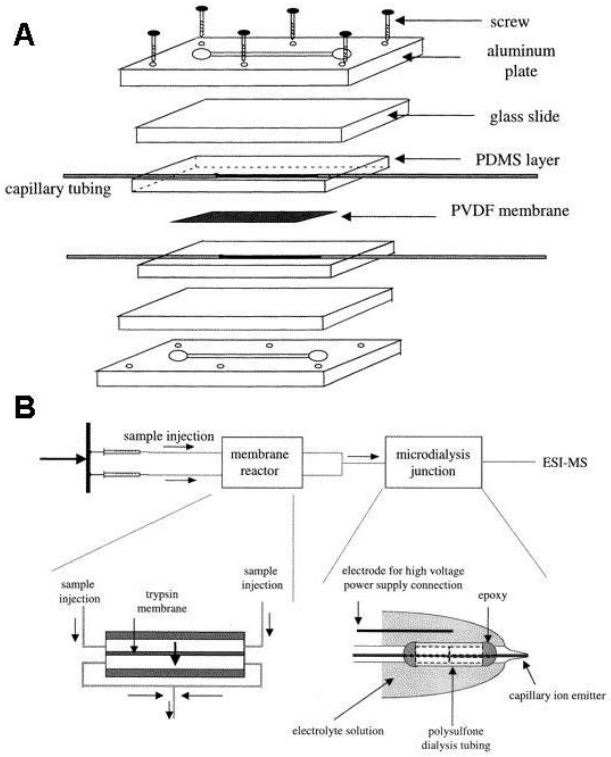

Figure 1.7 (A) Schematic of a membrane reactor assembly. (B) Schematic of the setup for performing ESI MS analysis of peptide mixtures from a trypsin membrane reactor (Reproduced form Analytical Chemistry, 73, 2001, 2648-2655).

A microfluidic device was also described by Wang and co-workers [64] in which an electrospray interface to MS was integrated with a CE channel, an injector and a protein digestion bed situated on a monolithic substrate (see Figure 1.8). To perform analysis, an 800 µm wide, 150 µm deep and 15 mm long channel served as a reactor bed for trypsin, which was immobilized on 40 – 60 µm diameter beads. Separation was performed in channels feeding into a capillary attached to the chip with a low dead volume coupler. Then, sample including melittin, cytochrome *c* and bovine serum albumin (BSA), was pumped through the reactor bed at flow rates between 0.5 and 60 µL/min and the application of the device for rapid digestion, separation and identification of proteins was demonstrated. A flow rate of 1 or 0.5 µL/min was found to be adequate for complete digestion of cytochrome C or BSA, corresponding to a digestion time of 3 – 6 min at room temperature.

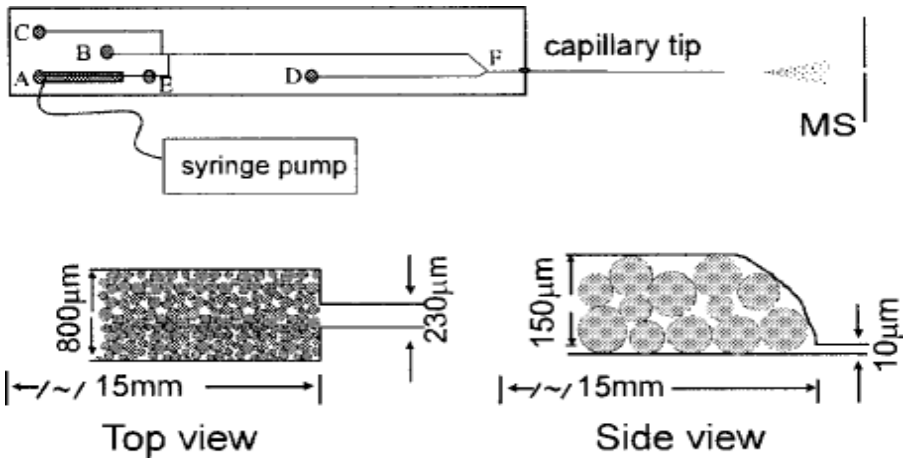

Figure 1.8 Schematic of an integrated enzyme reaction bed and CE microchip. Top and side views show a blow up of the packed trypsin bead (Reproduced from Rapid Communications in Mass Spectrometry, 14, 2000, 1377-1383).

Hardouin *et al*. [83] reported a nano-HPLC-Chip-MS device that integrated a sample enrichment column, a nanoscale C_{18} reverse-phase separation column and a nanoelectrospray tip. The chip, which was obtained from Agilent Technologies, Santa Clara, CA, USA, was automatically loaded and positioned into an MS nanospray chamber and resulted in reproducible retention times of protein digests. To enhance protein identification, the method combined m/z data generated from the MS with highly reproducible peptide retention times (RT) from the nano-LC. Based on 24 relative standard devations (RSDs) associated with retention times of different tryptic ions of the CLIC1_HUMAN protein an average RT RSD of 1.2% was calculated. Proteins were separated and digested off chip prior to the nano-HPLC-Chip-MS analysis using conventional 2-D SDS PAGE, protein spot excision from the 2-D gels post separation and digestion of protein spots with trypsin. The nano-HPLC-Chip-MS technique was able to analyze and detect as low as 10 fmol of BSA digest.

Sedgwick *et al*. [84] described a polydimethylsiloxane (PDMS) microfluidic device that was capable of isolating single A431 human epithelial carcinoma cells, electroporating the cells and lysing single cells. The cells expressed a green fluorescent protein-labeled β-actin, which allowed for the visualization and monitoring of the cell's cytoskeleton by confocal fluorescence microscopy during

trapping and electroporation of the cells. Electroporation was carried out using dielectrophoresis (DEP) by applying an electric field across a pair of 10 µm spaced saw-tooth gold microelectrodes that were perpendicular to the channels. The schematic representation of this device is shown in Figure 1.9. The back-end of the device's column was loaded with streptavidin-coated latex 10 µm microspheres, which were previously incubated with biotinylated anti-β-actin antibody for 1 h. The bead bed was used to capture the actins after cell lysis.

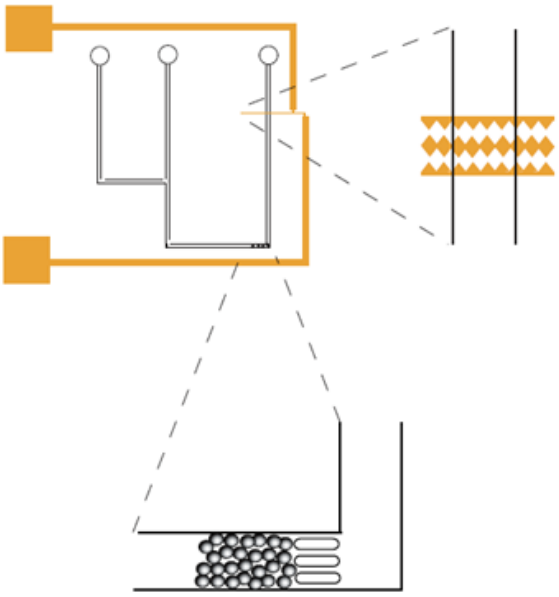

Figure 1.9 Schematic representation showing the saw-tooth gold electrodes (on a glass slide) positioned with the PDMS microchannels, and the bead bed for protein capture created by trapping microsphere with three approximately 25 µm PDMS pillars. Simple microchannels of depth approximately 50 µm and width approximately 100 µm were used, with two inlets (one for the cell suspension and one for introducing the micro-spheres and/or a buffer for flushing through the system) and a single outlet (Reproduced from Journal of The Royal Society Interface, 5, 2008, S123-S130).

Long *et al*. [85] coupled a pre-concentration SPE device to microchip electrophoresis (chip SPE-CE) in an integrated multilayer PDMS device separated with a nanoporous thin membrane interconnect that prevented solution leakage. The SPE, carried out in the upper unit, could be performed either by pressure or electroosmosis. The representation of the system is shown in Figure 1.10. The SPE device was made by loading the upper channel with a suspension of C_{18}-coated 10 µm silica beads. Sample was delivered to the bead bed from R1 to R2 (see Figure 1.10) followed by

washing with 20/80 (v/v) acetonitrile-borate buffer and then elution of concentrated analytes from the SPE column with 60/40 (v/v) acetonitrile-borate buffer. To introduce an injection plug into the lower CE device, a 2 s pulse voltage was applied between R2 and R4. CE detection was monitored by laser-induced fluorescence (LIF). Although the system was tested with a dye-labeled ephedrine solution, its application can be extended to proteins as well. Similar systems in the sense of integrating a pre-concentrator to a separation device have been reported as well [55, 86-90].

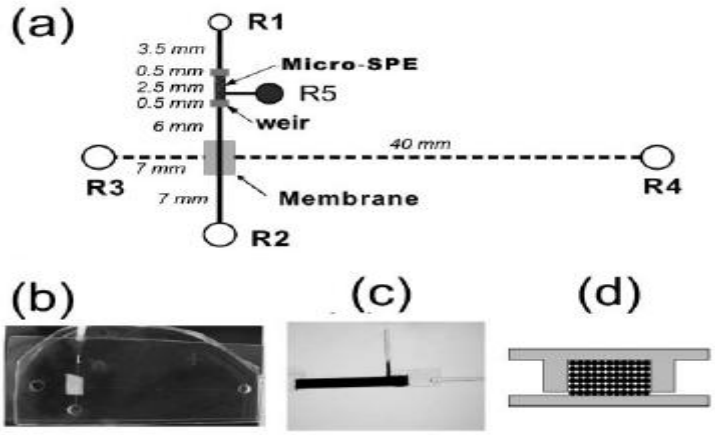

Figure 1.10 (a) Layout of the integrated SPE-CE multilayer device consisting of a small piece of nanoporous membrane sandwiched between the upper (continuous line) and lower (broken line) PDMS layers. (b) Photograph of the multilayer device. (c) and (d) Micrograph and schematic diagram of the packed μ-SPE column between two shallow weirs (Reproduced from *Lab Chip* 2007, *7*, 1819-1824).

1.5.2.2 Integrated Systems with Three Devices

Gottschlich *et al.* [91] developed a microfluidic device that integrated enzymatic reactions, electrophoretic separation of the reactants from the products and post-separation labeling of the proteins and peptides prior to fluorescence detection was accomplished (see Figure 1.11). A tryptic digestion of oxidized insulin β-chain was performed in 15 min under stopped flow conditions in a heated channel serving as the reactor and the separation was completed in 60 s. Localized thermal control of the reaction channel was achieved using a resistive heating element. The separated reaction products were then labeled with naphthalene-2,3-dicarboxaldehyde (NDA) and detected by fluorescence detection.

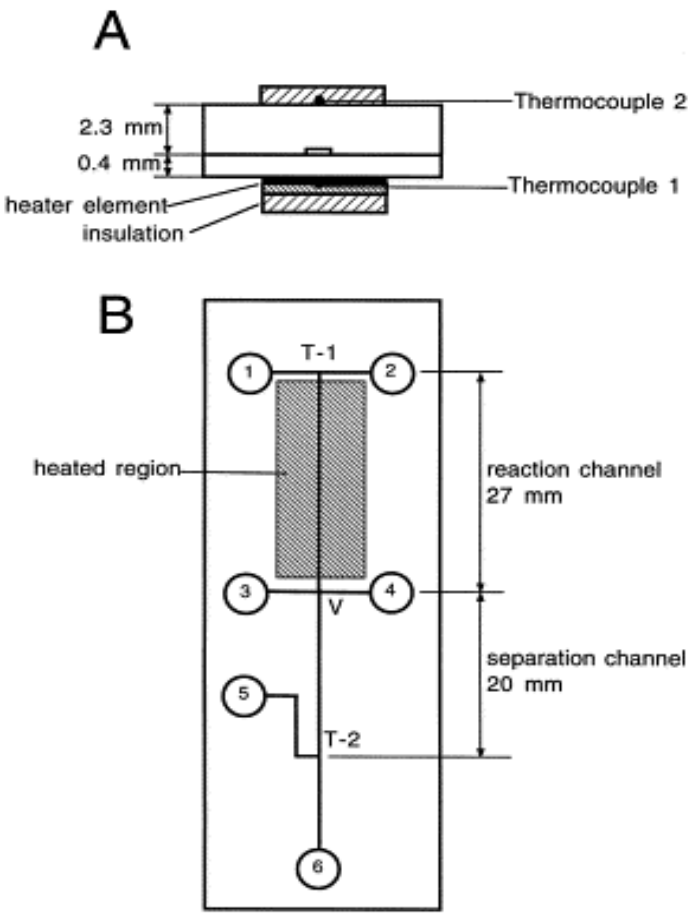

Figure 1.11 (A) Cross-sectional view of a microchip, heating element, and thermocouples. (B) Diagram of the microchip used for on-chip proteolytic reactions, separations and postcolumn labeling for generating fluorescent moieties. The fluid reservoirs are: (1) substrate, (2) enzyme, (3) buffer, (4) sample waste, (5) NDA, and (6) waste (Reproduced from Journal of Chromatography B, Biomedical Sciences and Applications, 745, 2000, 243-249).

A PDMS microfluidic device has been reported by Dodge and co-workers [92] that combined on-line protein electrophoretic separation, selection, and digestion of a protein of interest for identification by MS (see Figure 1.12). The microfluidic system included eight integrated valves and one micropump dedicated to control of flow operations. To evaluate the system performance, myoglobin was successfully isolated from BSA, then selected using integrated valves and digested in a rotary micromixer. Proteolytic peptides were recovered from the micromixer for protein identification. Total analysis from sample injection to protein identification was performed within 30 min, with sample volumes in the range of tens of nanoliters.

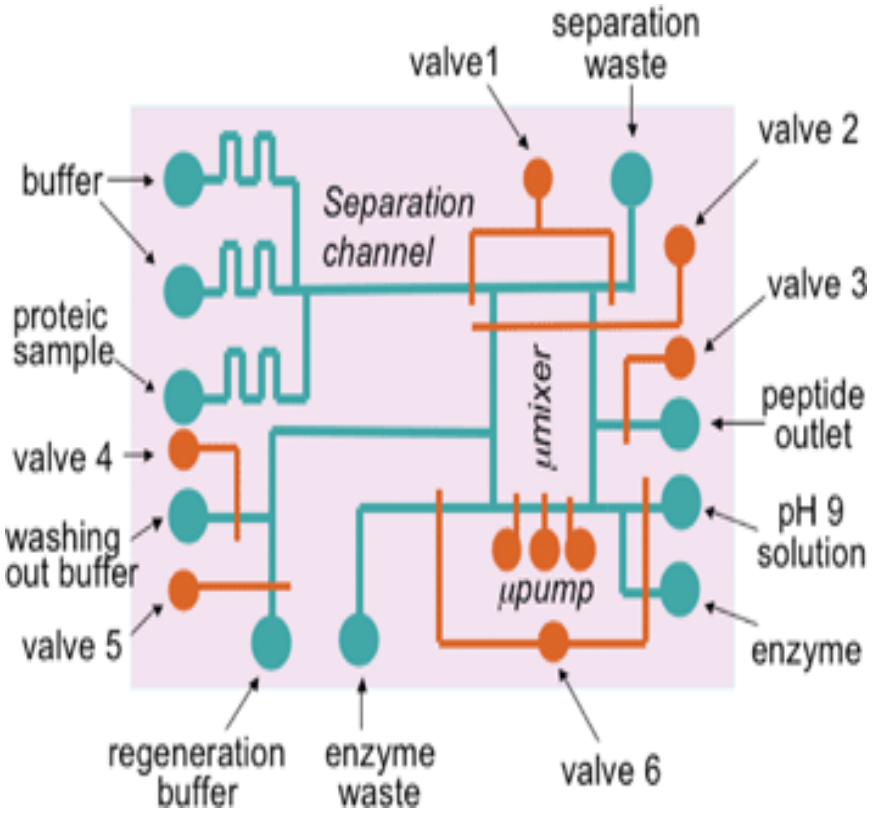

Figure 1.12 Drawing of an integrated PDMS microfluidic device. It was comprised of four modules: an injection/separation module in which pumping was entirely supported by electroosmotics; a protein trapping module; a circular micromixer where pumping was mechanically achieved; and an enzyme reaction module. Fluidic channels are in red, actuation channels are in blue-green. Valve actuation channels were filled with water in order to avoid air entering the fluidic channels through the PDMS membranes. Integrated valves are numbered from 1 to 6 (Reproduced from The Analyst, 131, 2006, 1122-1128).

An integrated microfabricated system composed of a proteolytic reactor and chromatographic column with direct interface to ESI-MS was reported by Carlier *et al*. [93]. The system is represented in Figure 1.13 and was fabricated from SU-8 and used to perform protein digestion, sample purification, salt removal, and chromatography followed by MS analysis. The chromatographic end of the chip was terminated with a nano-ESI interface. The digestion module was composed of tryspin covalently attached to a monolithic polymer, which was also used to prepare a hydrophobic stationary phase for the desalting or separation of peptides prior to MS analysis. Monoliths were made *in situ* by photo-polymerizing ethylene dimethacrylate (EDMA) monomers in the presence of lauryl methacrylate (LMA) or butyl methacrylate (BMA) crosslinkers.

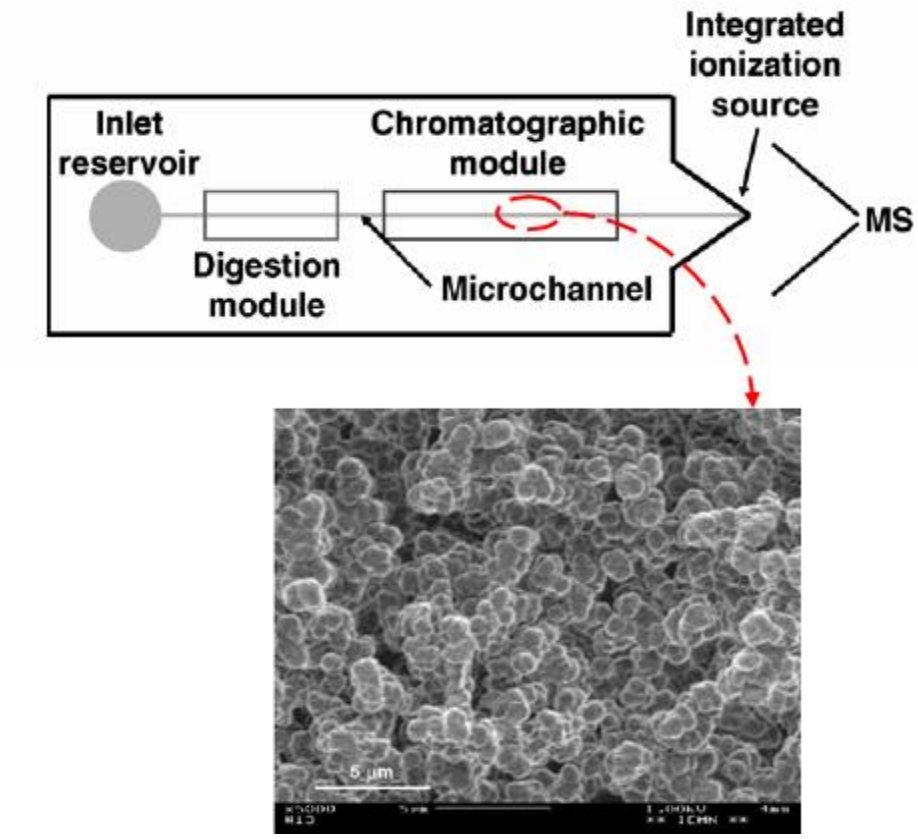

Figure 1.13 Top: Schematic representation of the SU-8 based microfluidic system which includes and enzymatic micro-reactor, a chromatographic device and an integrated ionization emitter tip. Bottom: Scanning electron microscopy photograph of a section of a monolithic phase prepared from LMA/EDMA. (Reproduced from Journal of Chromatography, 1071, 2005, 213-222).

Huh *et al*. [94] developed an integrated microfluidic system as shown in Figure 1.14, which was used to first successfully disrupt cells by mixing at an optimized speed of 500 rpm for 10 min. Mixing was made possible by embedding a microdisk in the microchamber and applying an external rotating magnetic. Elution buffer was then introduced into the chamber to shuttle the lysed sample into a fritless solid-phase extraction (SPE) device that was made by *in situ* photo-polymerizing ethylene glycol dimethacrylate (EGDMA) and acrylamide (AAm) monomer solutions. Most cellular debris and negatively charged proteins from a recombinant gold binding peptide (GBP)-fusion *E. coli* were bound to the SPE surface allowing for up to 60% of the total proteome to be shuttled to a detection device where GBP-fusion proteins were electrochemically detected using three gold electrodes integrated in the microchannels or gold microarrays.

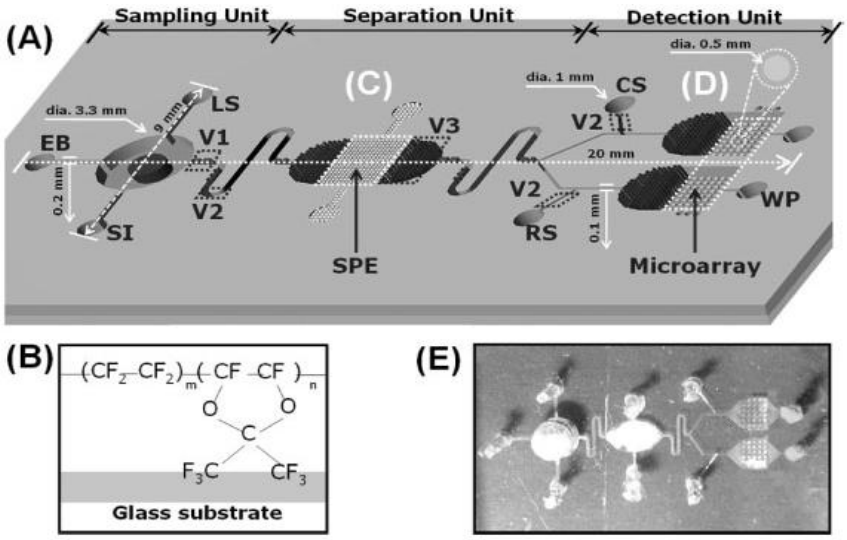

Figure 1.14 Integrated microfluidic system for on-chip analysis of biomolecules. (A) Schematic representation of the fully integrated microfluic system showing the sample mixing zone for disruption of cells, the sample purification zone with SPE, and the gold microcircle patterned analysis zone for detection infectious pathogens. Reservoirs in the mixing chamber were labeled as SI, EB, and LS for sample inlet, elution buffer, and lysis solution, respectively. Detection reservoirs were labled as RS, CS, and WP for reaction sample, control sample, and waste port, respectively. (B) Chemical structure of Teflon AF 1600 used for the hydrophobic film valve (V2). (C) The AAm functionalized SPE was packed by *in situ* polymerization. (D) Gold microarray for the detection of infectious viral disease. (E) Photograph of the integrated system coupled with a magnetic stirrer. The cylinder-type micropillar for packing SPE is for removing debris (V3). Device dimension are 10.0 (width) x 18.0 (length) x 5 (height) mm. (Reproduced from Electrophoresis, 29, 2008, 2960-2969).

Li *et al*. [95-97] developed a variety of integrated systems amenable to the rapid analysis of trace tryptic protein digests with the most recently reported system shown in Figure 1.15 [95]. The system was endowed with an autosampler, which introduced peptides first to the pre-concetration device of the system. The pre-concentration device was composed of c-myc-specific antibodies immobilized protein G-Sepharose beads packed into a large channel (2.4 μL) of the chip. The bead-based bed enabled an affinity selection of targeted antigenic peptides (20 ng/mL spiked in human plasma) prior to electrophoretic separation and subsequent MS quadruple/time-of-flight (Q TOF) MS analysis. A throughput of up to 12 samples/h and on-chip detection limit of ~5 nM (or 25 fmol) were reported. However, peptide samples were generated off-chip as tryptic digests of isolated protein spots from 2-D IEF/SDS PAGE of protein extracts of human prostatic cancer cells (LNCaP).

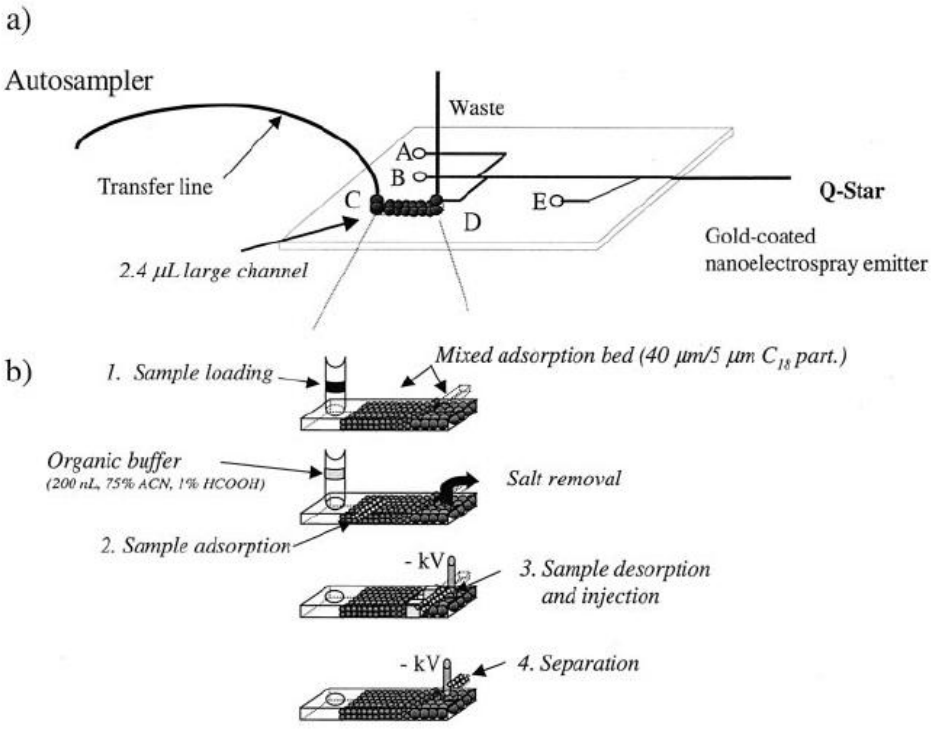

Figure 1.15 Schematic representation of the auto-sampler chip-CE-time-of-flight interface. (a) microfluidic device comprising a large flow channel (800 um wide, 150 um deep, and 22 mm long) located between wells C and D and packed with C_{18} reverse phase. Sample plugs (typically 8-10 µL) are introduced from the auto-sampler to well C via a capillary transfer line. Wells A, B, and E correspond to waste, separation buffer (0.2% aqueous HCOOH), and internal standard (1 µg/mL angiotensin I in separation buffer), respectively. (b) Sequential steps involving sample clean-up, desorption, injection, and separation (Reproduced from Molecular & Cellular Proteomics, 1, 2002, 157-168).

1.5.2.3 Integrated Systems with Four or More Devices

Srivastava *et al*. [98] recently reported an integrated quartz-based microfluidic platform termed the phosphoFlow Chip (pFC) (see Figure 1.16), which was used to monitor internal responses of the RAW 264.7 murine macrophage by profiling only phosphorylated proteins. Using fluorescence microscopy, real-time observation of cell phenotype was plausible prior to flow cytometry. The approach involved cell introduction, infection of the cells, phosphor-epitope staining, fluorescence imaging and flow cytometry. The system consisted of two fluidically isolated spiral incubation chambers for the simultaneous execution of both assays with adherent cells and the control with non-adherent cells. The system's capacity was reported to be ~2000 cells per assay and 350 nL of fluid

volume. The technique was capable of monitoring early signaling events that took less than 30 min for sample preparation and analysis [98].

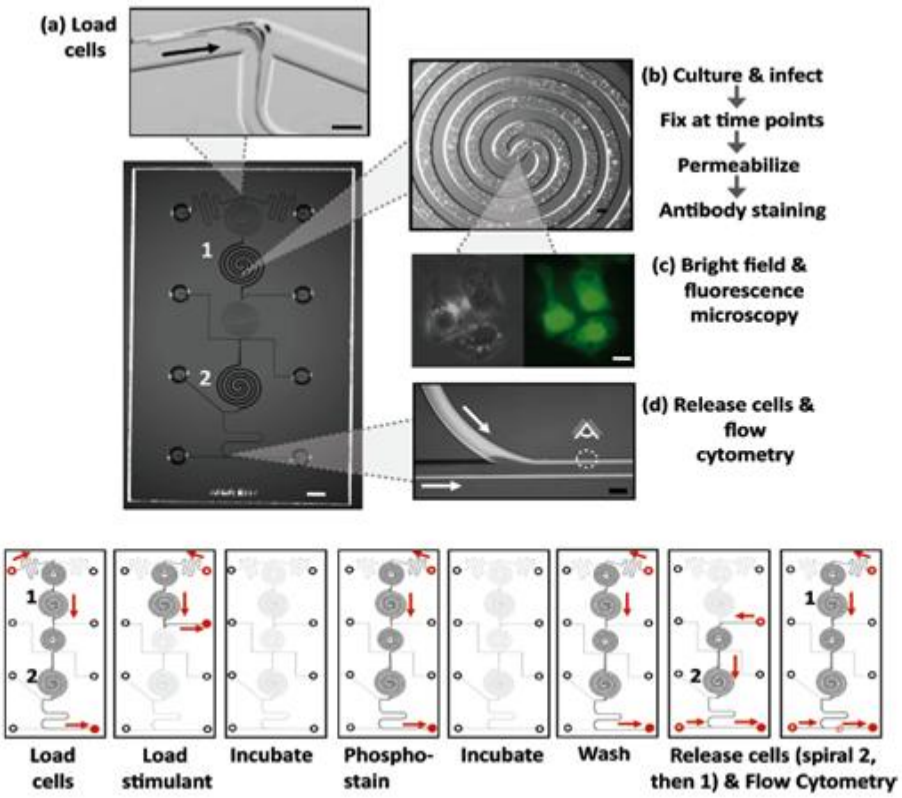

Figure 1.16 Top panel: pFC device for phosphor-profiling of adherent cells. Device operation proceeds from top to bottom. The two wide spirals (1 and 2) for simultaneous infection and control assay. (a) Macrophage cells are introduced into the pFC via pressure-driven flow, (b) incubation chambers (wide spirals, only one of the two is shown) where the automated pFC phosphorylation assay proceeds as (1) cell culture and infection, (2) phosphor-profiling (fixation, permeabilization, and staining with phosphor-specific antibodies), (c) imaging, and (d) flow cytometry. Scale bars: 2 mm (chip image), 100 um (a,d), 200 um (b), and 10 um (c). Bottom panel: Detailed step-by-step operation of the pFC platform, from loading cells to end-point detection by flow cytometry. Red arrows indicate the direction of flow, highlighted wells indicate external fluid valve to that inlet well is open (all others being closed), channels in dark gray support continuous flow while regions in light gray contain stagnant flow (Reproduced from Analytical Chemistry, 81, 2009, 3261-3269).

Stachowiak *et al.* [99] coupled an automated sample preparation (ASP) system to a chip gel electrophoresis protein profiling (CGE-PP) system to execute an autonomous microfluidic sample preparation and detection of aerosolized bacterial cells and spores based on protein profiling. The combined system, which was field deployable, was capable of differentiating between bacterial organisms. It operated by collecting aerosol samples using a collector, pre-concentrating the

organisms, thermo-chemically lysing the bacterial cells or spores, subjecting the resulting proteins to size exclusion chromatography prior to fluorescently labeling the proteins with dyes and finally separating the labeled proteins using gel electrophoresis to generate a protein profile. The entire task was completed in approximately 10 min with a sensitivity of 16 agent-containing particles per liter of air for *B. subtilis* spores. By profiling the proteins of pathogenic organisms, the technique can detect any pathogen unlike in PCR-based or immunoassay-based techniques where the pathogen's sequence primers or monoclonal antibodies, respectively, must be available. Figure 1.17 shows the schematic representation of the ASP system.

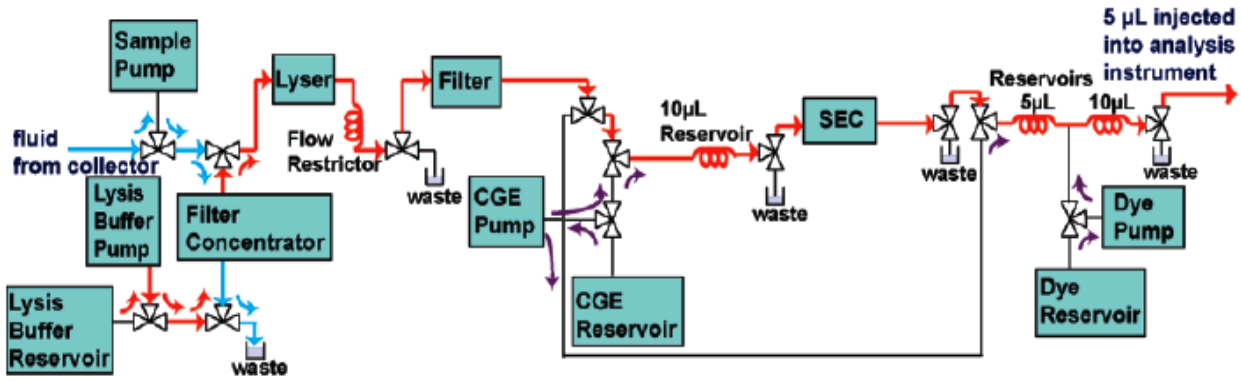

Figure 1.17 Schematic representation of the automated sample preparation system. Arrows indicate the flow direction. Blue lines and arrows represent the path taken by incoming sample from the aerosol collector before preconcentration. Red lines and arrows represent the path taken by sample after concentration by the filter. Port symbols represent position valves. Fluidic connections between ports perpendicular to each other are made and broken as the valve actuates. Ports parallel to one another are never connected (Reproduced from Analytical Chemistry, 79, 2007, 5763-5770).

Ethier *et al*. [100] assembled a reactor by coupling a 200 µm inner diameter capillary tubing into an inline micro-filter frit and then packing the capillary with strong cation exchange (SCX) beads, such that proteins were bound to the beads at low pH and digested at high pH where trypsin enzyme was activated. Buffers and slurry beads were pressure filled using nitrogen (see Figure 1.18). The system was dubbed "the proteomic reactor" and could rapidly extract proteins from cells, pre-concentrate, reduce, alkylate, and digest proteins. With an interstitial volume of ~50 nL, the pre-concentration range was between 20 to 2000-fold for material input volumes between 1-100 µL.

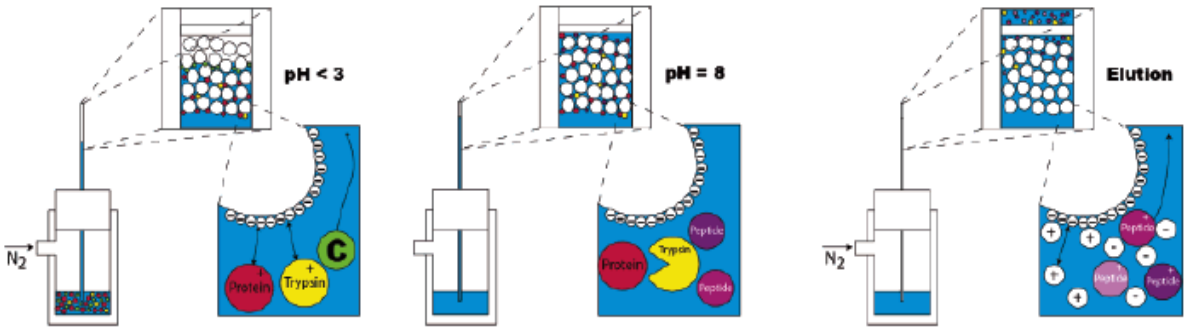

Figure 1.18 Left: Schematic representation of the proteomic reactor. Pressurized nitrogen was used to push the liquid into the reactor. The protein and trypsin are bound to the SCX material. Middle: Trypsin is activated by adjusting the pH to 8. The flow was stopped to let the digestion proceed without losing peptides. Right: Peptides were eluted by using an ammonium bicarbonate solution. (Reproduced from Journal of Proteome Research, 5, 2006, 2754-2759).

1.6 Concluding Remarks

To date, there is still no fully integrated multi-functional microfluidic system for automated protein analysis. The microchip system reported by Ethier *et al*. [100] in our opinion is one of the most comprehensive systems. It appears that it may be more feasible to implement the top-down approach on an integrated microchip platform compared to implementing the bottom-up approach owing to the fact that all proteins in the protein mixture are digested at once in one proteolytic step for the top-down approach. On the other hand, the bottom-up approach requires the digestion of individual proteins that have been separated previously, suggesting that proteins would have to be serially injected into the proteolytic reactor to be digested or the integrated microchip would have to possess several reactors so that one protein is digested in one reactor. If the former is implemented, then there would be an issue of cross contamination of peptides. However, for the latter is to be implemented, the question of how many reactors to be incorporated into the chip becomes an issue as there are a multitude of proteins that could result from the separation of a complex proteome.

Most integrated protein analysis systems reported thus far are comprised of only two devices as shown in Table 1. There are challenges facing the development of fully integrated systems for protein analysis. Different devices may require different buffer conditions; therefore, isolation of the various

Table 1.1 Integrated Microfluidic Systems for Protein Analysis with two or more protein processing devices combined prior to MS interface

Devices or Units Combined	Chip	Sample Analyzed	Efficiency/Comments	Ref.
TWO PROCESSES OR DEVICES COMBINED				
Porous silica pre-concentration unit and μ-CGE separation	Glass	Mixture of up to 7 purified proteins	Pre-concentration factors of ~600 fold	[77]
Proteolytic reactor and IMAC affinity unit for peptide enrichment	Glass	Model proteins were analyzed individually	Capture bias on IMAC; system required further optimization due to non-specific binding	[78]
Monolithic based SPE and proteolytic reactor	Glass	Myoglobin	Sequence coverage of ~80% achieved for 20 uL of myoglobin (19 pmol/uL)	[79]
polystyrene beads for SPE desalting and a CE unit with ESI-interface	PDMS	Six-peptide mixtures dissolved in physiological salt solution	LOD is in the femtomole regime	[80]
SPE enrichment column and a reversed phase separation channel with a nanoelectrospray emitter	Glass	protein digests spiked into rat plasma samples	LOD of 1 – 5 fmol.	[81]
Protein digestion unit made of a trypsin adsorbed poly (vinylidene fluoride) porous membrane and transient capillary isotachophoresis/CZE with ESI-MS interface	PDMS	Three model proteins	A plug of 300 nL of cytochrome *c* solution (10 μg/mL) was analyzed	[82]
A monolithic protein digestion bed and CE unit interfaced with an ESI-MS	Glass	Three model proteins	3 – 6 min to complete digestion cytochrome *c* or BSA	[64]
Enrichment column and nanoscale C_{18} reversed phase separation column interfaced with ESI- tip	Glass	Peptides resulting from proteins digested off-chip	Highly reproducible retention times from the nano-LC and 10 fmol of BSA digest was detected	[83]
Cell lyses and protein capture and visualization	PDMS	green fluorescent protein-labeled β-actin	Capture bed was decorated with anti-β-actin antibody	[84]
C18-coated silica bed SPE unit and CE unit	PDMS	dye-labeled ephedrine protein	CE detection was monitored by laser induced fluorescence	[85]

Table 1.1 Continued

Devices or Units Combined	Chip	Sample Analyzed	Efficiency/Comments	Ref.
THREE PROCESSES OR DEVICES COMBINED				
Proteolytic reactor, peptide separation, and post-column labeling	Glass	Oxidized insulin β-chain	Tryptic digestion in 15 min, and peptide separation in ~60 s	[91]
Protein separation, mechanical protein trapping/selection, and proteolytic digestion	PDMS	Myoglobin and BSA	Device included 8 valves and a micropump. Total analysis was under 30 min nanoliter sample volume	[92]
Proteolytic reactor, desalting bed made of a hydrophobic monolithic stationary phase, and a chromatographic unit with ESI interface	SU-8	Cytochrome *c*	800 fmol cytochrome c digest was separated by nano-LC coupled to ESI-MS	[93]
Cell lysis, SPE unit, and a microarray	PDMS	*E. coli* cell lysate	Up to 60% of the total proteome were shuttled to microarray unit	[94]
SPE unit, salt removal unit, and a separation unit with nano-spray.	Glass	antigenic peptides spiked in human plasma	Device provided a HTP of 12 samples/h and LOD of ~5 nM (or 25 fmol)	[95-97]
FOUR OR MORE PROCESSES OR DEVICES COMBINED				
Cell culture, cell infection, phosphor-epitope staining, cell imaging, and flow cytometry	Quartz	Phosphorylated proteins from maurine cell lysate	~2000 cells per assay can be analyzed and 350 nL of fluid volume	[98]
Pre-concentration of bacterial cells, thermo-chemical lysis, size exclusion chromatography of proteins prior, fluorescent labeling the proteins, and μ-CGE	Glass	Bacterial cell lysates	Field deployable chip with total analysis time ~10 min and a LOD of 16 agent-containing particles per liter of air for *B. subtilis* spores.	[99]
Cell lysis, protein extraction, preconcentration, sample clean-up, protein modification (reduction/alkylation), and protein digestion	Glass	Mouse testicular cell lysate	As little as 300 cells can be used	[100]

processing steps becomes important. For example, the separation buffer conditions required to optimally separate proteins prior to protein digestion may be completely different. The integrated chip presented by Yue *et al.* [78] required different pH buffer solutions for trypsin digestion and IMAC enrichment. Thus, when proteins were flowed through the trypsin beads to the IMAC beads, 4% acetic acid was pumped through a side inlet to the IMAC microchannel at the same time to adjust the pH of the digested protein solution from pH 8.0 to pH 4–5. In their work, Peterson *et al*. [79] used acetonitrile to release accumulated proteins from a SPE bed that was directly coupled to a proteolytic digestion reactor and reported a high protein recovery. However, the use of pure organic solvent to release the proteins would be impractical where a separation step followed the extraction step because pure organic solvents may not be compatible with the subsequent chromatographic process, which the authors anticipated to incorporate in their future designs.

There is also the issue of incomplete digestion or prolonged digestion times due to the limited amount of immobilized trypsin. One way to alleviate the problem is to provide high surface area to immobilize trypsin and this can be achieved by replacing large diameter beads onto which trypsin has been attached with smaller diameter particles or by immobilization of the trypsin onto a sol–gel matrix that is formed within the channel [78]. Furthermore, there is the issue of cross-contamination between peptide ions within the reactor. To minimize the issue of cross-contamination, a 10-min Tris-buffer flush may be required between each protein digestion [78]. Unfortunately, flushing the reactor after each proteolytic digestion may not be amenable for a complete top-down protein analysis where each separated protein would be sequentially injected from an up-stream separation into the bioreactor.

Pre-concentrating protein samples after extraction and before separation in an integrated system for a total proteomic analysis is very important – enough material is needed downstream during protein digestion and subsequently for peptide mass analysis. One way, to improve the concentration factor is by pre-concentrating the sample directly in the separation injector so that all of the concentrated

sample can be then injected into the separation channel for analysis [77]. However, peak distortions and loss of resolution during μ-CE can be observed following long pre-concentration times [77]. Finally, the issue of dead volumes develop when capillary connections and other junctions, such as fluid inlets, outlets and microdialysis junctions are used, which can degrade separation performance, introduce sample carryover or sample loss. For example, Gao and co-workers [82] estimated ~4 μL for the void volumes associated with their miniaturized trypsin membrane reactor.

Fabricating a practical integrated chip for acomplete protein analysis is possible. To begin with, the ruggedness and stability of the trypsin reactor has been shown to be impressive. Trypsin has been shown to maintain its activity for at least two weeks when a bioreactor was properly stored at 4 ^{o}C when not in use [78]. This aspect of an integrated system is delicate as it is the only device decorated with degradable biomaterials. But, to achieve a complete protein analysis on chip in the near future, a combination of both the top-down and bottom-up approaches (dubbed the *top-bottom "combo" approach*) may be called for. The modified processing pipeline would be as follows: (1) Cell lysis and protein extraction; (2) protein separation, where due to the high complexity of the proteome, the separated protein plugs are a mixture of proteins instead of individual proteins as required by the top-down approach; (3) digestion of the protein mixture digestion just like in the bottom-up approach where the non-separated proteins are digested apriori; and (4) peptide separation and introduction into the mass spectrometer. So, if we were to implement the top-down combo approach on a mammalian cell proteome, which contains ~10,000 proteins per cell [20] using our proposed ideal integrated microchip shown in Figure 1, we would first separate the 10,000 proteins after cell lysis and extraction by a SDS μ-CGE/MEKC [101] (Unit II). For the sake of argument, let us assume that we were able to resolve ~2,500 proteins using this technique [62]. This means that each protein band would contain about four different proteins on average. To ensure that there would be enough trypsin to digest the four different proteins, the solid-phase micro-reactors (Unit III) would be endowed with nanopillars

[102] to increase the surface area prior to the attachment of trypsin. Considering that the tryptic digestion of cytochrome *c* (104 amino acids) results in ~10 peptides [34], the average protein containing about 360 amino acids is expected to generate roughly 35 peptides (for top-down approach) or 140 peptides for four proteins (for the top-bottom approach). There has not been any report where microchip 2-D separations were coupled to ESI or MALDI MS. For the separation unit shown in Figure 1, an average protein peak volume of ~10 pL [101] is expected, but in order to make the microchip 2-D separation coupled to ESI or MALDI MS a reality, MS interfaces must be optimized for small sample volumes; for example, MALDI deposition with small deposited spot sizes for a higher local concentration [31]. In addition, having sufficient signal to noise ratio (SNR) is needed for the mass spectral readout as well. About 1.4×10^{-15} mole is expected from the 10 pL protein peak volume [101] considering an average concentration of 3 nM [101] for an individual protein and an average protein molecular mass of 46 kDa.

1.7 References

[1] Anderson, N. L., Anderson, N. G., *Molecular & Cellular Proteomics* 2002, *1*, 845-867.

[2] Clarke, S., *International Journal of Peptide and Protein Research* 1987, *30*, 808-821.

[3] Wittenberg, G., Danon, A., *Plant Science* 2008, *175*, 459-466.

[4] Glozak, M. A., Sengupta, N., Zhang, X. H., Seto, E., *Gene* 2005, *363*, 15-23.

[5] Peng, J. M., Schwartz, D., Elias, J. E., Thoreen, C. C., *et al.*, *Nature Biotechnology* 2003, *21*, 921-926.

[6] Tan, S., Tan, H. T., Chung, M. C. M., *Proteomics* 2008, *8*, 3924-3932.

[7] Guidotti, G., *Annual Review of Biochemistry* 1972, *41*, 731-&.

[8] Coiras, M., Camafeita, E., Lopez-Huertas, M. R., Calvo, E., *et al.*, *Proteomics* 2008, *8*, 852-873.

[9] Garcia, M. A., Meurs, E. F., Esteban, M., *Biochimie* 2007, *89*, 799-811.

[10] Geisow, M., *Nature* 1977, *270*, 476-477.

[11] Wilkins, M. R., Sanchez, J. C., Gooley, A. A., Appel, R. D., *et al.*, *Biotechnology and Genetic Engineering Reviews, Vol 13*, Intercept Ltd, Andover 1996, pp. 19-50.

[12] Ishihama, Y., Schmidt, T., Rappsilber, J., Mann, M., *et al.*, *Bmc Genomics* 2008, *9*.

[13] *www.ncbi.nlm.nih.gov*.

[14] Anderson, N. L., Anderson, N. G., *Electrophoresis* 1998, *19*, 1853-1861.

[15] Hu, S., Michels, D. A., Fazal, M. A., Ratisoontorn, C., *et al.*, *Anal. Chem.* 2004, *76*, 4044-4049.

[16] de Hoog, C. L., Mann, M., *Annual Review of Genomics and Human Genetics* 2004, *5*, 267-293.

[17] Wilkins, M. R., Pasquali, C., Appel, R. D., Ou, K., *et al.*, *Bio-Technology* 1996, *14*, 61-65.

[18] Schramm, A., Apostolov, O., Sitek, B., Pfeiffer, K., *et al.*, *Klinische Padiatrie* 2003, *215*, 293-297.

[19] Kussmann, M., Affolter, M., Fay, L. B., *Combinatorial Chemistry & High Throughput Screening* 2005, *8*, 679-696.

[20] Venter, J. C., Adams, M. D., Myers, E. W., Li, P. W., *et al.*, *Science* 2001, *291*, 1304-+.

[21] Lander, E. S., Linton, L. M., Birren, B., Nusbaum, C., *et al.*, *Nature* 2001, *409*, 860-921.

[22] Lion, N., Rohner, T. C., Dayon, L., Arnaud, I. L., *et al.*, *Electrophoresis* 2003, *24*, 3533-3562.

[23] Kim, H., Page, G. P., Barnes, S., *Nutrition* 2004, *20*, 155-165.

[24] Lay, J. O., Borgmann, S., Liyanage, R., Wilkins, C. L., *Trac-Trends Anal. Chem.* 2006, *25*, 1046-1056.

[25] Ahmed, N., Rice, G. E., *J. Chromatogr. B* 2005, *815*, 39-50.

[26] Reinders, J., Lewandrowski, U., Moebius, J., Wagner, Y., Sickmann, A., *Proteomics* 2004, *4*, 3686-3703.

[27] Ransohoff, D. F., *Nat. Rev. Cancer* 2005, *5*, 142-149.

[28] Coombes, K. R., Morris, J. R. S., Hu, J. H., Edmonson, S. R., Baggerly, K. A., *Nat. Biotechnol.* 2005, *23*, 291-292.

[29] Haynes, P. A., Yates, J. R., *Yeast* 2000, *17*, 81-87.

[30] Emmett, M. R., Caprioli, R. M., *J. Am. Soc. Mass Spectrom.* 1994, *5*, 605-613.

[31] Lee, J., Soper, S. A., Murray, K. K., *Journal of Mass Spectrometry* 2009, *44*, 579-593.

[32] Li, J. J., Kelly, J. F., Chemushevich, I., Harrison, D. J., Thibault, P., *Anal. Chem.* 2000, *72*, 599-609.

[33] Mellors, J. S., Gorbounov, V., Ramsey, R. S., Ramsey, J. M., *Anal. Chem.* 2008, *80*, 6881-6887.

[34] Musyimi, H. K., Guy, J., Narcisse, D. A., Soper, S. A., Murray, K. K., *Electrophoresis* 2005, *26*, 4703-4710.

[35] Figeys, D., vanOostveen, I., Ducret, A., Aebersold, R., *Anal. Chem.* 1996, *68*, 1822-1828.

[36] Laurell, T., Marko-Varga, G., *Proteomics* 2002, *2*, 345-351.

[37] Laurell, T., Nilsson, J., Marko-Varga, G., *TrAC, Trends in Analytical Chemistry* 2001, *20*, 225-231.

[38] Ekins, R., Chu, F., Biggart, E., *Analytica Chimica Acta* 1989, *227*, 73-96.

[39] Fodor, S. P. A., Read, J. L., Pirrung, M. C., Stryer, L., *et al.*, *Science (Washington, DC, United States)* 1991, *251*, 767-773.

[40] Khrapko, K. R., Lysov, Y. P., Khorlyn, A. A., Shick, V. V., *et al.*, *FEBS Letters* 1989, *256*, 118-122.

[41] Southern, E. M., Maskos, U., Elder, J. K., *Genomics* 1992, *13*, 1008-1017.

[42] Paegel, B. M., Emrich, C. A., Wedemayer, G. J., Scherer, J. R., Mathies, R. A., *Proceedings of the National Academy of Sciences of the United States of America* 2002, *99*, 574-579.

[43] Mueller, O., Hahnenberger, K., Dittmann, M., Yee, H., *et al.*, *Electrophoresis* 2000, *21*, 128-134.

[44] Bousse, L., Mouradian, S., Minalla, A., Yee, H., *et al.*, *Analytical Chemistry* 2001, *73*, 1207-1212.

[45] Lion, N., Rohner, T. C., Dayon, L., Arnaud, I. L., *et al.*, *Electrophoresis* 2003, *24*, 3533-3562.

[46] Li, P. C. H., Harrison, D. J., *Anal. Chem.* 1997, *69*, 1564-1568.

[47] Di Carlo, D., Jeong, K. H., Lee, L. P., *Lab Chip* 2003, *3*, 287-291.

[48] Waters, L. C., Jacobson, S. C., Kroutchinina, N., Khandurina, J., *et al.*, *Anal. Chem.* 1998, *70*, 158-162.

[49] Taylor, M. T., Belgrader, P., Furman, B. J., Pourahmadi, F., *et al.*, *Anal. Chem.* 2001, *73*, 492-496.

[50] Lee, S. W., Tai, Y. C., *Sensors and Actuators a-Physical* 1999, *73*, 74-79.

[51] Lu, H., Schmidt, M. A., Jensen, K. F., *Lab Chip* 2005, *5*, 23-29.

[52] Kutter, J. P., Jacobson, S. C., Ramsey, J. M., 2000, pp. 93-97.

[53] Kutter, J. P., Jacobson, S. C., Matsubara, N., Ramsey, J. M., *Anal. Chem.* 1998, *70*, 3291-3297.

[54] Lion, N., Gellon, J. O., Jensen, H., Girault, H. H., *J. Chromatogr. A* 2003, *1003*, 11-19.

[55] Yang, W. C., Sun, X. H., Pan, T., Woolley, A. T., *Electrophoresis* 2008, *29*, 3429-3435.

[56] Service, R. F., *Science* 2001, *294*, 2074-2077.

[57] Smith, R. D., *Nat. Biotechnol.* 2000, *18*, 1041-1042.

[58] Wang, H., Hanash, S., *J. Chromatogr. B* 2003, *787*, 11-18.

[59] Chen, X. X., Wu, H. K., Mao, C. D., Whitesides, G. M., *Anal. Chem.* 2002, *74*, 1772-1778.

[60] Molloy, M. P., Brzezinski, E. E., Hang, J. Q., McDowell, M. T., VanBogelen, R. A., *Proteomics* 2003, *3*, 1912-1919.

[61] Chen, H., Fan, Z. H., *Electrophoresis* 2009, *30*, 758-765.

[62] Osiri, J. K., Shadpour, H., Park, S., Snowden, B. C., *et al.*, *Electrophoresis* 2008, *29*, 4984-4992.

[63] Yang, S., Liu, J. K., Lee, C. S., Devoe, D. L., *Lab Chip* 2009, *9*, 592-599.

[64] Wang, C., Oleschuk, R., Ouchen, F., Li, J., *et al.*, *Rapid Communications in Mass Spectrometry* 2000, *14*, 1377-1383.

[65] Jin, L. J., Ferrance, J., Sanders, J. C., Landers, J. P., *Lab Chip* 2003, *3*, 11-18.

[66] Lee, J., Musyimi, H. K., Soper, S. A., Murray, K. K., *J. Am. Soc. Mass Spectrom.* 2008, *19*, 964-972.

[67] Kim, Y. D., Park, C. B., Clark, D. S., *Biotechnology and Bioengineering* 2001, *73*, 331-337.

[68] Sakai-Kato, K., Kato, M., Toyo'oka, T., *Anal. Chem.* 2003, *75*, 388-393.

[69] Peterson, D. S., Rohr, T., Svec, F., Frechet, J. M. J., *Anal. Chem.* 2002, *74*, 4081-4088.

[70] Krenkova, J., Foret, F., *Electrophoresis* 2004, *25*, 3550-3563.

[71] Hood, L., *Journal of Proteome Research* 2002, *1*, 399-409.

[72] O'Connor, C. D., Pickard, K., *Microarrays & Microplates* 2003, 61-88.

[73] Chang, H.-T., Huang, Y.-F., Chiou, S.-H., Chiu, T.-C., Hsieh, M.-M., *Current Proteomics* 2004, *1*, 325-347.

[74] Soper, S. A., McCarley, R. L., Chen, G., Shadpour, H., Musyimi, H. K., Patent disclosure filed at Louisiana State University Patent Office (Reference No. 0622, 25547) 2006.

[75] Musyimi, H. K., Shadpour, H., Chen, G., McCarley, R. L., *et al.*, *Micro Total Analysis Systems 2006, Proceedings of the mTAS 2006 Symposium*, 2006, in press.

[76] Baba, Y., *Analytical and Bioanalytical Chemistry* 2002, *372*, 14-15.

[77] Foote, R. S., Khandurina, J., Jacobson, S. C., Ramsey, J. M., *Analytical Chemistry* 2005, *77*, 57-63.

[78] Yue, G. E., Roper, M. G., Balchunas, C., Pulsipher, A., *et al.*, *Analytica Chimica Acta* 2006, *564*, 116-122.

[79] Peterson, D. S., Rohr, T., Svec, F., Frechet, J. M. J., *Analytical Chemistry* 2003, *75*, 5328-5335.

[80] Dahlin, A. P., Bergstroem, S. K., Andren, P. E., Markides, K. E., Bergquist, J., *Analytical Chemistry* 2005, *77*, 5356-5363.

[81] Fortier, M.-H., Bonneil, E., Goodley, P., Thibault, P., *Analytical Chemistry* 2005, *77*, 1631-1640.

[82] Gao, J., Xu, J., Locascio, L. E., Lee, C. S., *Analytical Chemistry* 2001, *73*, 2648-2655.

[83] Hardouin, J., Duchateau, M., Joubert-Caron, R., Caron, M., *Rapid Communications in Mass Spectrometry* 2006, *20*, 3236-3244.

[84] Sedgwick, H., Caron, F., Monaghan, P. B., Kolch, W., Cooper, J. M., *Journal of the Royal Society Interface* 2008, *5*, S123-S130.

[85] Long, Z. C., Shen, Z., Wu, D. P., Qin, J. H., Lin, B. C., *Lab Chip* 2007, *7*, 1819-1824.

[86] Broyles, B. S., Jacobson, S. C., Ramsey, J. M., *Anal. Chem.* 2003, *75*, 2761-2767.

[87] Ramsey, J. D., Collins, G. E., *Anal. Chem.* 2005, *77*, 6664-6670.

[88] Proczek, G., Augustin, V., Descroix, S., Hennion, M. C., *Electrophoresis* 2009, *30*, 515-524.

[89] Tuomikoski, S., Virkkala, N., Rovio, S., Hokkanen, A., *et al.*, *J. Chromatogr. A* 2006, *1111*, 258-266.

[90] Hatch, A. V., Herr, A. E., Throckmorton, D. J., Brennan, J. S., Singh, A. K., *Anal. Chem.* 2006, *78*, 4976-4984.

[91] Gottschlich, N., Culbertson, C. T., McKnight, T. E., Jacobson, S. C., Ramsey, J. M., *Journal of Chromatography, B: Biomedical Sciences and Applications* 2000, *745*, 243-249.

[92] Dodge, A., Brunet, E., Chen, S., Goulpeau, J., *et al.*, *Analyst (Cambridge, United Kingdom)* 2006, *131*, 1122-1128.

[93] Carlier, J., Arscott, S., Thomy, V., Camart, J. C., *et al.*, 2005, pp. 213-222.

[94] Huh, Y. S., Park, T. J., Lee, E. Z., Hong, W. H., Lee, S. Y., *Electrophoresis* 2008, *29*, 2960-2969.

[95] Li, J. J., LeRiche, T., Tremblay, T. L., Wang, C., *et al.*, *Molecular & Cellular Proteomics* 2002, *1*, 157-168.

[96] Li, J. J., Tremblay, T. L., Wang, C., Attiya, S., *et al.*, *Proteomics* 2001, *1*, 975-986.

[97] Li, J. J., Wang, C., Kelly, J. F., Harrison, D. J., Thibault, P., *Electrophoresis* 2000, *21*, 198-210.

[98] Srivastava, N., Brennan, J. S., Renzi, R. F., Wu, M. Y., *et al.*, *Anal. Chem.* 2009, *81*, 3261-3269.

[99] Stachowiak, J. C., Shugard, E. E., Mosier, B. P., Renzi, R. F., *et al.*, *Anal. Chem.* 2007, *79*, 5763-5770.

[100] Ethier, M., Hou, W. M., Duewel, H. S., Figeys, D., *Journal of Proteome Research* 2006, *5*, 2754-2759.

[101] Shadpour, H., Soper, S. A., *Anal. Chem.* 2006, *78*, 3519-3527.

[102] Chen, G., McCandless, G. T., McCarley, R. L., Soper, S. A., *Lab Chip* 2007, *7*, 1424-1427.

2 Surface Modification of PMMA Microchips for Separations*

2.1 Introduction

The increasing need for high-speed separations that offer excellent performance for the analysis of biomolecular material for applications that require processing of large amounts of material, as in genome sequencing, has lead to a surge in conducting separations using microchip electrophoresis platforms. The attractiveness of this separation platform includes: High efficiencies on par with capillary separations; fast analysis times due to the smaller footprint; the ability to integrate sample pre-processing steps onto the separation using a single monolithic device; and smaller load volumes [1]. Other advantages include reduced effects from biased injections as well as the potential portability of such devices when integrated with the peripheral components of the system, such as power supplies and detectors. Since their introduction, several groups have performed optimization studies for microchip electrophoresis devices focusing on the sieving matrices, channel dimensions, and various other electrophoretic conditions [2-5]. A number of different electrophoretic separation analyses of biomolecules such as proteins, amino acids, PCR products, short oligonucleotides, DNA restriction fragments, and DNA sequencing ladders have been performed using a multitude of microfluidic devices [6, 7].

For the analysis of many biomolecules, the surface characteristics of the substrate material employed for the separation must be taken into careful consideration, because the surface-to-volume ratio is high indicating that solute-wall interactions can affect performance and for electrophoretic separations, the chemical composition of the wall affects the electroosmostic flow (EOF). The performance of glass-based devices can be easily predicted and controlled due to the well studied characteristics of their surfaces including the effects different end groups (i.e. Si-O-Si-C vs. Si-C) have on covalent coatings [8-10].

**Reprinted with permission from the Electrophoresis journal.*

Electroosmotic properties of various covalent, adsorbing and dynamic coatings as well as the regeneration processes required for multiple usages of glass or fused silica substrates have also been investigated [11]. As such, many of the modification procedures optimized for capillary tubes are transferable to glass-based microdevices. Employing polymer substrates as microfluidic devices has several advantages over glass-based substrates such as the wide choice of manufacturing techniques for their fabrication, minimized manufacturing constraints when producing high aspect-ratio microstructures, and the cost efficiency for mass production [12]. Given the variety of polymers available for device fabrication, many polymer-based devices have been used in their native form with varying degrees of success for microseparations [13-15]. Yet, regardless of the type of polymer employed, concerns with the material properties arise, which can hinder efficient separations, specifically analyte-substrate interactions and inconsistencies with the EOF properties [16, 17].

Groups have recently begun investigating modification procedures to stabilize and alter the EOF properties of various elastomers and thermoplastics, showing that covalent and dynamic coatings as well as ultraviolet grafting procedures provide means to modify the surface for separations [18-21]. Locascio and co-workers demonstrated the use of excimer laser ablation to modify the surface chemistry of various polymers to obtain specific EOF properties [22, 23]. In patent applications described by Amigo and McCormick of ACLARA Biosciences (5,935,401 and 6,056,860), the authors provided examples of using interpenetrating monomers or polymers into the substrate that had been machined and could be further elaborated for EOF suppression or preventing non-specific adsorption. In their examples, dimethylacrylamide (DMA) was allowed to penetrate PMMA substrates from which linear polyacrylamides could be grafted. Alternatively, absorbed coatings have been used for polycarbonate (PC), poly(methyl methacrylate) (PMMA), polystyrene (PS), and polymer-PDMS hybrid chips to stabilize the EOF for biomolecular separations [24]. However, one of the major drawbacks when developing modification chemistries is that the procedure employed

for one particular type of polymer may not necessarily transfer to another substrate with the same degree of success [16].

In the case of PMMA, research groups have been successful in separating a multitude of biomolecules including proteins, peptides, and double-stranded DNA using this material [25-28]. Although many publications have demonstrated the analysis of short oligonucleotides and double-stranded DNA fragments using PMMA devices in their native state, surface modifications have been incorporated to enhance the separation through stabilizing or altering the EOF. Muck et al. varied the EOF by fabricating PMMA devices through a UV-initiated polymerization, whereby improvements in target ion and neurotransmitter separations were demonstrated [29]. Galloway and co-workers were able to separate DNA and PCR products with a C-18 stationary phase immobilized onto an amine-modified PMMA device [30]. Dang and co-workers have reported that PMMA produced highly irreproducible separations of oligosaccharides when used in its native state, but exhibited an improved performance after incorporating various dynamic coatings [31].

Proteins are known to be notoriously hydrophobic and to adsorb to channel surfaces as a result; therefore, oligonucleotides are better suited as test samples to monitor electrophoretic performance in separation channels. In fact, attempt to separate single stranded DNA (ssDNA) fragments has been conducted in an unmodified PMMA microdevice [32]. Although PMMA proved to be a suitable substrate for fluorescence detection due to its low autofluorescence level, resolution between fragments with single base-pair differences required for DNA sequencing, which was attributed to potential analyte/wall interactions as indicated by peak tailing in the electropherograms and/or an inhomogeneous EOF. Locascio and co-workers demonstrated that the fabrication method employed, in this case hot-embossing, can produce hot-spots of functional groups, distorting the plug-like flow associated with most electrically-driven systems [33]. Later work in our group successfully demonstrated the separation of ssDNA fragments using similar dye-labeling chemistry and detection

methods employing a glass-based microdevice [34], suggesting that some modification to the surface would be necessary before PMMA could be routinely used for separation of ssDNA fragments for DNA sequencing. Shi and Anderson have reported the use of a polymeric microdevice for the separation of ssDNA fragments and successfully achieved single base-pair resolution using a polyolefin device coated with poly-dimethylacrylamide/diethylacrylamide [35]. The authors attributed their ability to achieve single base resolution primarily to their matrix selection, a 4% w/v of 5.5 MDa LPA; however, they did not investigate the significance of their coating material and whether the same resolution was achievable using the native polyolefin. The coating employed in this study required ~36 hours for preparation [36]. Data was shown for three consecutive separations of short-tandem repeats and suggested significant variations in migration times between the first and third runs when operated with a single coating.

In this work, we present a simple modification procedure to covalently coat PMMA microchannels to produce higher efficiency separations compared to the native material through reduction of analyte/wall interactions and suppression of the EOF. Based on modification procedures previously outlined in our group [37, 38], PMMA surfaces were aminated through exposure to either UV modification or lithiated diamine prior to surface coating with a linear polyacrylamide. The LPA was able to polymerize through acrylamide anchors covalently attached to the amine surfaces. Stepwise characterization of the modified surfaces was performed by measuring the EOFs and contact angles. An LIF system was then employed to detect near-IR dye-labeled ssDNA fragments in the modified PMMA channels; the results of which were compared to those obtained in native PMMA.

2.2 Materials and Methods

2.2.1 Chip Fabrication and Electrophoresis

We have reported a method for the fabrication of microchip electrophoresis devices from a nickel master using micro-replication methods [30]. The technique utilizes X-ray or UV lithography

to develop a mold master with electroplated nickel microstructures (LiGA). This nickel master is later used for the production of microdevices by hot embossing polymer substrates. For the embossing process, a PHI Precision Press model number TS-21-H-C(4A)-5 (City of Industry, CA) was used. This process consisted of heating a PMMA wafer (GE Polymershapes, Metairie, LA) to 155°C and pressing against the metal master using 1000 lbs of pressure for 3 min. The embossed device consisted of an 11 cm long serpentine channel (effective length = 9.5 cm) incorporating two opposite turns with a double T injector 500 μm long and 0.5 cm side-arm channels (see Figure 2.1). The channel dimensions were 25 μm wide and 120 μm deep. Reservoirs were created by drilling 1 mm holes into the 3 mm thick PMMA wafers. A finished device was prepared by thermally annealing a thin PMMA cover slip (0.5 mm) to a clean device by securing the assembled polymer pieces between two glass plates and heating to 107°C for 12 min in a convection oven.

A linear polyacrylamide (LPA) sieving matrix was prepared from high-viscosity-average molecular mass powder (~6 MDa) (Polysciences Inc., Warrington, PA) dissolved in 1X TTE (50 mM Tris/50 mM TAPS/2 mM EDTA) buffer with 7 M urea for electrophoretic separation of DNA fragments. The 4% (w/v) LPA was replaced between each run from the anodic end of the separation channel. The electrophoresis buffer, consisting of 1X TTE buffer, was also changed after each run. The matrix was pre-electrophoresed for 3 min at 200 V/cm through the separation channel with sample and waste reservoirs floating. DNA samples were loaded by applying 230 V/cm across the injection channel for 120 s with the anodic and cathodic buffer reservoirs floating. Electrophoretic separations were run at 130 V/cm; sample leakage into the injection cross was prevented by applying pull-back voltages of 250 and 180 V/cm to the sample and waste reservoirs, respectively. The microdevice was heated to 50°C by a Kapton flexible heater (Omega Engineering Inc., Stamford, CT) mounted to the cover slip of the microchip with a pressure sensitive adhesive; the temperature was monitored via a self-adhesive thermocouple (Omega Engineering Inc., Stamford, CT).

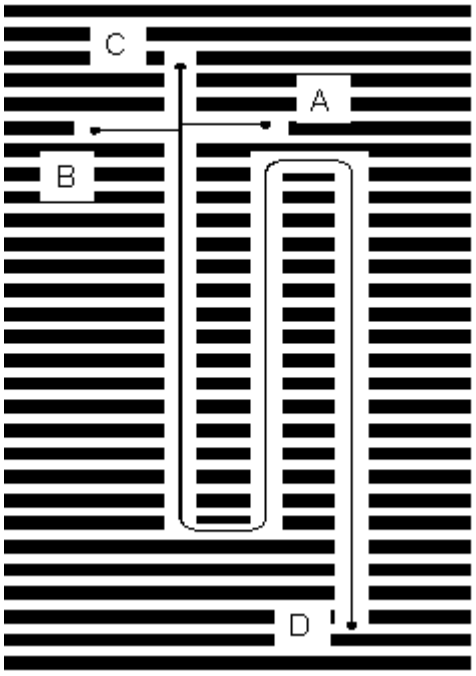

Figure 2.1 Illustration of topographical layout for the PMMA microchip. The separation microchannel was 11 cm in length with channel dimensions of 25 μm in width and 120 μm in depth. The solid rectangular structures were included into the device to aid in the thermal annealing of the PMMA cover slip to the microchip. Reservoirs were formed from 1 mm holes mechanically drilled through the 5 mm thick chip; A = sample, B= waste, C = buffer, D = anode / detection. The microchip used a "double T" injector with the distance between the side channels being 500 μm and a total injection volume of ~1.5 nL

2.2.2 Channel Surface Modification

The functional scaffold from which the LPA coating was built was produced either chemically or photo-chemically. The following procedures were used to modify PMMA microchannel surfaces. For the chemical method, the surface of the channels were aminated following a protocol outlined by Henry and co-workers [37]. This involved preparation of a N-lithiodiaminoethane solution from a reaction of 6 mmol dry ethylenediamine (Aldrich, Milwaukee, WI) with 1 mmol n-butyllithium (2.0 M in cyclohexane, Aldrich). The channels were filled with the lithiated diamine solution and allowed to incubate for 2-5 min before flushing and drying the channel under a stream of nitrogen (see Figure 2.2A). In the photochemical method, the channels were aminated by first irradiating pristine PMMA with a UV light source (15 mW/cm^2, 254 nm; ABM Series 60 exposure system, San Jose, CA) for 20

min, rinsing with 10% v/v isopropyl alcohol, and drying under a flow of N_2. After thermal annealing of a cover slip to the microdevice, the channel was filled with a buffered solution (100 mM phosphate, pH 7.0) containing N-(3-dimethylaminopropyl)-N-ethylcarbodiimide (EDC) (Sigma, St. Louis, MO) and 0.58 mmol dry ethylenediamine for at least 40 min (Figure 2.2B).

Following either amination process, the following steps were carried out (see Figure 2.2C). To provide an anchor for grafting the LPA layer, methyl acrylic acid was covalently attached to the aminated PMMA surface by exposing the amine-modified channels to a solution of 50 mM [0.8% (w/v)] EDC and 0.5 M [4.2% (v/v)] methacrylic acid for 30 min. To passivate the surface, the channels were flushed and filled with a degassed solution of 4% (w/v) acrylamide containing 0.01% (v/v) N,N,N',N'-tetramethylethylenediamine (TEMED) and 0.01% (w/v) ammonium persulfate (Sigma). This was allowed to polymerize in the channel for at least 4 h after which the channels were rinsed with water and dried.

2.2.3 Electroosomotic Flow Measurements

The EOF measurements were carried out in the microchannels described above using a method employed by Zare and co-workers [39]. Microchannels were filled entirely with a buffer of low ionic strength at an appropriate pH. In this case, the buffer was 0.5X TTE (pH = 7.4), which was selected to minimize changes in the EOF from the run conditions that were used for the DNA separations. Pt electrodes were placed into two reservoirs at opposite ends of the microchannel. An electric field was applied between the electrodes using a Spellman high voltage power supply (CZ1000R, Plainview, NY) and a baseline current was established. Upon stabilization, one reservoir was emptied and filled with a 1X TTE buffer (pH = 7.4). Pt electrodes were placed into the two reservoirs containing the high and low ionic strength buffers and an electric field was applied operated at a field strength of 150 V/cm. A strip-chart recorder (Kipp and Zonen Inc., Bohemia, NY) plotted changes in the current and it was monitored until the current reached a plateau. The time to reach this point was used to calculate

the linear velocity (cm/s). The linear velocity was then divided by the applied electric field to produce the electroosmotic mobility [cm^2 / (V s)]; the EOF was averaged over five consecutive runs.

2.2.4 Contact Angle Measurements

Sessile drop water contact angle measurements were conducted with a VCA 2000 Contact Angle System (VCA, Billerica, MA). A single drop of 18 MΩ•cm water, (~2 μL) was placed onto the polymer surface via a syringe, at which time the right and left contact angles were immediately measured. The contact angle values were calculated using the manufacturer's software. Each value reported represents an average of 5 drops of water in several locations on the investigated polymer surface.

2.2.5 Instrumentation

We obtained fluorescence intensity data using an in-house constructed near-IR laser-induced fluorescence system shown in Figure 2.3. The excitation source consisted of a 780 nm diode laser (Thorlabs model LT024MD/MF, Newton, NJ) powered by a custom built power supply with tunable output power. The laser was filtered by a bandpass filter (CWL = 780 nm, Omega Optical, Brattleboro, VT) before being directed through a dichroic mirror to a reflective mirror (>99% reflectance) after which the light was focused onto the channel using a 40x microscope objective (Nikon, Natick, MA). To position the microdevice with respect to the laser beam, an X-Y-Z translational stage (Newport, Irvine, CA) was utilized. The resulting emission was then collected through an objective, routed again through the dichroic mirror and filtered through a longpass filter (CWL = 800 nm, Omega Optical, Brattleboro, VT) and a bandpass filter (CWL = 820 nm, Omega Optical, Brattleboro, VT). The filtered fluorescence emission was ultimately focused onto a single photon avalanche diode (SPAD, PicoQuant model SPCM 200B, Berlin, Germany). The LIF signal was acquired on a personal computer equipped with an I/O connector board (National Instruments model CB-68LP, Austin, TX) and a pulse converter (IBH model TB-01, Glasgow, UK). Data acquisition software was written in LabView.

2.2.6 Sample Preparation

The labeling dye, IRD800 (Li-COR Biotechnology, Lincoln, NE), was used in these experiments; the dye possessed absorption and emission wavelengths of 780 and 810 nm, respectively. The acid form of the dye was converted to a succinimidyl ester prior to covalently linking it to the 5' end of an M13 forward (-29) sequencing primer (17mer) through a C6 amino linker; the dye-labeled primer was purified by reverse-phase HPLC. Primer samples were concentrated from lyophilized product in distilled water and later diluted in the appropriate buffer for sample analysis.

2.3 Results and Discussion

2.3.1 Manipulation of Electroosmotic Flow in PMMA Microdevices

Previously reported procedures for modifying PMMA substrates have provided a basis for covalently attaching a polymer coating onto the wall of PMMA to stabilize or suppress the EOF and minimize potential analyte/wall interactions. One method (see Figure 2.2A) relies upon reaction of the methyl ester functional groups in the PMMA backbone with N-lithioethylenediamine to produce an amide linkage and creating an NH_2-terminated PMMA surface, which has a surface coverage of ~5 nmol cm^{-2} [37]. EOF measurements obtained for pristine and NH_2-terminated PMMA were found to be 2.95 (±0.95) x 10^{-4} $cm^2/V{\cdot}s$ and -1.46 (±0.14) x 10^{-4} $cm^2/V{\cdot}s$, respectively, agreeing with previously obtained measurements [37]. The negative value on the EOF for the amine-terminated surface indicates that the EOF is reversed in direction (cathode to anode). The EOF measurements for this and each subsequent modification step are summarized in Table 2.1.

Alternatively, the PMMA was functionalized with terminal amine groups through UV activation and subsequent reaction with ethylenediamine (see Figure 2.2B). Exposing PMMA to UV light produces a carboxylate group from the methyl esters found on native PMMA due to a photo-induced oxidation reaction. The reader is referred to Table 2.1 for a side by side comparison of EOF measurements for both UV activated PMMA surfaces and the chemically activated PMMA surfaces.

Figure 2.2 Scheme showing the modification procedures used to terminate PMMA surfaces with amine functional groups by (A) reaction with a lithiated diamine solution or (B) exposure to UV radiation proceeded by EDC coupling of ethylenediamine to the carboxylated surface**.** (C) Surface modification scheme for grafting PMMA surfaces with LPA. The amine-terminated PMMA is first reacted with methacrylic acid in the presence of EDC to covalently bind it to the surface. These groups then serve as a scaffold for subsequent polymerization of acrylamide after initiation with APS and TEMED.

A

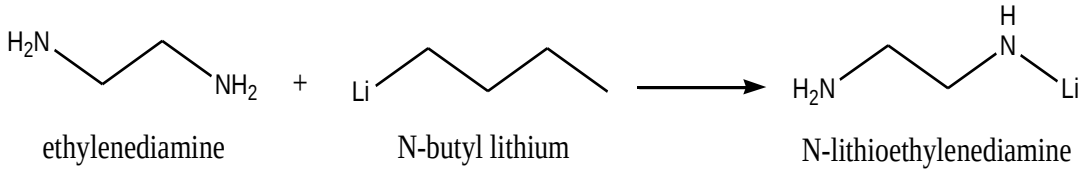

ethylenediamine N-butyl lithium N-lithioethylenediamine

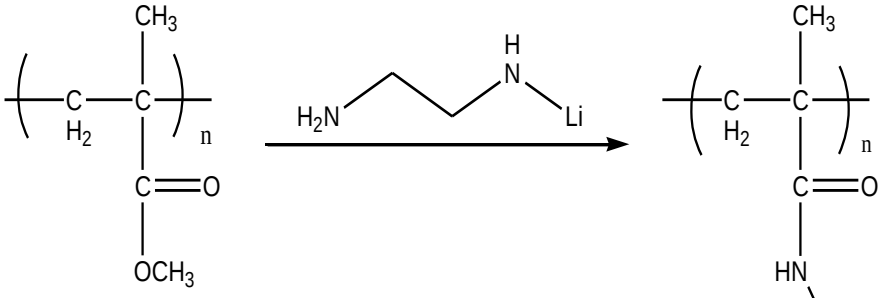

PMMA backbone

Amine-terminated PMMA

B

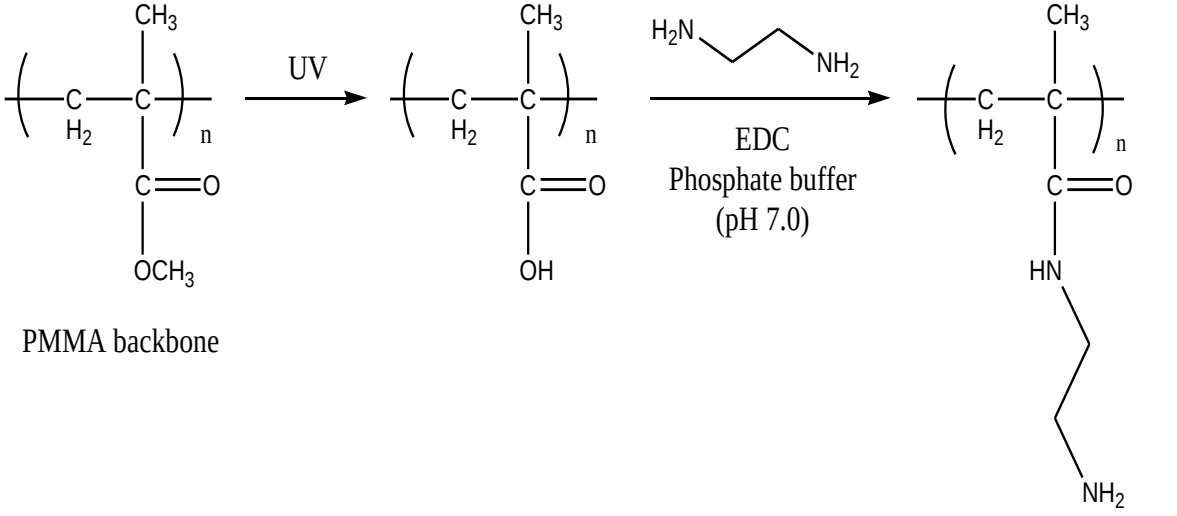

PMMA backbone

Amine-terminated PMMA

Figure 2.2 Continued

C

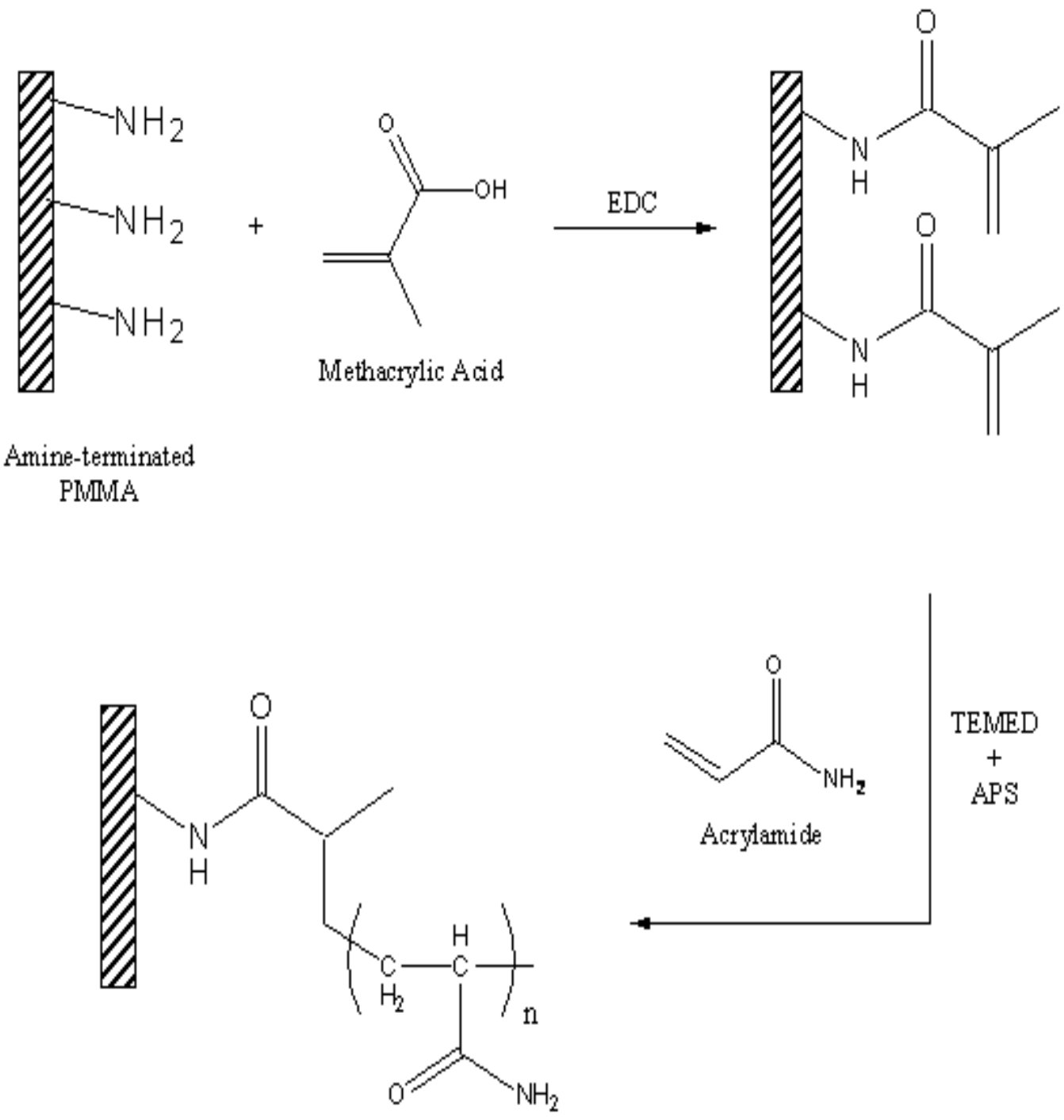

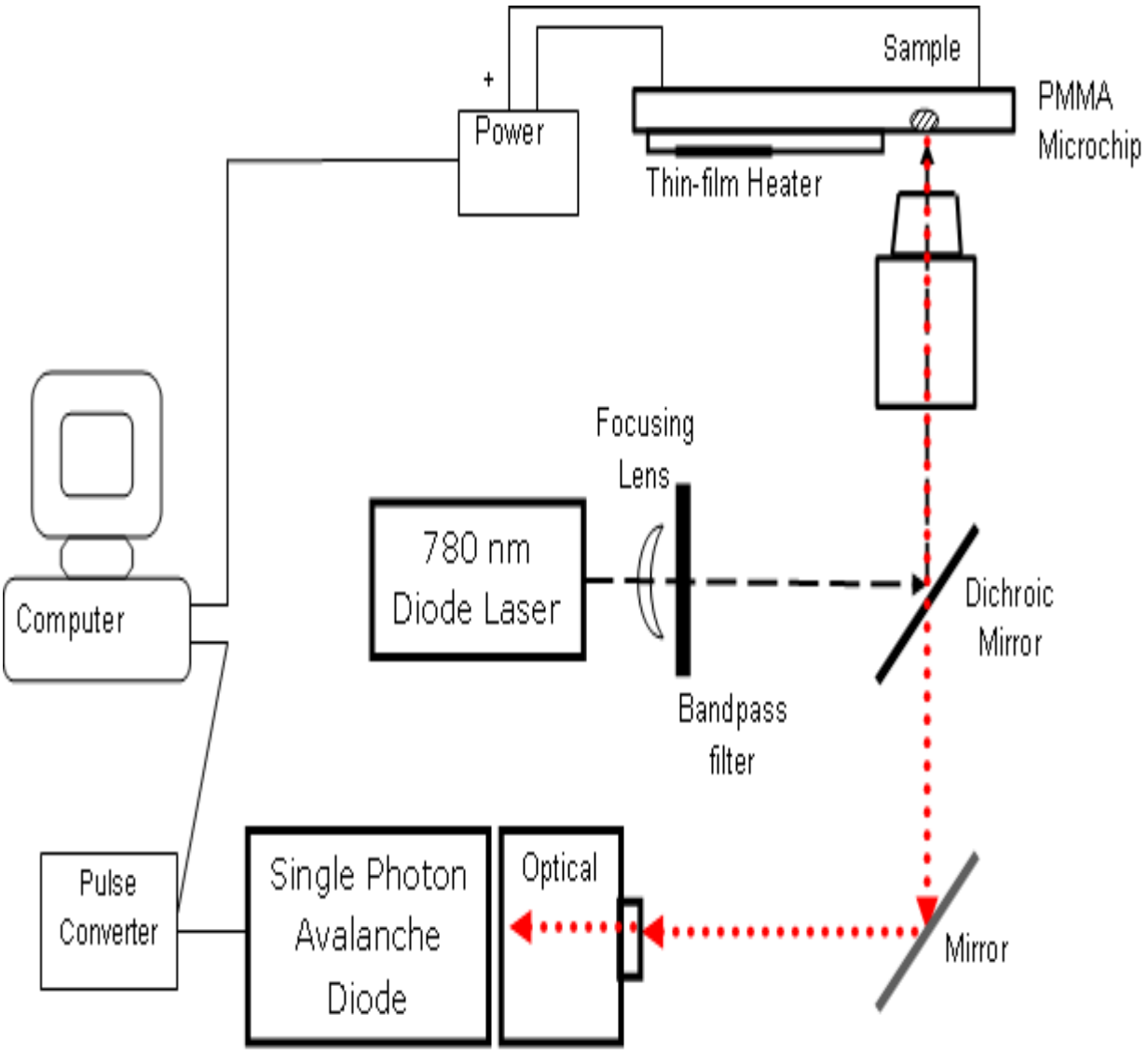

Figure 2.3 Schematic diagram of the near-IR laser-induced fluorescence system, which provided an excitation wavelength of 780 nm

Reacting the carboxyl groups with ethylenediamine in the presence of EDC produces an amine-terminated surface. In this method, the number of amine sites is governed by the dose of UV light, which has been shown to produce carboxylic acids with a surface coverage of ~1.3 nmol cm^{-2} [41]. EOF measurements for these amine-terminated surfaces were -1.34 (±0.21) x 10^{-4} $cm^2/V{\cdot}s$, agreeing with that obtained for aminated PMMA produced via activation with the lithiated diamine.

Table 2.1 Electroosmotic flow (EOF) values for PMMA and PMMA modified with an LPA layer attached via a chemical or photochemical procedure. These measurements were conducted on three different PMMA chips containing the indicated surface coating and therefore, the standard deviations shown represent inter-chip variability in the EOF.

Terminating Groups	EOF (cm^2/Vs) (Chemical)	EOF (cm^2/Vs) (Photochemical)
Pristine (unmodified) PMMA	$2.95 \pm 0.95 \times 10^{-4}$	————
UV-activated PMMA	————	$4.43 \pm 0.58 \times 10^{-4}$
Amine-terminated PMMA	$-1.46 \pm 0.14 \times 10^{-4}$	$-1.34 \pm 0.21 \times 10^{-4}$
Methyl acrylamide-terminated PMMA	$1.41 \pm 0.16 \times 10^{-4}$	$1.49 \pm 0.11 \times 10^{-4}$
LPA-coated PMMA	$3.36 \pm 0.13 \times 10^{-5}$	$3.27 \pm 0.15 \times 10^{-5}$

Both amine-terminated surfaces were subsequently reacted with ~50 mM methacrylic acid. In the presence of an excess of EDC [N-(3-Dimethylaminopropyl)-N'-ethylcarbodiimide], the carboxyl groups of methacrylic acid react with the amine groups at the PMMA surface to form an amide bond. Following this modification, the EOF reversed in direction compared to the amine-terminated surface, with a value of 1.41 (±0.16) x 10^{-4} cm^2/V·s and 1.49 (±0.11) x 10^{-4} cm^2/V·s for the chemical and photochemical modifications, respectively. The resulting methacrylamide terminal groups at the surface serve as a scaffold for the next reaction.

Finally, polymerization of a 4% (v/v) acrylamide solution was initiated through the addition of TEMED and 10% APS and allowed to incubate within the methacrylamide-modified microchannels. The radical polymerization process formed covalent bonds between the methacrylamide groups at the channel surface and the acrylamide in solution. The incubation time was extended to ensure proper chain formation for coating the channel wall in its entirety to allow maximum EOF suppression. The LPA-coating reduced the EOF to 3.36 (±0.13) x 10^{-5} cm^2/V·s and 3.27 (±0.15) x 10^{-5} cm^2/V·s for the chemical and photochemical methods, respectively. However, we noticed that these EOF values were stable for extended periods of time and large number of electrophoretic runs (> 20), indicating the

stability of the underlying linkage chemistry. While the EOF values reported above are still about an order of magnitude larger than LPA-coated capillaries [42], after storage of these microchips in buffer (pH ~8) for > 3 weeks, no significant changes in the EOF were observed. The stability of these coatings are comparable to that observed for a Si-C linkage in a capillary, which showed an EOF of 5.21 x 10^{-6} $cm^2/V \cdot s$ [42] after 30 days of storage in pH=8 buffer compared to a Si-O-Si-C linkage, which produced an EOF of 1.04 x 10^{-4} $cm^2/V \cdot s$ after the same storage conditions.

In order to determine the stability of the LPA layer grafted to the functionalized PMMA surface, the EOF was monitored as a function of electrophoresis run number when the device was electrophoresed (15 min run time at E = 150 V/cm) with the running buffer (no sieving gel) used for the ssDNA separations (1X TTE, pH = 8.0 with 7 M urea). The results indicated that the EOF remained constant over > 20 runs with a value that was determined to be 3.2 x 10^{-4} cm^2 V^{-1} s^{-1} for run 1 and 3.6 x 10^{-4} cm^2 V^{-1} s^{-1} for run 20. These results indicate the stability of the LPA coating on the PMMA surface using the linkage chemistry adopted herein when operated under relatively high field strengths.

2.3.2 Contact Angle of Modified Surfaces

During the modification steps, sessile drop water contact angle measurements were taken on the native and modified PMMA as a simple monitor of the changes induced on the surface as a result of the modification procedures. The contact angles changed from 69 ± 2° for pristine PMMA to 32 ± 3° after termination with amine groups, agreeing with values reported in the literature [37]. For the UV-modified PMMA surfaces, the contact angle was 51 ± 2° after rinsing with ddH_2O and changed to 36 ± 4° after modification with the diamine. The value of the UV-modified PMMA differs from those reported previously (i.e., 24°); however, those results were obtained prior to rinsing the surface with IPA to remove low molecular weight polymers formed during the photochemical modification [41]. The value of the methacrylamide-terminated PMMA surfaces increased to 80 ± 3° and 82 ± 2° for both

the chemical and photochemical methods, respectively. In either case, after polymerization forming the linear polyacrylamide onto these surfaces, the contact angle decreased to 41 ± 3°. In all instances, there were no differences observed for the left and right advancing contact angle measurements.

2.3.3 Performance of the Modified PMMA Microdevice

To determine what effects coating the PMMA channel had on the electrophoretic separation of single-stranded DNA (ssDNA) using an LPA sieving matrix (4%), analyte migration time and the efficiency (plates per meter) obtained for electrophoretic runs on native and PMMA-modified surfaces were monitored. As a model, an IRD800-labeled oligonucleotide (17mer) was used. One of the earlier problems encountered when using pristine PMMA for electrophoresis of ssDNA was that variances in the EOF were significant, contributing to increased run-to-run variability in terms of analyte mobility. For evaluation, 20 sequential runs were completed in both pristine and LPA-coated PMMA (chemical and photochemical) devices. As seen in Figure 2.4, the pristine channel resulted in an average migration time of 258 (±14) s when averaged over the 20 runs. The average plate numbers generated over these 20 runs was 3.76 x 10^5 plates/m, comparable to results reported earlier [32].

In comparison, the migration time observed for the 17mer using the LPA-coated PMMA devices resulted in more stable results over the entire 20 runs. The chemically modified devices gave an average migration time of 227 (±8) s, indicating not only faster migration of the dye-labeled oligonucleotides compared to pristine PMMA due in part to a lower EOF, but also a much lower standard deviation between runs. The plate numbers generated for the separations in the coated devices were 1.15 x 10^6 plates/m, comparable in magnitude to those obtained in fused silica capillaries possessing an LPA-coating [43]. For the microdevices coated with LPA through an UV-initiated modification, the average migration time was 225 (±6) s over the 20 runs, comparable to those obtained with the device coated through the chemical method, and the average efficiency was 9.74 x 10^5 plates/m.

Inspection of the data shown in Figure 2.4 indicates that the migration times for the pristine device showed incremental decreases until after the 10^{th} run, in which the migration times remained fairly constant with a value similar to those obtained for the LPA-coated devices. When incorporating LPA as a coating material in silica capillaries, it is common to see degradation of the coating after multiple runs due to hydrolysis at the surface assisted by the application of a high electric field [44, 45]. However, we do not believe that the observed trends in the migration times for the LPA-coated devices was suggestive of coating degradation because the migration times remained rather constant for all 20 runs. Rather, we suspect that passive adsorption of the sieving matrix, LPA, onto the native PMMA walls resulted in reductions in the EOF to a level approaching that of the LPA-coated devices indicating that the LPA matrix exhibits some potential to dynamically coat PMMA surfaces [45]. Interestingly, the changes in plate numbers for both the pristine and LPA-coated devices closely resembled the changes in the migration times (see Figure 4), but in an inverse fashion. The plate numbers for the LPA-coated devices were rather constant over the 20 runs; for the pristine device, the plate numbers were low in the early runs and showed incremental increases until after the 10^{th} run in which it remained fairly constant with a value somewhat similar to that observed for the migration times.

Furthermore, former graduate student from the Soper research group, Dr. Shawn Llopis, using the LPA-coated PMMA chips, was able to obtain single base resolution of ssDNA that otherwise co-migrated in unmodified PMMA chips. This DNA sequencing work is briefly described below. In previous attempts to separate ssDNAs in a PMMA microdevice, it was not possible to achieve single base resolution as required for DNA sequencing [32]. We suspected that changes in the surface charge density on the walls of pristine PMMA due to either analyte adsorption or inhomogeneities in the surface charged groups contributed to low plate number generation. When separating DNA fragments containing single base-pair differences as required for sequencing, the effect of eddy migration

resulting from residual zeta-potential discontinuities can be significant, degrading resolution [44].

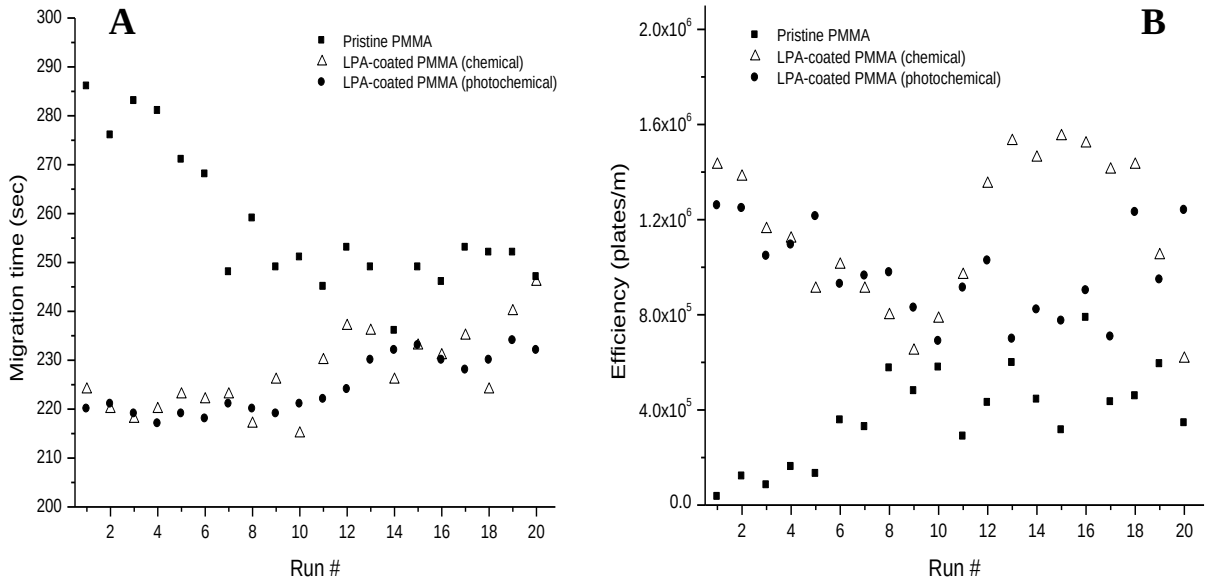

Figure 2.4 Electrophoretic analyses of IRD800-labeled oligonucleotides (17mer) electrophoresed at 115 V/cm in both pristine PMMA and LPA-coated PMMA microchips and their effects on migration times (A) and plate numbers (B) for 20 runs on the same devices**.**

By passivating the PMMA surfaces with LPA, the EOF within the channels was significantly reduced (see Table 2.1) suggesting that peak dispersion due to differences in the EOF would be reduced [21]. To benchmark the performance characteristics of this coating procedure, Dr. Llopis compared separations of IRD800-labeled T-tracts, prepared using dye-primer chemistry and Sanger cycle sequencing, in 4% LPA using both pristine and LPA-passivated PMMA microchannels.

Using a modified procedure of that outlined for the Amersham 7-deaza primer cycle sequencing kit she prepared Sanger sequencing reactions using an M13mp18 single-stranded DNA template [40]. Thermal cycling was carried out in a Genius series 96-well thermal cycler (Techne Inc., Minneapolis, MN) using the following thermal cycling conditions (40 cycles): (i) 92 °C for 2 s; (ii) 55 °C for 30 s; (iii) 72 °C for 60 s, followed by a final extension step at 72 °C for 7 min. Prior to use, excess salts, enzymes, dNTPs and ddNTPs were removed from the sample by a solid-phase reversible

immobilization (SPRI) technique incorporating CleanSEQ^{TM} magnetic particles (Agencourt, Beverly, MA).

Under optimized conditions, ssDNA fragments were electrokinetically injected into the separation channel of a pristine PMMA device and separated at 115 V/cm in a 4% LPA matrix (50° C). This run yielded plate numbers of 3.39 x 10^5 plates/m for base 122 and resolution values of 0.24 between bases 102 and 104 and 0.47 between bases 364 and 370 (data not shown). However, fragments with single base-pair differences co-migrated. In comparison, the same fragments were loaded onto a channel coated with LPA (chemical) and the T-terminated ladder was electrophoresed using conditions similar to those used for the pristine PMMA. For this separation, an efficiency of 3.91 x 10^5 plates/m for base 122 was calculated and the resolution values of 0.37 between bases 102 and 104 and 0.64 between bases 364 and 370. Also, it was observed in that electropherogram (not shown) that single base resolution with resolution values of 0.18 and 0.21, were observed for specific bases 199, 200 and 208, 209, respectively. This evolution was realized when an LPA modified PMMA chip was used.

While the results are promising, there are several reasons why we are still limited in consistently achieving electrophoretic separations with single base resolution for this device and coating procedure. During our optimization studies, we focused predominantly on using a reduction in the EOF as our primary metric for evaluating performance enhancement. There are other factors that are important as well for optimizing the electrophoretic performance required for sequencing, such as the physical and chemical nature of the coating material. For example, the thickness of the polymer coating may play an integral role in determining electrophoretic performance in terms of plate numbers. It has been noted that when the polymer coating becomes too thick, molecules may partition into and out of the coating resulting in reduced electrophoretic performance [46]. In striving for maximum reductions in the EOF using our coating procedure, we may have polymerized the LPA

layer past its optimal range. The nature of the sieving matrix also plays an integral role in determining resolution, especially for microchips that use short separation columns. Matrices that offer high selectivity can improve electrophoretic resolution and higher selectivity capabilities, such as the newly developed “nanogels” [47, 48].

2.4 Conclusions

To fully realize the potential of polymer microfluidic devices for routine high throughput separation applications, the reliability of the devices must be improved in terms of their walls’ chemical composition. To this end, a novel procedure was discussed that can covalently anchor an LPA coating to the PMMA wall to stabilize and suppress the EOF of PMMA as well as reduce potential solute-wall interactions. It was found that PMMA devices modified using UV or chemically grafted LPAs to the PMMA substrate demonstrated reliable performance. In the case of the UV activation method, a simple 15 min exposure with broadband UV radiation followed by a coupling reaction with methacrylic acid and a subsequent LPA polymerization step was required to produce the coating. Using the coatings described herein, better electrophoretic performances were demonstrated for LPA-coated PMMA chips in cases where the pristine device could not. In Chapters 3 and 4 we considered dynamic coatings using methyl hydroxyethyl cellulose (MHEC) for suppressing EOF and improving the separation performance during separations.

2.5 References

[1] Schmalzing, D., Adourian, A., Koutny, L., Ziaugra, L., *et al.*, *Analytical Chemistry* 1998, *70*, 2303-310.

[2] Zhang, C. X., Manz, A., *Analytical Chemistry* 2001, *73*, 2656-2662.

[3] Vazquez, M., McKinley, G., Mitnik, L., Desmarais, S., *et al.*, *Analytical Chemistry* 2002, *74*, 1952-1961.

[4] Landers, J. P., *Analytical Chemistry* 2003, *75*, 2919-2927.

[5] Liu, S. R., Shi, Y. N., Ja, W. W., Mathies, R. A., *Analytical Chemistry* 1999, *71*, 566-573.

[6] Kan, C. W., Fredlake, C. P., Doherty, E. A. S., Barron, A. E., *Electrophoresis* 2004, *25*, 3564-3588.

[7] Dolnik, V., Liu, S. R., Jovanovich, S., *Electrophoresis* 2000, *21*, 41-54.

[8] Cobb, K. A., Dolnik, V., Novotny, M., *Analytical Chemistry* 1990, *62*, 2478-2483.

[9] Kohr, J., Engelhardt, H., *J. Chromatogr. A* 1993, *652*, 309-316.

[10] Cifuentes, A., Canalejas, P., Diez-Masa, J. C., *J. Chromatogr. A* 1999, *830*, 423-438.

[11] Horvath, J., Dolnik, V., *Electrophoresis* 2001, *22*, 644-655.

[12] Soper, S. A., Ford, S. M., Qi, S., McCarley, R. L., *et al.*, *Analytical Chemistry* 2000, *72*, 642A-651A.

[13] Liu, Y. J., Ganser, D., Schneider, A., Liu, R., *et al.*, *Analytical Chemistry* 2001, *73*, 4196-4201.

[14] Sia, S. K., Whitesides, G. M., *Electrophoresis* 2003, *24*, 3563-3576.

[15] Fiorini, G. S., Chiu, D. T., *Biotechniques* 2005, *38*, 429-446.

[16] Belder, D., Ludwig, M., *Electrophoresis* 2003, *24*, 3595-3606.

[17] Herr, A. E., Molho, J. I., Santiago, J. G., Mungal, M. G., *et al.*, *Analytical Chemistry* 2000, *72*, 1053-1057.

[18] Makamba, H., Kim, J. H., Lim, K., Park, N., Hahn, J. H., *Electrophoresis* 2003, *24*, 3607-3619.

[19] Liu, Y., Fanguy, J. C., Bledsoe, J. M., Henry, C. S., *Analytical Chemistry* 2000, *72*, 5939-5944.

[20] Hu, S. W., Ren, X. Q., Bachman, M., Sims, C. E., *et al.*, *Analytical Chemistry* 2002, *74*, 4117-4123.

[21] Hu, S., Ren, X., Bachman, M., Sims, C. E., *Electrophoresis* 2003, *24*, 3679-3688.

[22] Johnson, T. J., Ross, D., Gaitan, M., Locascio, L. E., *Analytical Chemistry* 2001, *73*, 3656-3661.

[23] Pugmire, D. L., Waddell, E. A., Haasch, R., Tarlov, M. J., Locascio, E., *Analytical Chemistry* 2002, *74*, 871-878.

[24] Doherty, E. A. S., Meagher, R. J., Albarghouthi, M. N., Barron, A. E., *Electrophoresis* 2003, *24*, 34-54.

[25] Chen, Y. H., Chen, S. H., *Electrophoresis* 2000, *21*, 165-170.

[26] Wainright, A., Nguyen, U. T., Bjornson, T., Boone, T. D., *Electrophoresis* 2003, *24*, 3784-3792.

[27] Herr, A. E., Molho, J. I., Drouvalakis, K. A., Mikkelsen, J. C., *et al.*, *Analytical Chemistry* 2003, *75*, 1180-1187.

[28] Abad-Villar, E. M., Tanyanyiwa, J., Fernandez-Abedul, M. T., Costa-Garcia, A., Hauser, P. C., *Analytical Chemistry* 2004, *76*, 1282-1288.

[29] Muck, A., Wang, J., Jacobs, M., Chen, G., *et al.*, *Analytical Chemistry* 2004, *76*, 2290-2297.

[30] Galloway, M., Stryjewski, W., Henry, A., Ford, S. M., *et al.*, *Analytical Chemistry* 2002, *74*, 2407-2415.

[31] Dang, F., Zhang, L., Hagiwara, H., Mishina, Y., Baba, Y., *Electrophoresis* 2003, *24*, 714-721.

[32] Llopis, S. D., Stryjewski, W., Soper, S. A., *Electrophoresis* 2004, *25*, 3810-3819.

[33] Johnson, T. J., Waddell, E. A., Kramer, G. W., Locascio, L. E., *Appl. Surf. Sci.* 2001, *181*, 149-159.

[34] Zhu, L., Stryjewski, W. J., Soper, S. A., *Anal. Biochem.* 2004, *330*, 206-218.

[35] Shi, Y. N., Anderson, R. C., *Electrophoresis* 2003, *24*, 3371-3377.

[36] Sassi, A. P., Barron, A., AlonsoAmigo, M. G., Hion, D. Y., *et al.*, *Electrophoresis* 1996, *17*, 1460-1469.

[37] Henry, A. C., Tutt, T. J., Galloway, M., Davidson, Y. Y., *et al.*, *Analytical Chemistry* 2000, *72*, 5331-5337.

[38] Soper, S. A., Henry, A. C., Vaidya, B., Galloway, M., *et al.*, *Analytica Chimica Acta* 2002, *470*, 87-99.

[39] Huang, X. H., Gordon, M. J., Zare, R. N., *Analytical Chemistry* 1988, *60*, 1837-1838.

[40] Lassiter, S. J., Stryjewski, W., Legendre, B. J., Erdmann, R., *et al.*, *Analytical Chemistry* 2000, *72*, 5373-5382.

[41] Wei, S. Y., Vaidya, B., Patel, A. B., Soper, S. A., McCarley, R. L., *J. Phys. Chem. B* 2005, *109*, 16988-16996.

[42] Nakatani, M., Skibukawa, A., Nakagawa, T., *J. Chromatogr. A* 1994, *661*, 315-321.

[43] Thomas, G., Sinville, R., Sutton, S., Farquar, H., *et al.*, *Electrophoresis* 2004, *25*, 1668-1677.

[44] Dolnik, V., Xu, D., Yadav, A., Bashkin, J., *et al.*, *J. Microcolumn Sep.* 1998, *10*, 175-184.

[45] Doherty, E. A. S., Berglund, K. D., Buchholz, B. A., Kourkine, I. V., *et al.*, *Electrophoresis* 2002, *23*, 2766-2776.

[46] Zhao, Z. X., Malik, A., Lee, M. L., *Analytical Chemistry* 1993, *65*, 2747-2752.

3 Generating High Peak Capacity 2-D Maps of Complex Proteomes Using Microchip Electrophoresis*

3.1 Introduction

There are many applications which require the ability to track protein expression for a large panel of markers in a given proteome such as that required for the discovery of new biomarkers that can be used for the diagnosis and/or prognosis of diseases [1]. A common method for large-scale protein analysis involves the use of two-dimensional electrophoresis, which commonly employs an isoelectric focusing (IEF) dimension, which separates the proteins based upon their isoelectric point (pI), followed by sodium dodecyl sulfate polyacrylamide gel electrophoresis (SDS-PAGE), which sorts proteins through differences in their molecular weights. To determine the identity of the various proteins comprising these 2-D maps, the spots can be subjected to high resolution MS/MS analysis directly (top-down proteomics) or digested via proteolytic enzymes followed by MS analysis (bottom-up proteomics) [2]. High-resolution 2-D gel electrophoresis is not restricted to discovery-based projects, but can also be used for generating fingerprints for determining phenotypes from certain biological samples [3-6].

A biological sample that holds great promise for clinical diagnostics is blood serum, which is the soluble component of blood following clotting. While the exact number of unique protein components comprising different serum proteomes is difficult to ascertain due to the vast number of sources of proteins to this biological fluid as well as the large number of post-translational modifications and splice variants they can undergo, it has been estimated that the human serum proteome can contain >10,550,000 different protein constituents [7]. The complexity is compounded by the large dynamic range; nearly 10^9 to 10^{10} with albumins making up nearly 55% by weight. Serum proteins can originate from necrotic or apoptotic cells, active secretion or leakage from intact cells or tissues, endogenous proteins such as immunoglobulins that have active functions in the serum, or

*Reprinted with permission from the Electrophoresis journal.

foreign proteins produced by infectious organisms. Several different serum-based proteomic projects have been undertaken in a variety of organisms, such as human [8], mouse [9] and horse [10].

The wide range of protein components that can potentially exist in complex biological samples, such as mammalian serum, makes it difficult to analyze these types of materials using one-dimensional (1-D) separations due to the limited peak capacity afforded by these separation platforms. While interesting advancements have been reported using 1-D SDS-PAGE [11], the total number of proteins contained in the serum proteome alone demands peak capacities well beyond that achievable by 1-D formats.

Giddings recognized that the combination of two different separation techniques can provide a significantly higher peak capacity, P, than the individual 1-D mechanisms as long as the dimensions comprising the multi-dimensional separation are orthogonal [12]. If the separation mechanisms of the multi-dimensional separation are orthogonal, the number of resolved components is given by the product of the peak capacity contained within the individual separation dimensions [13]. For example, using 2-D electrophoresis consisting of IEF and SDS-PAGE, 3,700 spots were identified from the human serum proteome following cleanup using affinity chromatography or size exclusion chromatography to remove the highly abundant albumin proteins [8].

While IEF/SDS-PAGE continues to be the workhorse for many proteomic projects, it does have some shortcomings [14]. IEF/SDS-PAGE is a laborious and time-consuming process involving extensive gel pouring and pH gradient formation as well as long operational times (~24 h) to generate the required 2-D map. In addition, following the separation, protein bands require staining for visualization and subsequent band extraction from the gel for follow-up identification purposes, which can result in sample loss [15, 16]. Also, conventional IEF/SDS-PAGE tends to exclude important membrane proteins by the IEF buffers due to their poor solubility in these buffering systems [17, 18]. Furthermore, the staining and visualization techniques associated with IEF/SDS-PAGE show poor

mass detection limits; important regulatory proteins, which are typically low in abundance, are often not detected during analysis [19]. Finally, IEF is not compatible with covalent fluorescence labeling that can improve the limit of detection for low abundant proteins [20, 21].

Because of the shortcomings associated with 2-D IEF/SDS-PAGE, several groups have demonstrated the utility of capillary-based 2-D separations. For the analysis of real protein samples, researchers have used capillary sieving electrophoresis coupled to micellar electrokinetic capillary chromatography [3, 22, 23], size-exclusion liquid chromatography and reversed-phase liquid chromatography [24] or nano-reverse phase liquid chromatography coupled to strong cation-exchange chromatography [25].

While the capillary-based multi-dimensional separation reports have demonstrated success in reducing electrophoresis development time and eliminate such tasks as gel pouring, increasing demands on proteomic studies have necessitated the need to further reduce electrophoresis development times, generate higher throughput by performing multiple separations in parallel, process smaller samples and integrate front-end processing to the 2-D separation. These demands have spawned the area of microchip electrophoresis (μ-CE), which is viewed as attractive alternative to their capillary counterparts.

Recently, several groups have reported on μ-CE 2-D separations for the analysis of model proteins using IEF and capillary zone electrophoresis (CZE) as the separation mechanisms [26, 27] or IEF coupled to capillary gel electrophoresis (CGE) [28-31]. We have recently reported on a polymer-based microchip made in PMMA for the 2-D separation of 10 model proteins labeled with AlexaFluor 633, which contained an isothiocyanate group appropriate for labeling the proteins' primary amine groups [32]. In that study, SDS-PAGE (L_{eff} = 30 mm) was used in the first dimension and micellar capillary electrophoresis (MEKC, L_{eff} = 10 mm) was used in the second dimension. Because a high degree of retention correlation between dimensions can reduce a 2-D separation to what is, in fact, a 1-

D separation [33], the information content of any multi-dimensional system is the sum of the mean information content of each individual dimension minus the cross-information [34]. Therefore, evaluating cross-information through a quantitative analysis is important for gauging the utility of a particular multi-dimensional separation [33]. Calculations were employed to quantitatively determine the degree of orthogonality between the SDS-PAGE and MEKC separation dimensions, which was found to be 77%, generating a peak capacity of ~1,000 in a 12 min development time [32].

Unfortunately, many of the μ-CE examples to-date has focused primarily on demonstrating proof-of-concept of the multi-dimensional separation using model systems, which have limited the number of components analyzed with the constituents present in similar concentrations, both of which do not represent "true" biological samples. To address this issue, Mathies and co-workers [35] recently reported a microchip differential gel electrophoretic (DIGE) separation in which *E. coli* proteins were separated by coupling an IEF dimension with parallel DIGE channels. Unfortunately, the authors did not report the peak capacity of their system, but stated the absence of SDS in the second dimension limited the orthogonality of the 2-D separation.

The peak capacity using a microchip configured in a 2-D separation format has been reported by Ramsey's group [36]. In that work, the 2-D separation was obtained for tryptic digests of bovine serum albumin. Also, Jikun Liu *et al.* [37] has reported a 2-D microchip system combining IEF and parallel SDS gel electrophoresis in which proteins from an *E. coli* cell lysate were analyzed. As a measure of reproducibility, the authors calculated the average relative standard deviation (RSD) in peak migration times for 11 selected peaks and found this reproducibility metric to be 4.1%.

In this work, we report the use of a polymer-based microchip for 2-D profiling of fetal calf serum (FCS) proteins within 30 min with exquisite peak capacities using SDS μ-CGE in the first dimension and μ-MEKC in the second dimension. Our readout strategy relied upon the use of laser-induced fluorescence (LIF), which was accomplished by labeling the FCS proteins covalently with a

thiol-reactive AlexaFluor 633 dye prior to the µ-CE 2-D separation. The SDS µ-CGE was performed using L_{eff} = 60 mm while the µ-MEKC separation utilized L_{eff} = 50 mm. We validated and compared our µ-CE separation results of the FCS proteins to conventional 2-D IEF/SDS-PAGE using the appropriate separation performance metrics.

3.2 Materials and Methods

3.2.1 Chip Fabrication

PMMA was selected as the µ-CE substrate because of its suitable physiochemical properties for this application, such as minimal non-specific adsorption artifacts and low levels of autofluorescence, improving the detection limits for ultra-sensitive fluorescence detection [38]. Microchips were made according to procedures described previously [39]. Briefly, microstructures were micromilled into a brass plate (0.25" thick alloy 353 engravers brass, McMaster-Carr, Atlanta, GA, USA) using a Kern MMP 2522 micromilling machine (KERN Mikro-und Feinwerktechnik GmbH & Co., Germany). Once fabricated, the mold master produced PMMA replicates using hot-embossing.

Hot-embossing required heating the molding tool to 160^{o}C and pressed into the PMMA plate with a pressure of 1,100 psi for ~410 s using a PHI Precision Press (PHI-Tulip, City of Industry, CA, USA). Following embossing, the PMMA substrate was cooled to room temperature and removed from the molding die. The embossed PMMA substrate was cleaned with 50% isopropanol in ultrapure water. Finally, a PMMA cover plate (0.125 mm) was thermal fusion bonded to the substrate by heating in a temperature programmable furnace to 107^{o}C, slightly above the Tg of PMMA. Figure 3.1A shows a topographical layout of the microchip used in this work.

All channels were 50 µm deep and 20 µm wide. Buffer, sample or waste containment reservoirs are shown in Figure 3.1A where letters A to F in the figure represent 1.5 mm diameter solution reservoirs on the PMMA microchip.

3.2.2 LIF Detection, Power Supply and Data Analysis

Fluorescence detection was accomplished using an in-house constructed LIF system. A schematic diagram of this detection system is shown in Figure 3.1B. Details of the detector operation and ancillary components are reported elsewhere [38]. Programmed high-voltages were applied to the solution reservoirs (A to F, see Figure 3.1A) of the microchip with six independently-controlled high-voltage power supplies. The software for LIF data acquisition and control of the power supplies was created using LabVIEW (National Instruments, Austin, TX, USA). Raw 2-D electropherograms were converted to 2-D images and then to three-dimensional (3-D) landscape representations (see Results and Discussion) by dividing the LIF signals from successive runs for each MEKC cycle and plotting the electropherogram at the corresponding cycle on the SDS μ-CGE axis. This procedure was performed using ImageJ software (National Institute of Health, Bethesda, MD, USA).

3.2.3 Depleting High Abundant Albumin Content from Sample

Prior to fluorescence labeling and the 2-D gel separations, a SwellGell Blue albumin removal kit (Pierce, Rockford, IL, USA) was used to remove the albumins from the serum sample. Briefly, a SwellGell disc was placed in a mini-spin column and hydrated for 20 s with a total of 380 μL of ultrapure water followed by vortexing for 2 s. After removing the hydration water by centrifugation, the spin column was placed in a 2 mL collection tube and loaded with 100 μL of the FCS sample (36 mg/mL) and centrifuged at 12,000x for 1 min. Based on the observation that ~55% of serum is albumin [7, 9, 10], we determined that 1.98 mg of albumin was removed for every 100 μL of FCS sample processed.

3.2.4 Protein Florescence Labeling

The proteins contained in the albumin-cleared FCS samples (Invitrogen, Carlsbad, CA, USA) were covalently labeled with AlexaFluor 633 (excitation/emission = 633/652 nm) thiol reactive dye

Figure 3.1 (A) Topography of the 2-D microchip used for these studies. The channels were 50 µm deep and 20 µm wide in all cases. The 1st and 2nd dimension channels were 7 cm (filled with gel media) and 6 cm (filled with MEKC buffer), respectively, in terms of their total column lengths. The effective column lengths for the 1st and 2nd dimensions were 6 cm and 5 cm, respectively. (B) Diagram of the in-house constructed LIF system used for the µ-CE separation. The system was configured in an epi-illumination format and was equipped with 40x microscope objective (NA = 0.65) used to focus the laser excitation radiation into the microseparation channel. An x-y-z micro-translational stage (not shown) was used to position the chip above the objective. A He-Ne laser served as the excitation source and a 633 nm band-pass filter was used to filter the excitation wavelength prior to launching into the microchip. The fluorescence emission was collected by the same objective, passed through the dichroic filter and spectrally filtered using a 653 nm band-pass filter with the photons transduced using a photomultiplier tube.

A

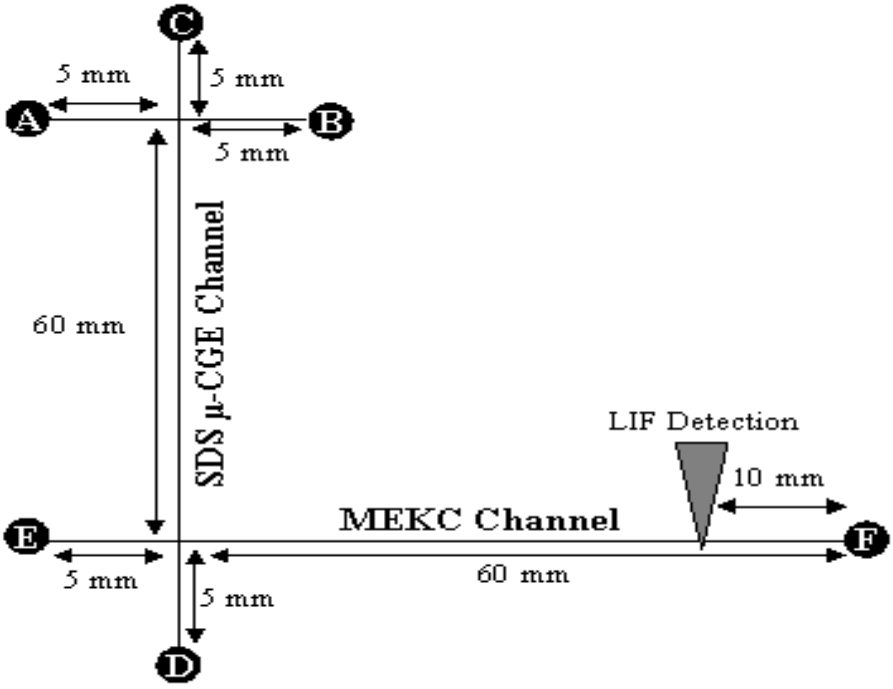
C
A
B
D
E
F
5 mm
5 mm
5 mm
60 mm
SDS μ-CGE Channel
LIF Detection
10 mm
MEKC Channel
5 mm
60 mm
5 mm

B

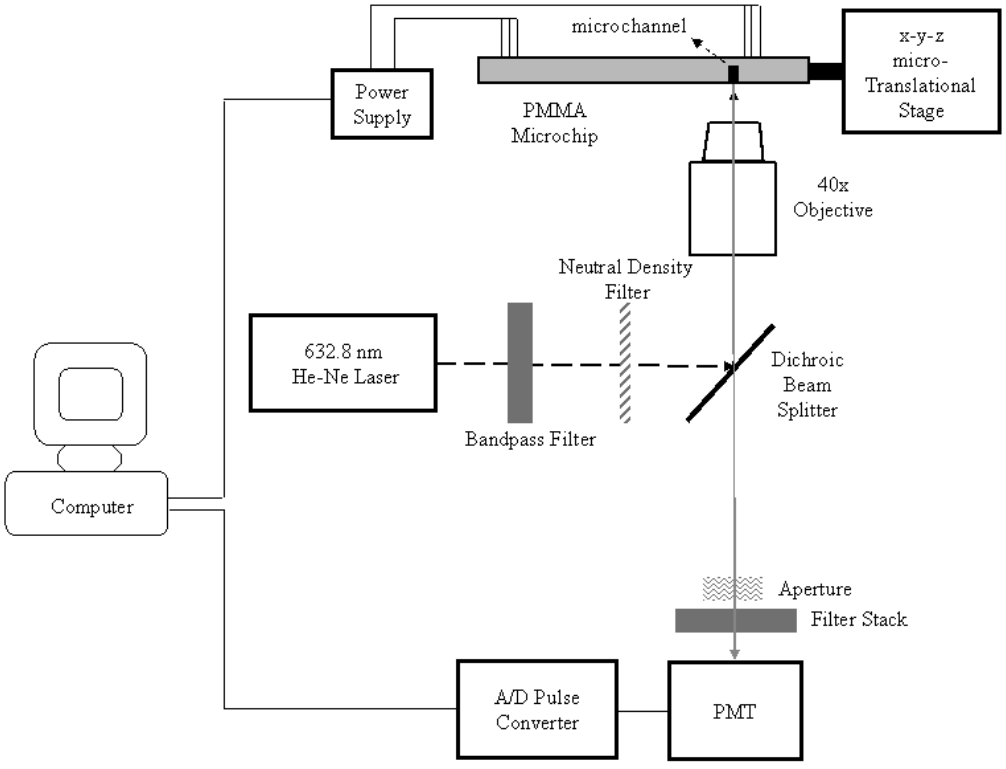
microchannel
x-y-z
micro-
Translational
Stage
Power
Supply
PMMA
Microchip
40x
Objective
Neutral Density
Filter
632.8 nm
He-Ne Laser
Dichroic
Beam
Splitter
Bandpass Filter
Computer
Aperture
Filter Stack
A/D Pulse
Converter
PMT

(Invitrogen) following the manufacturer's guidelines. Briefly, proteins containing cystine residues were first reduced to cysteines by adding tris-(2-carboxyethyl) phosphine (TCEP) to the FCS sample. Cysteines were then reacted with the AlexaFluor 633 dye in an approximate 1:10 molar ratio, respectively, for approximately 2 h after which the excess dye was selectively removed by running the derivatized sample through a 3 kDa filtration column (Millipore Corp., Billerica, MA, USA). AlexaFluor-conjugated cystine/cysteine containing proteins from the FCS sample were then diluted in the µ-CE run buffer in a 1:5 volume ratio (FCS sample:run buffer) and heated to 95°C for 5 min. Prior to use in the microchip, all solutions were filtered with a 0.2 µm Nylon-66 membrane syringe filter (Cole-Parmer Instrument Co., Vernon Hills, IL, USA) except for protein solutions, which were centrifuged (5 min, ~6,000 rpm) to remove any particulates.

3.2.5 Microchip 2-D Electrophoretic Separations

Prior to the electrophoretic separation, a solution of 5 mg/mL of methyl hydroxyethyl cellulose (MHEC) was dissolved in 1X PBS (pH = 7.2, Sigma-Aldrich, St. Louis, MO, USA) and was flushed through the fluidic channels through reservoir A (see Figure 3.1A) while applying vacuum to reservoir F. Prior to the µ-CE 2-D separation, the first dimension channel (see Figure 3.1A) was filled with a seiving matrix, which consisted of a SDS 14-200 linear polyacrylamide gel (Beckman Coulter Inc., Fullerton, CA, USA) containing 0.05% w/v MHEC. The gel filling was monitored using brightfield microscopy to make sure the gel was allowed to fill the chip exactly at the interaction of the 1^{st} and 2^{nd} dimensions. The second dimension channel was then filled with the MEKC buffer, which was composed of 12 mM Tris-HCl containing 0.4% w/v SDS and 0.05% w/v MHEC (pH = 8.5). Reservoir A was then emptied and subsequently filled with 2 µL of the FCS sample containing the labeled proteins. The sample was injected into the sampling channel (see A-B, Figure 3.1A) at 200 V/cm while B was poised at a positive voltage. The 2^{nd} dimension separations were programmed to start after 10 s electrophoresis run time in the 1^{st} dimension (SDS µ-CGE). The SDS µ-CGE separation was carried

out at 300 V/cm using L_{eff} = 60 mm (see C-D channel, Figure 3.1A). Each 2nd dimension MEKC cycle consisted of a 10 s run (MEKC development time) operated at a field strength of 400 V/cm, which was found to be a sufficient time to assure that all of the components injected into the 2nd dimension reached the LIF detection zone (L_{eff} = 50 mm). Sample eluting from the 1st dimension was injected into the 2nd dimension following a 1 s run period in the 1st dimension. During the MEKC run cycle, the applied field in the 1st dimension was ceased, parking the components in the 1st dimension during the 2nd dimension run.

3.2.6 Protein 2-D Slab Gel Separation Using IEF/PAGE and Protein Staining

An immobilized pH gradient (IPG) buffer (pH 3.0 to 10.0) was immobilized onto a 24 cm IEF strip (Immobiline dry strip, pH 3.0 to 10.0 non-linear gradient). The IPG buffer and Immobiline strip as well as dithiothreitol (DTT), bromophenol blue, Ettan IPGphor and Ettan DALT*twelve* 2-D electrophoresis reagents were all purchased from Amersham Pharmacia Biotech (Piscataway, NJ, USA) and the Dodeca silver stain kit, SDS, 3-([3-Cholamidopropyl]-dimethyl-ammonio-1-propane-sulfonate (CHAPS), ammonium persulfate, urea, and N,N,N^9,N^9, -tetramethyl-ethylenediamine (TEMED) were purchased from Bio-Rad (Hercules, CA, USA).

FCS protein contents were determined by the Bradford method [40] to determine the amount of proteins used for the IEF/SDS-PAGE 2-D separations. The FCS proteins were mixed with 10 μl of lysis buffer composed of 8 M urea, 4% CHAPS, 40 mM DTT, and 2% w/v IPG buffer. The 24 cm Immobiline dry strip containing the FCS proteins was rehydrated overnight in a 450 μl rehydration solution composed of 8 M urea, 2% CHAPS, 20 mM DTT, Bromophenol and 0.5% IPG buffer. IEF was then performed sequentially (20°C) for 1 h at 500 V, 1 h at 1 kV, and 8 h and 20 min at 8 kV for a total run time of 10 h and 20 min using an Ettan IPGphor Instrument (GE Healthcare, Piscataway, NJ, USA). The focused strip was first equilibrated for 15 min in a 7 ml SDS equilibration buffer composed of 50 mM Tris-HCl, pH 8.8, 6 M urea, 30% w/v glycerol, 2% w/v SDS, and 0.002% w/v bromophenol

blue with 1% w/v DTT. This step was followed by a second equilibration for 15 min in 7 ml of a SDS equilibration buffer containing 2.5% w/v Iodoacetamide. After equilibration, IPG gel strips were embedded in a 0.5% agarose solution (Amresco, Solon, OH, USA) at the top of the SDS-polyacrylamide gel.

The SDS-polyacrylamide gel (12.5%) was prepared in a 1.5 mm gel cassette purchased from Amersham. The gel was 235 mm wide, 190 mm long and 1.5 mm thick. The 2nd dimension SDS-PAGE was conducted (20°C) at a constant voltage of 110 V on the Ettan DALT*twelve* System, which required ~15 h development time. Proteins contained within the SDS-PAGE gel were then stained with a Dodeca silver stain kit (Bio-Rad) for spot visualization and all stained gels were scanned using an UMAX PowerLook II scanner (UMAX data systems, City, Taiwan).

3.2.7 Software Analysis of Data

To obtain a 2-D image of the microchip electrophoresis data, a text file of a typical raw 2-D run formatted into a 2-D matrix was input into ImageJ. The matrix was constructed such that each column represented one MEKC cycle. The 2-D image obtained from ImageJ comprised of a total available area of 60,000 pixel^2 (200 × 300 pixel). The 2-D image map from IEF/SDS-PAGE was adjusted to a total area of 60,000 pixel^2 to match that of the microchip. Images were then converted into binary formats prior to the determination of the average size of each spot in the 2-D map using ImageJ.

3.3 Results and Discussion

3.3.1 Column Lengths for Generating High Peak Capacities (P)

To increase P for the analysis of complex samples such as the FCS proteome compared to our previously reported 2-D μ-CE system [32], we used a 60 mm long effective separation length for the first (SDS μ-CGE) dimension and increased the effective column length to 50 mm in the 2nd (MEKC) dimension. Because $P \alpha L_{eff}$, we reasoned that an increase in the total 2-D column length from 4 cm to 11 cm (175% increase in the effective column length) would result in P ≥2,750 compared to our

previously reported P of ~1,000. This column length increase comes at the expense of a longer electrophoretic development time, but more effectively accommodates the higher number of proteins expected in the FCS sample compared to the 10-model protein set used in our previous report [32].

3.3.2 Representation of the FCS Proteome Using Thiol-Labeling Dyes Only

Cysteine is unique amongst the 20 amino acids in that it contains a highly reactive sulf-hydryl group that can be oxidized to form intramolecular disulfide linkages (*i.e.,* cystine). A relatively low occurrence of cysteine has been reported in proteins comprising the proteome of several organisms, with the occurrence level dependent upon the complexity of the organism [41]. For example, human and mouse proteins possess a level of occurrence of cysteine residues estimated to be ~2.26% [41]. According to the SwissProt data bank, proteins comprising many proteomes including many mammalian proteomes contain on average 360 amino acids per protein (49.2 kDa, assuming an amino acid average molecular weight of 136.7 Da). Therefore, approximately 8.1 cysteine residues would be found in the "average" protein comprising the FCS sample, which would be available for labeling using the maleimide functional group appended to the fluorescent moiety. The question remains; are some proteins not represented in the 2-D profile because they do not contain a cysteine residue? Statistically, this may occur for proteins with amino acid compositions below approximately 45 amino acid residues.

3.3.3 Effects of Dye-Labeling on the Electrophoreteic Mobility of the Proteins

Because the proteins are pre-labeled with AlexaFluor 633, which is an anion (net -2 charge), mobility shifts of the proteins may be expected based on the addition of charge and friction resulting from the added mass of the dye(s) with the perturbation dependent upon the extent of labeling. However, this perturbation is expected to be small due to the relatively large size of the SDS/protein complexes compared to the dye molecules and the large amount of negative charge carried by the

SDS/protein complexes. For example, a 49.2 KDa average molecular weight protein (360 amino acid residues) would carry a load of ~242 SDS molecules per protein assuming 1.4 g of SDS per gram of protein. Therefore, labeling of 8.1 cysteine residues per average protein would add approximately 6% charge to this complex when the solution pH is near the proteins' pI. Because the electrophoresis is performed in reverse polarity, the additional negative charge added by the dye(s) would increase its electrophoretic mobility, which would be compensated by the mass of dye(s) conjugated to the protein resulting in reductions in the electrophoretic mobility. AlexaFluor 633 has a molecular weight of ~1,300 Da; for 8 dyes per average protein, a mass increase of ~10,400 Da would occur, which is a 21% increase. For a globular protein, the molecular weight (MW) dependence on the frictional component to the electrophoretic mobility is approximately $(MW)^{1/3}$, therefore, this reduction in the mobility is 2.8%, close to the 6% increase in charge noted above.

3.3.4 1-D µ-CGE of FCS Using SDS-PAGE

We were first interested in analyzing the peak capacity for a 1-D µ-CGE separation of the FCS proteins using L_{eff} = 60 mm. The results of this analysis are depicted in Figure 2. As can be seen from this electropherogram, approximately 24 bands could be observed with varying degrees of resolution and widths due to potential peak overlap arising from proteins with similar molecular weights. From this data (see bands marked with an asterisk in Figure 3.2), the average peak width was estimated to be 5.2 ±3.2 s, producing a plate number of 1.5×10^3. From these values and a separation window of 147 s (defined by the migration time difference between the last and first migrating components), we estimated a peak capacity for this 1-D separation of 28. Clearly, this is well below the necessary level required to analyze a sample as complex as that anticipated for a mammalian serum proteome.

3.3.5 2-D SDS-PAGE/MEKC Separations

In our 2-D electrophoresis separations, SDS-PAGE was used as the first dimension and MEKC as the second dimension. SDS forms complexes with proteins, which are subsequently electrophoresed

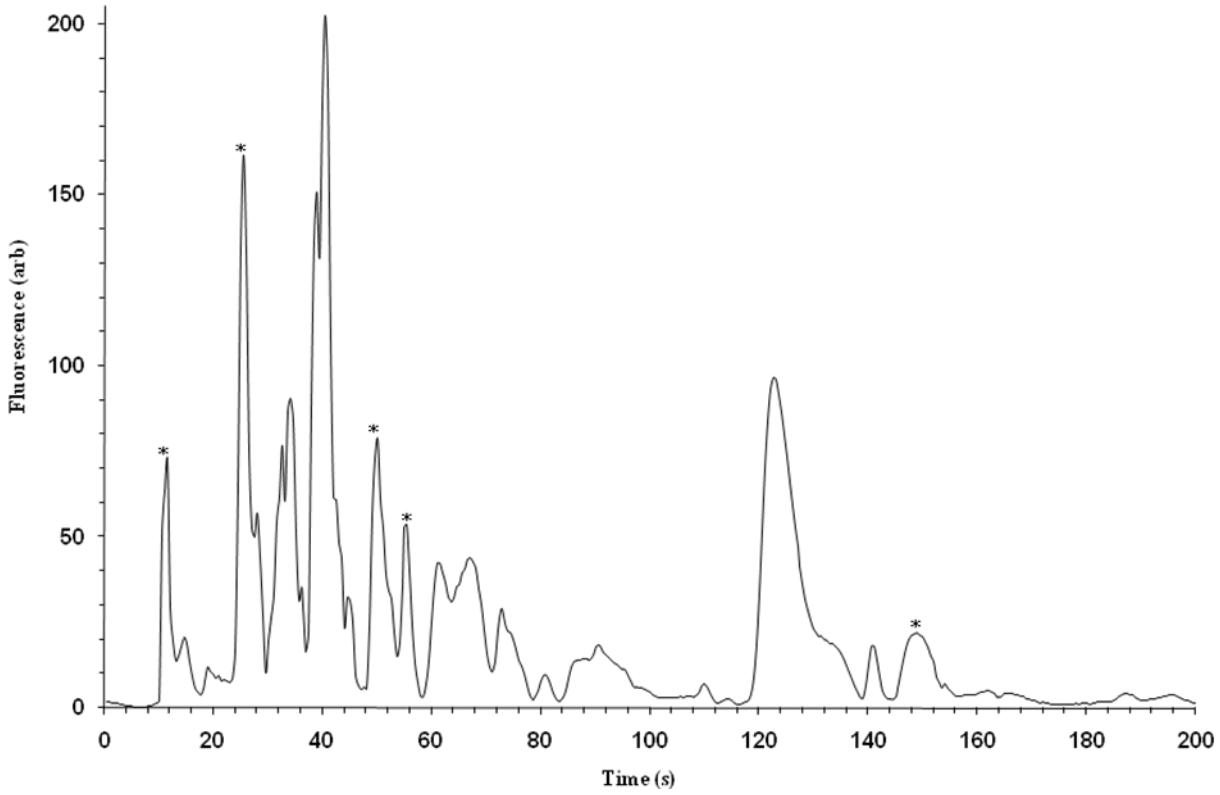

Figure 3.2. SDS µ-CGE 1-D separation of a FCS protein mixture. The protein sample, which was labeled with the thiol-specific fluorescent dye, AlexaFluor 633, was placed into reservoir A of the microchip (see Figure 1A) and electrokinetically injected into the separation channel at 200 V/cm. The 1-D SDS µ-CGE was performed at E = 300 V/cm. The total separation length was 7 cm with an effective length of 6 cm.

through a sieving matrix allowing for the separation of species primarily based on differences in their MWs. MEKC uses micelles as a pseudo-stationary phase with separation based on selective partitioning of solutes to these micelles. In our case, we are using SDS micelles as the pseudo-stationary phase, which provides an attractive interface to SDS-PAGE due to the fact that both dimensions use SDS. We have previously demonstrated that SDS-MEKC is highly orthogonal to SDS µ-CGE, making it an elegant format for producing high peak capacities for multi-dimensional electrophoretic analysis of intact proteins [32]. The degree of orthogonality between the SDS-PAGE and MEKC dimensions was evaluated using changes in migration order and migration times between a set of 10 model proteins. A plot of the normalized migration time for a SDS-PAGE 1-D separation

versus that of the SDS MEKC 1-D separation produced a scatter plot with minimal data points occurring on a diagonal (slope = 1.0, intercept = 0.0) providing an orthogonality value between these 2 separation mechanisms of 77%.

In the present 2-D format, electrophoretic zones are "parked" in the first dimension while the second dimension is affected in a serial fashion. Therefore, issues with zonal dispersion due to longitudinal diffusion should be considered since it can significantly impact the peak capacity of the 2-D separation. This was accomplished by calculating the height equivalent to a theoretical plate for longitudinal diffusion only (H_D) of the 1-D SDS μ-CGE dimension and comparing that value to H_{TOT} secured from the complete 2-D separation. A representative diffusion coefficient for proteins in a sieving matrix as used herein was taken as ~10^{-8} cm^2 s^{-1}, which is the measured diffusion coefficient of cytochrome C in polyacrylamides [42], resulting in $H_D = 5.9 \times 10^{-6}$ cm ($H_D = 2Dt/L$; t = time; L = column length, cm). The number of plates for a typical band migrating from the 2-D separation (see Figure 3.3) was 6.2×10^5, resulting in $H_{TOT} = 1.8 \times 10^{-5}$ cm. Therefore, the diffusional component to H_{TOT} was calculated to be approximately 33%.

For 159 10 s MEKC cycles, which represents the parking time (1,590 s), and a total separation time of 1,759 s, the percent contribution of diffusional spreading during the parking phases of the 2-D separation to H_D is roughly 90% or 5.3×10^{-6} cm. Clearly, reductions in the development time for the MEKC cycles can reduce H_D resulting from the parking phases of the separation, producing higher peak capacities. Interestingly, the diffusion coefficient for cytochrome C in free solution has been reported to be ~10^{-6} cm^2 s^{-1} [42], two-orders of magnitude higher than that in the viscous polyacrylamide sieving matrix. Therefore, using MEKC in the 1st dimension, where parking is required to allow development in the 2nd dimension would be inadvisable due to significant degradations in peak capacity arising from larger values of H_D compared to the SDS-PAGE dimension. The average peak width determined above from the SDS-PAGE dimension was then used to select the

appropriate sampling time into the second dimension, which was set at 1 s. Therefore, each peak was estimated to be sampled approximately 5 times upon transfer from the 1st dimension into the 2nd dimension. This over-sampling was necessary to obtain accurate 2-D profiles by minimizing band aliasing artifacts [26, 43]. In order to exhaustively sample all components migrating from the 1st dimension into the 2nd dimension, 159 MEKC cycles were required with each cycle run for 10 s (E = 400 V/cm). In addition, a 10 s run time was imposed on the 1st dimension prior to running sequential MEKC separations. Using these sampling and run times as well as the injection times (1 s) for sampling from the 1st dimension into the 2nd dimension, the development time for the full 2-D separation was estimated to be 1,759 s (29.3 min).

Given the dimensions of the microfluidic channels used herein, we calculated an injection volume of ~20 pL into the 2nd dimension. To calculate the transfer efficiency of material from the 1st dimension into the 2nd dimension, we used the column length in the 1st dimension, the average migration time for the components in the 1st dimension (see Figure 3.2) and the field strengths used for the 1st dimension separation as well as the electrophoresis time (1 s).

Based upon these considerations, we estimated a transfer efficiency of ~5%. To improve this transfer efficiency a lower field strength would need to be employed in the 1st dimension, but this comes at the expense of a longer electrophoresis development time. However, in spite of this transfer efficiency, the SNR provided by the laser-induced fluorescence system was sufficient for generating adequate profiles for moderately expressed proteins. A typical 2-D image of the FCS protein separation and the corresponding 3-D landscape image are shown in Figure 3A. The images secured from Figure 3A were imported into ImageJ for analysis. From the input data to ImageJ, the average size of each protein spot for the μ-CE run was determined to be 23 (±1.4) $pixel^2$, which yielded a peak capacity for this 2-D separation of 2,600 (±149). As noted previously, the anticipated peak capacity

was ~2,750 based on the extended column length used herein, which agrees favorably with the experimental value observed.

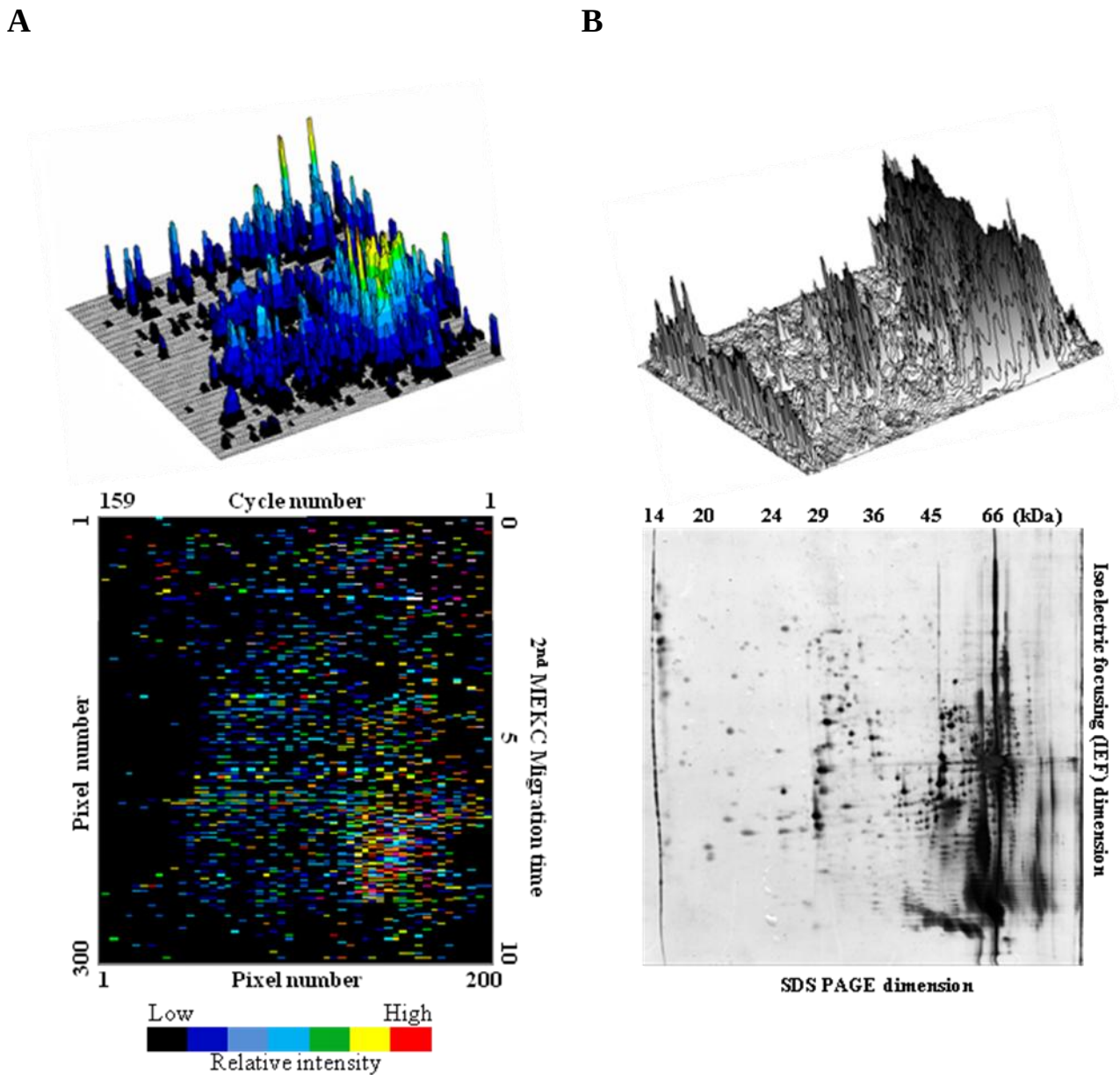

Figure 3.3. (A) SDS µ-CGE/µ-MEKC 2-D separation of a FCS protein mixture. The protein sample was placed into reservoir A (see Figure 1A) and electrokinetically injected into the separation channel at 200 V/cm. The 2-D SDS µ-CGE × MEKC were performed at 300 V/cm and 400 V/cm, respectively. A 10 s separation time was utilized in the first dimension prior to performing the serial 10 s MEKC cycles. A total of 159 MEKC cycles was used with a 1 s transfer time from the 1st to 2nd dimension. The bottom panel shows a 2-D image of the microchip FCS map, while the top panel shows a 3-D landscape of the FCS protein map. (B) 2-D image of a conventional IEF/2-D PAGE separation of the FCS protein sample (bottom panel) and the corresponding 3-D landscape proteins (top panel). Separation conditions are provided in the Experimental section.

3.3.6 Reproducibility of the 2-D Separations

Unfortunately, polymer microchips are susceptible to poor migration time reproducibility due in part to EOF variations [44]. In chapter 2, we discussed the importance of coating polymers surfaces prior to separations to suppress EOF and minimize migration time variability from run to run; therefore, PMMA channels were covalently modified by grafting linear polyacrylamides onto their surfaces. To suppress the EOF in the present case, MHEC (0.05% w/v) was simply added into the run buffer used for our protein separations. EOF in PMMA channels with buffer containing MHEC (0.05% w/v) as a dynamic coating agent has been measured to be around $1.20 \pm 0.07 \times 10^{-5}$ cm^2/Vs [32], which is comparable to $3.36 \pm 0.13 \times 10^{-5}$ cm^2/Vs for LPA-modified PMMA reported in chapter 2. As an indicator of the reproducibility of our separations, we calculated the average migration times for the four most intense peaks taken from the raw 2-D electropherograms collected for three different microchip separations. The average protein migration times were 166 s (RSD = 11.3%), 976 s (RSD = 2.8%), 1,303 s (RSD = 3.9%) and 1,467 s (RSD = 1.2%) giving an average RSD value of 4.8%, comparable to what has recently been reported for microchip-based 2-D separations using IEF and SDS-PAGE [37].

To further demonstrate the reproducibility of the full 2-D profile shown in Figure 3.3A, a second FCS sample was run using a different PMMA microchip. Figure 3.4 shows the resulting 2-D protein profile using similar separation conditions as described in Figure 3.3. Comparison of Figures 3.3A and 3.4 demonstrate good reproducibility of this 2-D separation assay.

3.3.7 Two-dimensional Slab Gel Separation of FCS Proteins

In order to make a comparison of the peak capacity for the microchip 2-D separation to that of a macro-scale version employing IEF/SDS-PAGE, we subjected the FCS sample to IEF/2-D PAGE. The FCS sample was processed in the same fashion as that used for the 2-D μ-CE case, except that proteins were not labeled with the AlexaFluor 633 dye prior to the electrophoresis.

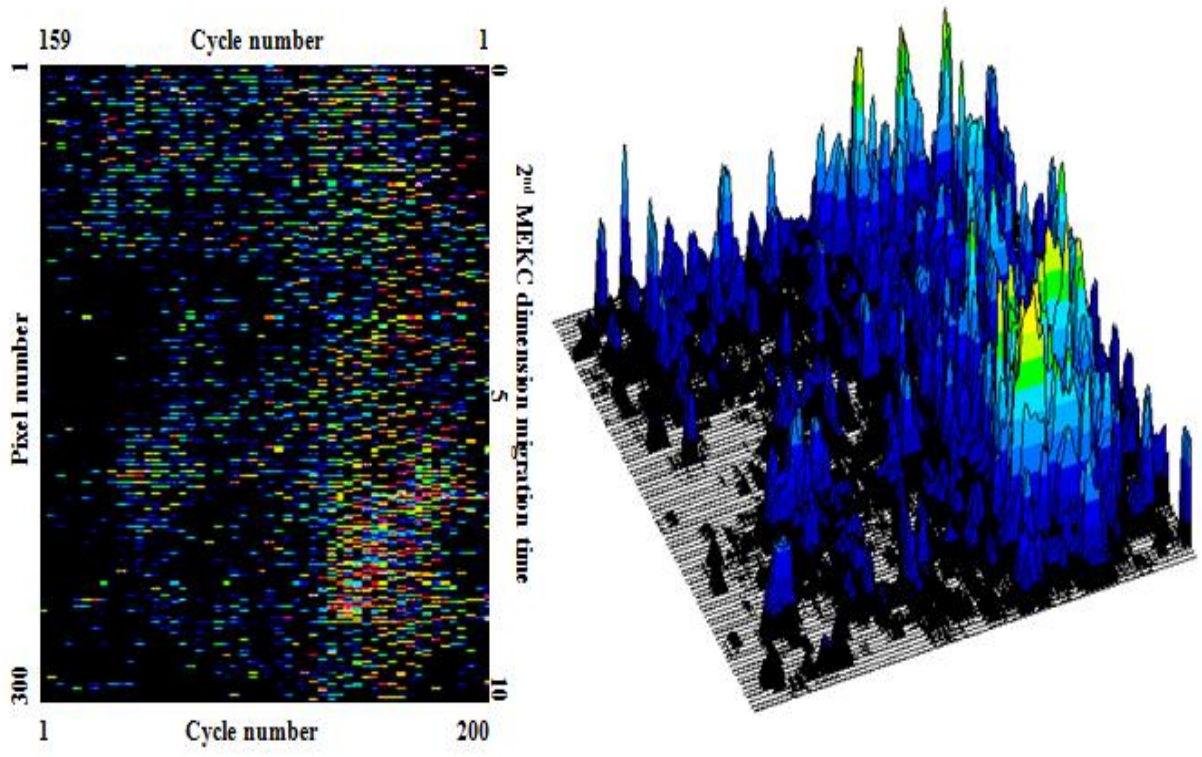

Figure 3.4 A 2-D protein profile of an FCS sample using similar conditions as those described in Figure 3A (left: 2-D image; right: 3-D landscape of proteins).

Protein visualization was accomplished by post-staining using a Ag-stain following the electrophoresis. A 2-D image of the stained gel is shown in Figure 3B. The image of the stained-gel was then subjected to ImageJ analysis. Using an input of 60,000 pixel^2 (200 x 300), the average spot size was determined to be 83.6 pixel^2, producing a peak capacity of 717, nearly 3-fold lower than that obtained for the 2-D μ-CE case. Depending on the complexity of the sample and the detection protocol employed, IEF/PAGE can produce ~2,000 protein spots per gel [45]. Our peak capacity number in the present case was only 717 due primarily to the inability to visualize low abundant proteins using the Ag staining employed here and the fact that some serum albumins were loaded onto the gel masking some the lower intensity bands.

A remarkable attribute of the 2-D μ-CE example is that it produced a peak capacity of 2,660 in 29.3 min, whereas only a peak capacity of 717 was generated for the standard gel, but required ~30 h

to complete. Therefore, the 2-D μ-CE produced protein spot generation rates of 88.7 min^{-1}, while the IEF/SDS-PAGE format possessed a spot production rate of only 0.4 min^{-1}, resulting in an approximate 222-fold increase in the protein spot production rate.

3.4 Conclusions

Separations on microchip platforms are garnering appeal for the analysis of complex biological samples because they can easily lend themselves to performance characteristics that rival their macro-scale counterparts using a much shorter operational time, generating data production rates that are impressive. In addition, these formats, due to their small footprint and lithographic fabrication techniques, will permit the development of multi-channel formats that can significantly improve the production rate of data. For example, if the 2-D format employed herein could be run in a 96-channel format in parallel, the protein spot production rate would be 8, 515 min^{-1}, an approximately 21,288-fold increase compared to conventional IEF/SDS-PAGE.

In the current report, we demonstrated the ability to generate peak capacities of 2,600 (±149) for a biological serum sample using an 11 cm effective separation length in both dimensions. If we increased the effective separation channel length 4-fold (i.e., 40 cm for both dimensions combined), the peak capacity of this 2-D format could potentially exceed 10,000 components. While this peak capacity is still far below the total number of protein components typically found in a serum proteome, isolating sub-populations of common protein types, such as glycosolated, phosphorylated protein types, could make this peak capacity tractable for exhaustive analysis of this complex sample. In addition, while we did not demonstrate the ability to interface this 2-D separation platform to mass spectrometry (MS) for discovery-based applications, interfacing of microchips to a variety of MS techniques have been demonstrated [46-50]. In addition, the integration of sample preparation steps to the chip platform prior to the 2-D separation will provide an autonomous system for discovery or diagnostic-based proteomic projects.

3.5 References

[1] Hood, L., *Journal of Proteome Research* 2002, *1*, 399-409.

[2] Lion, N., Rohner, T. C., Dayon, L., Arnaud, I. L., *et al.*, *Electrophoresis* 2003, *24*, 3533-3562.

[3] Hu, S., Michels, D. A., Fazal, M. A., Ratisoontorn, C., *et al.*, *Analytical Chemistry* 2004, *76*, 4044-4049.

[4] Hu, S., Zhang, L., Krylov, S., Dovichi, N. J., *Anal. Chem.* 2003, *75*, 3495-3501.

[5] Mitterdorfer, G., Mayer, H. K., Kneifel, W., Viernstein, H., *Proteomics* 2002, *2*, 1532-1538.

[6] Zhang, Z., Carpenter, E., Puyan, X. L., Dovichi, N. J., *Electrophoresis* 2001, *22*, 1127-1132.

[7] Anderson, N. L., Anderson, N. G., *Molc. & Cell. Proteomics* 2002, *1*, 845-867.

[8] Pieper, R., Gatlin, C. L., Makusky, A. J., Russo, P. S., *et al.*, *Proteomics* 2003, *3*, 1345-1364.

[9] Hood, B. L., Zhou, M., Chan, K. C., Lucas, D. A., *et al.*, *Journal of Proteome Research* 2005, *4*, 1561-1568.

[10] Miller, I., Friedlein, A., Tsangaris, G., Maris, A., *et al.*, *Proteomics* 2004, *4*, 3227-3234.

[11] Park, Y. M., Kim, J. Y., Kwon, K. H., Lee, S. K., *et al.*, *Proteomics* 2006, *6*, 4978-4986.

[12] Giddings, J., *Unified Separation Science*, 1991.

[13] Liu, H., Yang, C., Yang, Q., Zhang, W., Zhang, Y., *Journal of Chromatography, B: Analytical Technologies in the Biomedical and Life Sciences* 2005, *817*, 119-126.

[14] Righetti, P. G., Castagna, A., Herbert, B., *Analytical Chemistry* 2001, *73*, 320A-326A.

[15] Anderson, L., Anderson, N. G., *Proceedings of the National Academy of Sciences of the United States of America* 1977, *74*, 5421-5425.

[16] O'Farrell, P. H., *Journal of Biological Chemistry* 1975, *250*, 4007-4021.

[17] Righetti, P. G., *Journal of Biochemical and Biophysical Methods* 1988, *16*, 99-108.

[18] Santoni, V., Molloy, M., Rabilloud, T., *Electrophoresis* 2000, *21*, 1054-1070.

[19] Gygi, S. P., Corthals, G. L., Zhang, Y., Rochon, Y., Aebersold, R., *Proceedings of the National Academy of Sciences of the United States of America* 2000, *97*, 9390-9395.

[20] Richards, D. P., Stathakis, C., Polakowski, R., Ahmadzadeh, H., Dovichi, N. J., *Journal of Chromatography A* 1999, *853*, 21-25.

[21] Tsai, S. W., Loughran, M., Karube, I., *Journal of Micromechanics and Microengineering* 2004, *14*, 1693-1699.

[22] Michels, D. A., Hu, S., Dambrowitz, K. A., Eggertson, M. J., *et al.*, *Electrophoresis* 2004, *25*, 3098-3105.

[23] Kraly, J. R., Jones, M. R., Gomez, D. G., Dickerson, J. A., *et al.*, *Analytical Chemistry* 2006, *78*, 5977-5986.

[24] Opiteck, G. J., Ramirez, S. M., Jorgenson, J. W., Moseley, M. A., *Analytical Biochemistry* 1998, *258*, 349-361.

[25] Shen, Y. F., Jacobs, J. M., Camp, D. G., Fang, R. H., *et al.*, *Analytical Chemistry* 2004, *76*, 1134-1144.

[26] Herr, A. E., Molho, J. I., Drouvalakis, K. A., Mikkelsen, J. C., *et al.*, *Analytical Chemistry* 2003, *75*, 1180-1187.

[27] Wang, Y.-C., Choi, M. H., Han, J., *Analytical Chemistry* 2004, *76*, 4426-4431.

[28] Griebel, A., Rund, S., Schoenfeld, F., Doerner, W., *et al.*, *Lab on a Chip* 2004, *4*, 18-23.

[29] Li, Y., Buch, J. S., Rosenberger, F., DeVoe, D. L., Lee, C. S., *Analytical Chemistry* 2004, *76*, 742-748.

[30] Xu, A., Sluszny, C., Yeung, E. S., *Journal of Chromatography, A* 2005, *1087*, 177-182.

[31] Das, C., Zhang, J., Denslow, N. D., Fan, Z. H., *Lab on a Chip* 2007, *7*, 1806-1812.

[32] Shadpour, H., Soper, S. A., *Analytical Chemistry* 2006, *78*, 3519-3527.

[33] Venkatramani, C. J., Xu, J., Phillips, J. B., *Analytical Chemistry* 1996, *68*, 1486-1492.

[34] Erni, F., Frei, R. W., *Journal of Chromatography* 1978, *149*, 561-569.

[35] Emrich, C. A., Medintz, I. L., Chu, W. K., Mathies, R. A., *Analytical Chemistry* 2007, *79*, 7360-7366.

[36] Ramsey, J. D., Jacobson, S. C., Culbertson, C. T., Ramsey, J. M., *Analytical Chemistry* 2003, *75*, 3758-3764.

[37] Liu, J. K., Yang, S., Lee, C. S., Devoe, D. L., *Electrophoresis* 2008, *29*, 2241-2250.

[38] Shadpour, H., Musyimi, H., Chen, J., Soper, S. A., *Journal of Chromatography, A* 2006, *1111*, 238-251.

[39] Hupert, M. L., Guy, W. J., Llopis, S. D., Shadpour, H., *et al.*, *Microfluidics and Nanofluidics* 2007, *3*, 1-11.

[40] Bradford, M. M., *Analytical Biochemistry* 1976, *72*, 248-254.

[41] Miseta, A., Csutora, P., *Molecular Biology and Evolution* 2000, *17*, 1232-1239.

[42] Lewus, R. K., Carta, G., *Industrial & Engineering Chemistry Research* 2001, *40*, 1548-1558.

[43] Gottschlich, N., Jacobson, S. C., Culbertson, C. T., Ramsey, J. M., *Analytical Chemistry* 2001, *73*, 2669-2674.

[44] Llopis, S. L., Osiri, J., Soper, S. A., *Electrophoresis* 2007, *28*, 984-993.

[45] Gorg, A., Weiss, W., Dunn, M. J., *Proteomics* 2004, *4*, 3665-3685.

[46] Freire, S.L., Wheeler, A.R., *Lab Chip* 2006, 6, 1415-1423.

[47] Meng, Q., Qi, S., Soper, S.A., Limbach, P.A., *Anal. Chem.* 2001, 73, 1286-1291.

[48] Lazar, I.M., Ramsey, R.S., Ramsey, J.M., *Anal. Chem.* 2001, 73, 1733-1739.

[49] Chan, J.H., Timpermann, A.T., Qin, D., Aebersold R., *Anal. Chem.* 1999, 71, 4437-4444.

[50] Lazar, I.M., Ramsey, R.S., Sundberg, S., Ramsey, J.M., *Anal. Chem.*, 1999, 71, 3627-3631.

4 Ultra-fast 2-Dimensional Microchip Electrophoresis Using SDS µ-CGE and Microemulsion Electrokinetic Chromatography for Protein Profiling

4.1 Introduction

Two-dimensional (2-D) separations are the workhorse of the process flow pathway in proteomics and in most cases, 2-D separations consist of isoelectric focusing (IEF) in the first dimension and polyacrylamide gel electrophoresis (PAGE) in the second dimension on conventional slab gels. Unfortunately, this technique does not lend itself to full process automation, can be very labor intensive, is time consuming and has difficulties in sorting highly hydrophobic proteins, such as membrane proteins [1]. For these reasons, microchip 2-D separation techniques have been developed as alternatives to conventional slab gel techniques because they offer high separation efficiencies due to effective heat dissipation, minimal sample consumption due to smaller footprints and fast analysis times due to shorter column lengths, and the ability to use higher electric field strengths.

Microchip 2-D separations are tractable not only because they can provide automation capabilities and rapid separations with high resolving power, but also can produce viable interfaces between the separation dimensions to minimize unswept volumes between separation dimensions preserving plate numbers. Herr and co-workers [2] coupled IEF and capillary zone electrophoresis (CZE) in which three model proteins were separated resulting in a peak capacity of ~1,300 that was achieved within 5 min. Li and co-workers [3] integrated IEF with parallel sodium dodecyl sulfate micro-capillary gel electrophoresis (SDS µ-CGE) for a comprehensive 2-D separation of five model proteins and generated a peak capacity of ~1,700 in 10 min. Chen and co-workers [4] described a microfabricated 2-D IEF-PAGE prototype, in which three model proteins were separated in 1.5 min, but the peak capacity of this system was not reported. Emrich and co-workers generated protein profiles from a complex, cellular mixture of *E. coli* proteins using a 2-D differential gel electrophoretic technique (DIGE) with the second-dimension separation completed within 1 h [5]. Also, Yang and co-workers recently reported a 2-D IEF/PAGE separation of whole cell *E. coli* protein lysate with an

estimated peak capacity of 2,880 that was obtained within 12 min [6] and provided a spot production rate of 240 min^{-1}.

All of the aforementioned examples of microchip 2-D utilized IEF in the first dimension. Unfortunately, IEF requires an equilibration step prior to the focusing step [6], which further increases the overall development times of the entire 2-D separation. Furthermore, IEF is not compatible with highly hydrophobic proteins as these are not compatible with the aqueous IEF buffer [1]. To avoid some of the drawbacks associated with IEF [1], alternative techniques can be used such as CZE [7-10] or micellar electrokinetic chromatography (MEKC) [10-13].

Ramsey and co-workers separated peptides with a 2-D microchip system that combined open-channel electrochromatography (OCEC) with CZE [9] in which they reported a peak capacity of 150 that was obtained in 13 min. The same group also combined MEKC with CZE [10, 11] and reported a peak capacity of 1000 that was obtained in 10 min [11] and a peak capacity of 4,200 that was obtained in 15 min [10]. For microchip protein separations, Soper and co-workers coupled SDS μ-CGE and MEKC and reported peak capacities of 1,000 and 2,600 in less than 12 min and 30 min for ten model proteins [13] and serum proteins [1], respectively.

Microemulsion electrokinetic chromatography (MEEKC), though similar to MEKC, has emerged as an attractive alternative to traditional MEKC. Since its introduction by Watarai [14] in 1991 for the separation of fluorescent aromatic compounds, MEEKC has been widely applied for the separation of various analytes [15-17] including proteins [15, 18]. In MEEKC, the separation medium is a microemulsion, a transparent solution consisting of an oil (e.g., n-heptane), a surfactant (e.g., SDS), a co-surfactant (e.g., n-butanol), and water. The structure of oil in a water emulsion is similar to that of micelles in MEKC except that the microemulsion has an oil droplet as a core [18]. Figure 4.1 depicts the formation of micelles in aqueous buffer and its utilization in the second dimensional phase of a microchip 2-D SDS μ-CGE and MEKC protein separation.

Figure 4.1 (**A**) Depiction of micelle formation in aqueous buffer and its utilization in the second dimensional phase of a microchip 2-D SDS µ-CGE and MEKC protein separation. SDS micelles form in buffer above the SDS critical micellar concentration (0.24% w/v). The aggregate number for SDS is about 62 molecules forming a core diameter of ~17Å. In a reverse polarity mode (detection is anodic), SDS micelles migrate towards the anode due to their ionized sulfate group, which are negatively charge whereas the direction of EOF is towards the cathode. Separation in the MEKC is according the partition coefficient of proteins within the micelles and the aqueous phase and according to the charge to mass ratio of proteins when they are in the aqueous medium. More hydrophobic domains within a protein result in stronger hydrophobic character and more hydrophobic proteins tend to interact more with the micellar core. On the other hand, anionic proteins[a] experiences columbic repulsion, and may not even interact with the micelles. This is especially true when their entire hydrophobic domains are masked by SDS (see rods that are gold only or gold/blue without any black color). These proteins are separated based on their electrophoretic mobility in the aqueous medium with the proteins possessing the highest charge-to-mass ratio migrating the fastest. Overall, the migration of proteins is in the order of 1-6 with protein 1 migrating the fastest and protein 6 migrating the slowest. (**B**) Depiction of microemulsion formation in aqueous buffer and its utilization in the second dimensional phase of a microchip 2-D SDS µ-CGE and MEEKC protein separation. In MEEKC, SDS surfactants impart a net negative charge to the oil emulsions and the co-surfactant (n-butanol) reduces the surface tension between the oil and the aqueous phase resulting to a miscible oil/water system. The hydrophobic core diameter for the microemulsion is ~100Å. Separation in the MEEKC phase is similar to that of the MEKC, except that separation and partitioning of larger proteins is more possible. *a = anionic proteins acquire their charge in two ways: (1.) because the pH conditions for the separation is above their pKa and (2.) because SDS imparts a negative charge on the proteins during sample prep and during the first dimension separation.*

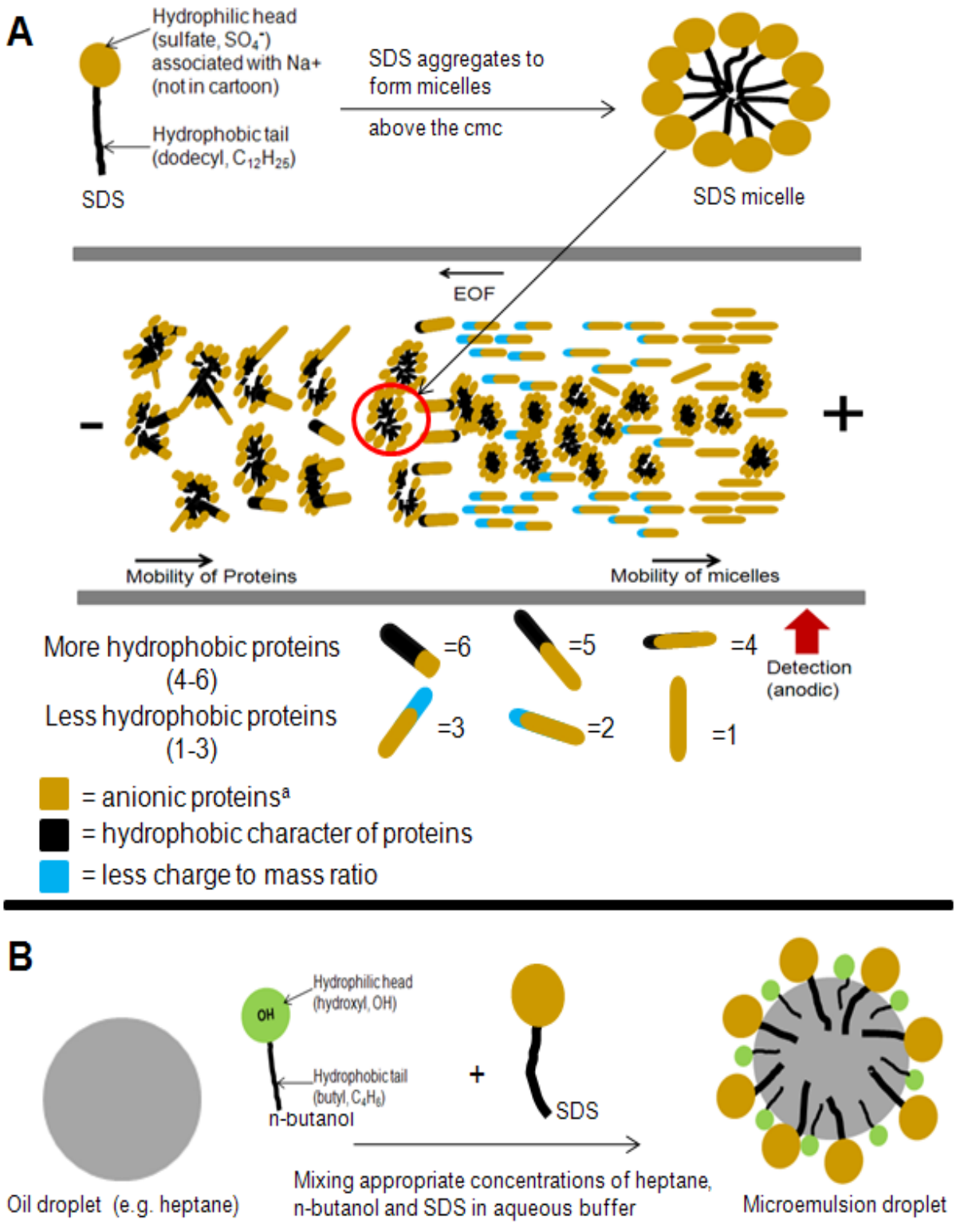
A
Hydrophilic head
(sulfate, SO_4^-)
associated with Na+
(not in cartoon)
Hydrophobic tail
(dodecyl, $C_{12}H_{25}$)
SDS
SDS aggregates to
form micelles
above the cmc
SDS micelle
EOF
−
+
Mobility of Proteins
Mobility of micelles
More hydrophobic proteins
(4-6)
Less hydrophobic proteins
(1-3)
=6
=5
=4
=3
=2
=1
Detection
(anodic)
= anionic proteins[a]
= hydrophobic character of proteins
= less charge to mass ratio
B
Oil droplet (e.g. heptane)
OH
Hydrophilic head
(hydroxyl, OH)
Hydrophobic tail
(butyl, C_4H_9)
n-butanol
+
SDS
Mixing appropriate concentrations of heptane,
n-butanol and SDS in aqueous buffer
Microemulsion droplet

In MEEKC, SDS surfactants impart a net negative charge to the microemulsions, whereas the co-surfactant reduces the surface tension between the oil and the aqueous phase resulting to a miscible oil/water system. Recent reports indicate that better separation efficiencies can be obtained using MEEKC compared to MEKC [18-25]. Due to their highly non-polar core, polar compounds typically remain in the aqueous electrolyte solution rather than partitioning into the microemulsion droplets. Therefore, it is expected that an anionic protein will experience columbic repulsion as it approaches the negatively charged droplet, but unmasked neutral or hydrophobic domains of proteins would strongly associate with the microemulsion droplets (Figure 4.1). Cationic species with pK_a values higher than the pH of the microemulsion solvent can form ion-pairs (IPs) with the anionic SDS surfactant layer on the emulsion surface. This interaction may be so strong that the species adsorb onto the microemulsion droplets [26]. Overall, analytes will interact with the emulsion droplets according to their partition coefficient. In a recent report [27], MEEKC was shown to result in better separation resolution (R_s) than MEKC for the analysis of the hydrophobic compound, bisphenol-A-diglycidyl ether and its derivatives under suppressed electroosmostic flow (EOF) operation. The authors showed that the improvement in R_s was due to a reduced retention factor (k) in MEEKC and not necessarily because of greater selectivity.

Despite the availability of experimental evidence demonstrating the utility of MEEKC compared MEKC in particular cases [28], it is surprising that MEEKC has not been used as a separation dimension in a multi-dimensional separation platform. In this work, we report a 2-D separation of a complex protein mixture, which combined SDS μ-CGE with MEEKC with the separation performed in a poly(methyl methacrylate), PMMA, microchip. Fluorescently-labeled *E. coli* proteins were profiled by this 2-D approach with the results compared to a comparable 2-D separation using SDS μ-CGE × MEKC. To achieve ultra-fast separations, short column lengths (effective length = 10 mm) were used for both dimensions.

4.2. Methods and Materials

4.2.1 Microchip Fabrication

The mold insert for embossing the PMMA chips was fabricated by high precision micromilling [29]. The mold insert was used to produce PMMA chips via hot embossing, which consisted of a PHI Precision Press model TS-21-H-C (4A)-5 (City of Industry, CA) that was used to replicate the microstructures into PMMA (MSC, Melville, NY) [30]. The embossed channels were 15 µm wide and 30 µm deep with effective separation lengths of 10 mm for both the SDS µ-CGE and MEEKC dimensions (C-D and E-F channels, respectively, see Figure 4.2). The injection channel (A-B, Figure

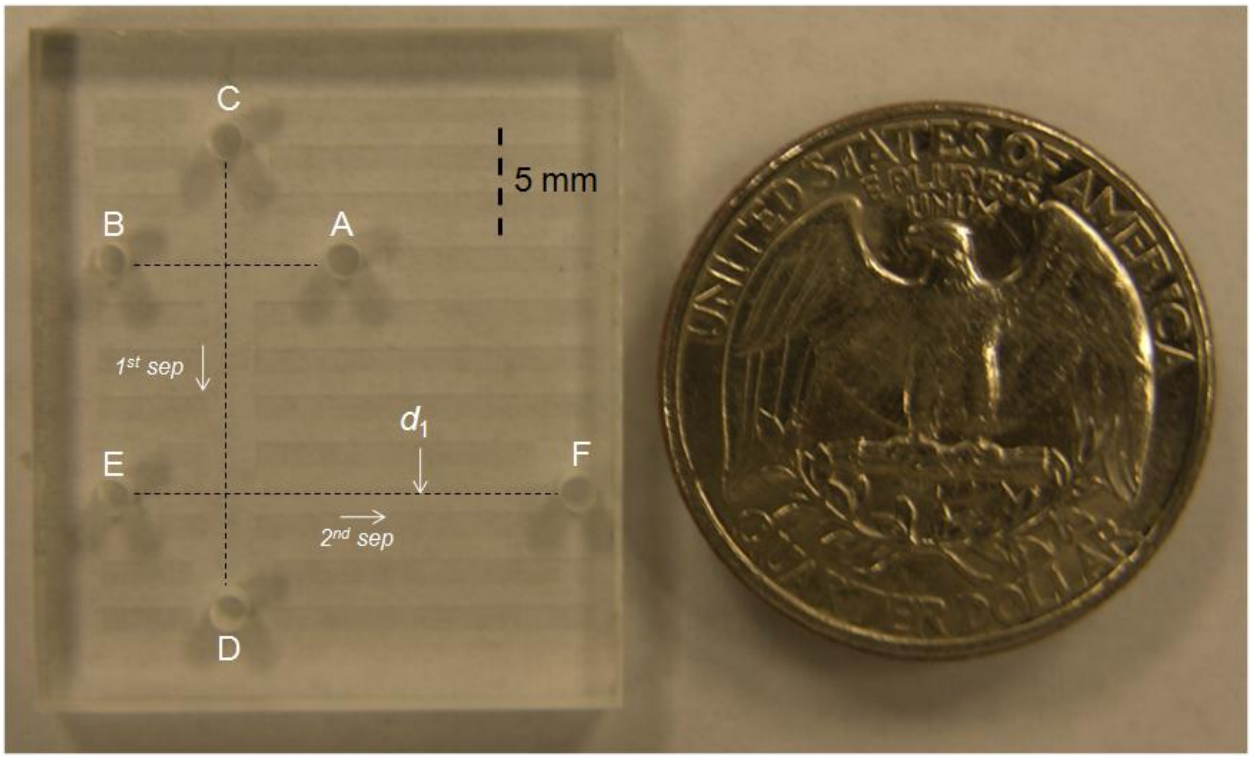

Figure 4.2 Photograph of the micro-electrophoresis chip used for the 2-D separations. The chip was fabricated in PMMA via hot-embossing from a lithographically prepared stainless steel molding tool. The channel width in all cases was 15 µm with a channel depth of ~30 µm. The solution reservoirs were; (A) sample reservoir; (B) sample waste reservoir; (C) SDS µ-CGE buffer reservoir; (D) SDS µ-CGE buffer waste reservoir; (E) MEKC or MEEKC buffer reservoir; (F) MEKC or MEEKC buffer waste reservoir. All reservoirs were mechanically drilled into the embossed substrate and were 2 mm in diameter. Platinum wires were used to apply high voltages to the reservoirs. For the SDS µ-CGE dimension, the injection and effective separation lengths were each 10 mm. The total separation channel length for a complete 2-D was 20 mm (i.e., 10 mm for both the 1st and 2nd dimensions). d_1 represents the LIF detection position for the 2-D separations.

4.2) was also 10 mm in length. The final device was assembled by thermal fusion bonding the molded piece to a 125-μm thick PMMA cover slip at 107°C in a convection oven for 15 min [30].

4.2.2 Laser-induced Fluorescence (LIF) Detection, Power Supply and Data Analysis

Fluorescence detection and data collection was accomplished using an in-house constructed LIF system and in-house written software. Details have been reported elsewhere [30]. Programmed high-voltage was applied to the reservoirs of the microchip with six independently controlled power supplies [30].

The software for data acquisition and control of the power supply was created using LabVIEW. Dye-labeled protein samples were first electrokinetically injected into the injection cross (A-B, Figure 4.2) by applying a positive potential at waste reservoir (B) while grounding the sample reservoir (A). Data were collected continuously from the start of the initial SDS μ-CGE after the injection step. SDS μ-CGE was initiated by applying a positive potential at the waste reservoir (D) and grounding reservoir C. In this particular case, proteins were sampled into the second dimension from the onset of the first dimension; therefore, proteins were allowed to separate in the second dimension after a 1 s electrophoretic run in the first dimension by applying a positive potential to reservoir E while grounding D. This 1 s separation in the first dimension transferred proteins into the second dimension for further separation. LIF was monitored on E-F at 10 mm (d_1) from the intersection of C-D and E-F (see Figure 4.2).

The 2-D protein landscapes were generated using ImageJ 1.34s software (National Institutes of Health, Bethesda, MD) by dividing the LIF temporal signals from each μ-MEEKC or μ-MEKC cycle and plotting the corresponding cycle with respect to the SDS μ-CGE axis [1, 13]. This process generated sets of 2-D separation data for the SDS μ-CGE × μ-MEEKC and SDS μ-CGE × μ-MEKC. We subsequently performed a student's t-test on the landscapes to determine statistical differences in the microchip 2-D techniques.

4.2.3 Emulsion Preparation, Protein Labeling and Purification

Solutions of heptanes (>99%), 1-butanol (>99%) and SDS powder were purchased from Sigma (St. Louis, MO). The separation buffer was prepared from 1.5 M Tris-HCl (Bio-Rad, Hercules, CA). Deionized water (18 MΩ) was obtained from an ultra-pure water system (Millipore, Milford, MA). Suitable amounts of heptane, 1-butanol and SDS powder were added to 12 mM Tris-HCl buffer at pH 8.5 to prepare the microemulsions for the MEEKC separation according to procedures reported in the literature [14, 31]. The solution was mixed by ultrasonification in a water bath for 30 min after which the solution was left to stand for 1 h at room temperature. The solution was filtered through a 0.2 µm Nylon-66 membrane syringe filter (Cole-Parmer Instrument Co., Vernon, IL) prior to use. It was important to ultrasonicate the solution adequately because the solution became turbid during standing at room temperature when the mixing step was insufficient [31]. However, when the preparation was done in the appropriate manner, the solution maintained a transparent appearance for several months at room temperature [32].

Soluble proteins were extracted from *E. coli* K12 (Bio-Rad) and were labeled with thiol reactive Alexa Fluor 633 dyes (Invitrogen, Carlsbad, CA) following the manufacturer's guidelines [1] after which the labeled proteins were purified using a gel filtration column (Millipore Corp., Billerica, MA). A total protein concentration determined by UV spectroscopy of ~40 nM was used for the separations. Samples were prepared in a buffer system composed of 12 mM Tris-HCl containing 0.1% w/v SDS at pH 8.5.

4.2.4 Electrophoretic Run Conditions

PMMA microfluidic devices were rinsed prior to each electrophoretic run with a solution of 2 mg/mL of methyl hydroxyethyl cellulose, MHEC (Fluka BioChemika, Switzerland), dissolved in 1X PBS buffer (pH 7.2) for electroosmotic flow (EOF) suppression [13]. All electrophoretic separations were carried out at ambient temperature in reverse mode (detection end anodic) for both SDS µ-CGE

and the MEEKC or MEKC dimensions. The SDS μ-CGE was performed using a seiving matrix consisting of SDS 14-200 (Beckman Coulter Inc., Fullerton, CA) mixed with 0.05% w/v MHEC. MEKC was conducted using 12 mM Tris-HCl containing 0.4% w/v SDS at pH 8.5 whereas MEEKC utilized 12 mM SDS, 8 mM heptane, 90 mM 1-butanol in 12 mM Tris-HCl and also 0.4% w/v SDS (pH 8.5). As a dynamic surface coating agent, MHEC at 0.05% w/v was added to both the MEKC and MEEKC separation buffers [13].

For the injection/separation scheme, 2-D separations were performed in channels A-B, C-D and E-F serving as injection, first dimension SDS μ-CGE and second dimension MEKC or MEEKC channels, respectively, and setting the LIF detection position at point d_1 (see Figure 4.2). Gel or run buffers were pressure filled into the channels after which reservoir A was replaced with the protein mixture while the rest of the reservoirs were filled with the running buffer. A 20 s clean up step was initially accomplished by applying +0.20 kV to reservoir A and grounding the other reservoirs (B - F, see Figure 4.1). Injection into the A-B channel was initiated by grounding the voltage to the sample reservoir (A, Figure 4.1) and applying a positive voltage (0.25 kV) to the waste reservoir (B, Figure 4.1) to fill the cross channel (points C - F were floated during injection). Following injection, a high positive voltage was switched to point D and point C was grounded (Figure 4.2). Then, pull back voltages (~10% of applied voltage to point D) were applied to the sample and waste reservoirs (A and B, see Figure 4.1). The electric field (E) used for SDS μ-CGE and the MEKC or MEEKC separations were 350 V/cm and 400 V/cm, respectively.

The 2-D separation was started by switching the high voltage applied to reservoir D (see Figure 4.1) to +0.70 kV and grounding reservoir C for 1 s. This allowed the lowest molecular weight proteins to reach the end of the first dimension. Reservoirs A and B were kept at +0.07 kV while reservoirs E and F were floated during the initial 1 s run. After that, point E was grounded and point F was set to +0.80 kV for 10 s allowing for the MEKC or MEEKC separation of the transferred proteins to occur.

Subsequently, 1 s SDS μ-CGE runs/injections from the first dimension into the second dimension and a subsequent 10 s MEKC or MEEKC separations were iteratively executed for nineteen more cycles making the total number of MEEKC or MEKC cycles equal to 20. During each MEKC or MEEKC cycle, effluents from the SDS μ-CGE dimension were parked by floating reservoirs C and D. MEKC or MEEKC separations were paused for 1 s after each 10 s MEKC or MEEKC separation by floating reservoirs E and F during which the SDS μ-CGE dimension was again run at E = 350 V/cm for that 1 s time, which resulted in the movement of proteins through the SDS μ-CGE dimension. This movement in channel C-D provided a new sample plug into the second dimension. In this serially implemented 2-D separation, the transfer/separation cycles were repeated until the entire separation was completed.

4.3 Results and Discussions

4.3.1 Representation of Proteins

Tremendous progress has been made towards understanding the *E. coli* proteome since O'Farrell published a 2-D IEF-PAGE analysis of the *E. coli* proteome in 1975 [34]. The protein sample used herein was a soluble extract from *E. coli* K12 W110, whose genome has been sequenced with a total of 4,226 proteins predicted for its proteome (www.ncbi.nlm.nih.gov). Considering that cytosolic proteins constitute 61.46% of the *E. coli* proteome [33], the cytosolic protein content was estimated to be 2,597. But since only those soluble proteins containing thiol groups were selectively labeled, it was important to ascertain the sub-population of cysteine containing proteins. We estimated that approximately 2,078 (80% of the cytosolic proteome) proteins contain at least one cysteine amino acid residue [35].

In the cytoplasm, cytosolic cysteines are often maintained in the thiol form by glutaredoxin and thioredoxin enzymes [35]. Nonetheless, cystines are still present because 6% of the entire *E. coli* K12 proteome contains disulfide linkages [36]; therefore, it was necessary to reduce the proteins prior to analysis (see section 4.2). Based on a 1.1% likelihood for the occurrence of cysteines on average in the

E. coli proteome [35], which consists of 340 amino acids [37], we deduced that between 3 - 4 sites were available for thiol labeling in each protein.

4.3.2 Start Time for Sampling into the Second Dimension

In our previous 2-D report [1], the second dimension was initiated close to the migration time of the first protein peak produced from the first SDS µ-CGE dimension, which amounted to a run time in the first dimension of 10 s. In the present work, we started the second dimension after 1 s of electrophoretic run time due to the shorter column length used herein compared to our previous reports and the fact that the *E. coli* proteome contains proteins with as low as 10 amino acid residues [37] (~1,367 Da). The short migration time (MT) of this relatively small protein can be verified using Equation 4.1 [13] to be less than 1 s. The migration time of the largest protein (~970 amino acids [37]) was also ascertained with equation 4.1 to be 105.19 s, but Equation 4.1 was generated for a 1-D SDS µ-CGE microchip device with a 40 mm total channel length and 30 mm effective length [13].

$$\log (MW) = 1.59 \times 10^{-2} MT + 3.45 \quad (4.1)$$

where MW is the protein molecular weight and MT is the migration time.

In the present case, the microchip's total (L) and effective (l) lengths for the first dimension were 20 mm and 10 mm, respectively; therefore, the MT for the largest protein was estimated to be 17.53 s using Equation 4.2 [38] for the present microchip.

$$MT/MT_1 = lL/l_1L_1 \quad (4.2)$$

where MT_1 is the estimated migration time (105.19 s) of the largest protein based on the previous chip [13], which possessed a 40 mm total length (L_1) and a 30 mm effective length (l_1).

By initiating the second dimension separation after a 1 s separation time in the first dimension, the need to perform a 1-D SDS µ-CGE to determine the migration time of the first peak in the first

dimension was negated. Eliminating 1-D SDS μ-CGE separations and starting the second dimension almost at the onset of the separation effectively reduced the total analysis time. Furthermore, the net negative charge (-2) of the dye appended to each protein should lower the migration time because the separation was performed in reverse polarity (detector end anodic). Conversely, the mass of the dye (~1,300 Da) should increase the MT. Nonetheless, the net mobility shift introduced by the dye on the protein was negligible [1] (Also see section 3.3.3).

4.3.3 Height Equivalent of a Theoretical Plate

A 1 s separation time in the first dimension and a 10 s separation time in the MEKC or MEEKC second dimension were implemented for a total cycle number of 20. This resulted in a total development of 220 s (11 s × 20). The total number of cycles provided an electrophoresis development time in the first dimension of 20 s, which provided sufficient time to sample every *E. coli* protein (including large proteins, see section 4.3.2) into the second dimension. The contributions to band broadening during these separations are shown in Equation 4.3 for the total plate height (H_{TOT});

$$H_{TOT} = H_D + H_{inj} + H_{oth} \quad (4.3)$$

where H_D, H_{inj}, and H_{oth} are contributions to the plate height from longitudinal diffusion, injection plug length, and other factors, respectively.

The height equivalent to a theoretical plate for longitudinal diffusion only (H_D) of the 1-D SDS μ-CGE dimension was calculated and compared to that value to H_{TOT} secured from the complete 2-D separation. A representative diffusion coefficient for proteins in a sieving matrix as used herein was taken as ~10^{-8} cm^2 s^{-1}, which is the measured diffusion coefficient of cytochrome C in polyacrylamides [39], resulting in $H_D = 4.4 \times 10^{-6}$ cm ($H_D = 2Dt/L$; t = time; L = column length, cm). The number of plates for a typical band migrating from the 2-D separation was 2.6×10^5 (see Figure 4.3), resulting in $H_{TOT} = 7.7 \times 10^{-6}$ cm ($H_{TOT} = L/N$; L = total effective length for 2-D separation, i.e., 20 mm).

Therefore, the diffusional component to H_{TOT} was calculated to be approximately 57%. For 20 10 s MEKC cycles, which represents the parking time (200 s), and a total separation time of 220 s, the percent contribution of diffusional spreading during the parking phases of the 2-D separation to H_D is roughly 91% or 4.0×10^{-6} cm.

Because shorter separation channels were used, we were also interested in ascertaining the contributions to the total H_{TOT} from injection or extra column variances. The injection volume (V_{inj}) of 45 pL for the present chip was significantly less than the total column volume (V_{TOT}) of 15 nL. $V_{inj} = L \times W \times D = 30\ \mu m \times 30\ \mu m \times 50\ \mu m$; where L, W, and D are the length, width and depth of the injection plug, respectively, and $V_{TOT} = L \times W \times D = 10\ mm \times 30\ \mu m \times 50\ \mu m$; where L, W, and D are the length, width, and depth of the effective separation channel, respectively). Also, H_{inj} was found to be less than 1% of H_{TOT} or 3.8×10^{-7} cm ($H_{inj} = l_{inj}^2/12l$; l_{inj} = length of injection plug (30 µm). Given an injection volume of 45 pL and a total protein concentration of ~40 nM for *E. coli* proteins, a total mass amount of ~8.3×10^{-14} g was analyzed. The average protein Mw was taken to be 46 kDa considering an average size of 340 amino acids per protein [37] and an average amino acid Mw of 136.7 Da.

While we were able to demonstrate ultra-fast separations and also negate the need to perform a 1-D separation of the protein sample, we however lost information pertaining to how many times one protein peak was sampled from the first dimension into the second dimension.

4.3.4 SDS µ-CGE × MEEKC

SDS gel electrophoresis has proven to be a valuable separation platform for proteome analyses due to the ability to sort the protein components on the basis of their molecular weights [40-42]. In addition, when the gel formulation is properly selected, SDS gel electrophoresis can provide efficient separations over relatively short column lengths [43]. Here, we focused on coupling SDS µ-CGE to a MEEKC dimension to perform 2-D separations of intact proteins using short separation lengths to

generate high protein spot production rates. Separation of compounds in MEEKC is based upon both a partitioning process between the microemulsion droplets and the water phase as well as differences in their electrophoretic mobilities [44, 45]. Manipulation of the microemulsion phase can influence the separation performance [20, 22, 31, 44-47]. Ionized macromolecules, such as proteins, possess very low affinity for the anionic surface phase of emulsion droplets [26].

The separation of large molecules can potentially be more feasible in MEEKC than MEKC because they can better partition into the core phase of the microemulsion droplet compared to micelles, which are typically used for MEKC and have a much smaller hydrophobic core [26] (hydrophobic core radius ~17 Å for SDS micelles [48]). On the other hand, the size of the MEEKC droplet core is up to 100 Å; hence, a higher solubilization capacity are possessed by emulsion droplets, which is further enhanced due to the "softness" of the hydrophobic oil making it more penetrable compared to a micellar surface [28]. The end result is that large, hydrophobic proteins that would normally not partition well into a micelle core may partition into the oil phase of a droplet. Furthermore, MEEKC can provide an increased rate of mass transfer and a wider migration range due to the increased core size [28]. By analyzing data obtained from profiling fluorescent dye labeled *E. coli* proteins using 2-D SDS μ-CGE × MEEKC with ImageJ processing, a protein 2-D contour map with a corresponding protein landscape profile was obtained (see Figure 4.3) with an average (n = 3) peak capacity of 481 ±18, which was obtained by dividing the total pixel area in the image of 90,000 pixels by an average spot size of 187 ±7 pixels. Also, a typical 2-D image provided a total number of spots of 103 ± 12. The results were compared to results from a similar separation that was carried out with a microchip 2-D SDS μ-CGE × MEKC (see section 4.3.6).

4.3.5 Orthogonality of SDS μ-CGE × MEEKC

We have previously shown MEKC to be orthogonal to SDS gel separation [13]. Though similar, MEEKC results in better resolution compared to MEKC [18]. For this reason, we cannot

assume that the two separation techniques have similar separation mechanisms. Therefore, we needed to determine the orthogonality between the SDS gel and MEEKC dimensions in order to assure that the 2-D separation operates properly. To determine orthogonality [13] between the SDS μ-CGE and MEEKC dimensions, we divided the 2-D image obtained from a typical SDS μ-CGE and MEEKC separation as shown in Figure 4.3 into 100 equal bins (i.e., 10 × 10 bin matrix) as an approximation of the 103 protein spots that was counted using the ImageJ software (see section 4.3.4; also see Figure 4.3).

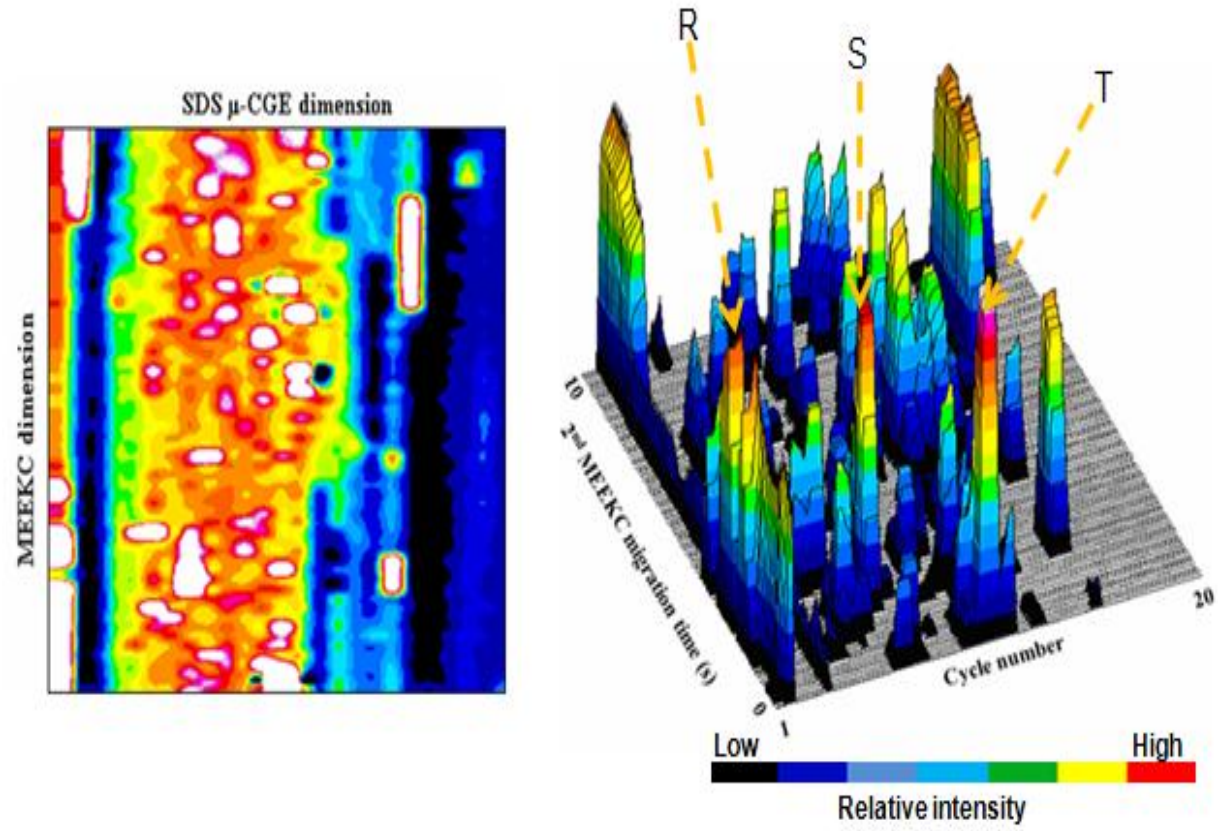

Figure 4.3 Left: 2-D contour image for the microchip 2-D SDS μ-CGE × MEEKC profile of a protein mixture isolated from *E. coli*. Fluorescently-labeled *E. coli* proteins were placed into reservoir A of the chip (see Figure 4.1) and electrokinetically injected into the separation channel at 200 V/cm. The 2-D SDS μ-CGE and MEEKC electrophoresis dimensions were performed at 350 V/cm and 400 V/cm, respectively. A 1 s separation time in the first dimension was allowed prior to performing a set of serial 10 s MEEKC runs. A total of 20 MEEKC cycles was used with a 1 s transfer time from the first into the second dimension**.** Right: Corresponding 3-D landscape image for the microchip 2-D SDS μ-CGE × MEEKC contour image shown on the left. The most intense peaks in the 2-D trace have been arbitrarily assigned letters R, S and T with T being the most intense peak followed by R and then S.

The total number of bins should be equal to number of protein spots generated by the 2-D technique [13]. Forty seven of the bins were determined to be unoccupied and by using Equation 4.5 an orthogonality of 67 (±4) % (n = 3) was calculated.

$$O = (\sum bins - \sqrt{P_{max}})/0.63\ P_{max} \quad (4.5)$$

where $\sum bins$ = number of bins in the 2-D image containing protein spots and P_{max} = the sum of all bins.

4.3.6 SDS µ-CGE × MEEKC vs. SDS µ-CGE × MEKC

In the SDS µ-CGE × MEEKC and SDS µ-CGE × MEKC 2-D separations conducted herein, identical sample, electric fields, buffer pH, injection times, cycle numbers and total separation times were employed except that the second dimension emulsion buffer in the former was replaced with a micellar buffer for the latter. A protein 2-D image with a corresponding profile was also generated for SDS µ-CGE × MEKC (Figure 4.4). An average (n = 3) peak capacity of 332 ±17 was calculated from a total pixel area of 90,000 pixels and an average spot size of 271 ±13 pixels.

We performed a simple student's *t*-test on the various separation metrics to determine if there were statistical differences between the two techniques in terms of these metrics. We observed a 45% increase ($p < 0.0005$) in peak capacity by switching the buffers from a micellar phase to one containing oil emulsions in the second dimension and the total time to generate a full 2-D profile was only 220 s for both SDS µ-CGE × MEEKC mode and SDS µ-CGE × MEKC mode. A production rate of 91 spots/min was associated with the microchip SDS µ-CGE × MEKC mode, which was less than 131 spots/min associated with the same microchip that utilized MEEKC as the second dimension instead of MEKC. The number of spots generated by the microchip 2-D, which employed oil emulsion, was 140% ($p = 0.005$) more compared to the microchip 2-D separation using micelles (103 ± 12 versus 43 ± 6 spots). We attribute this significant improvement in spot generation and peak capacity to the better plate numbers provided by the emulsion-based buffer.

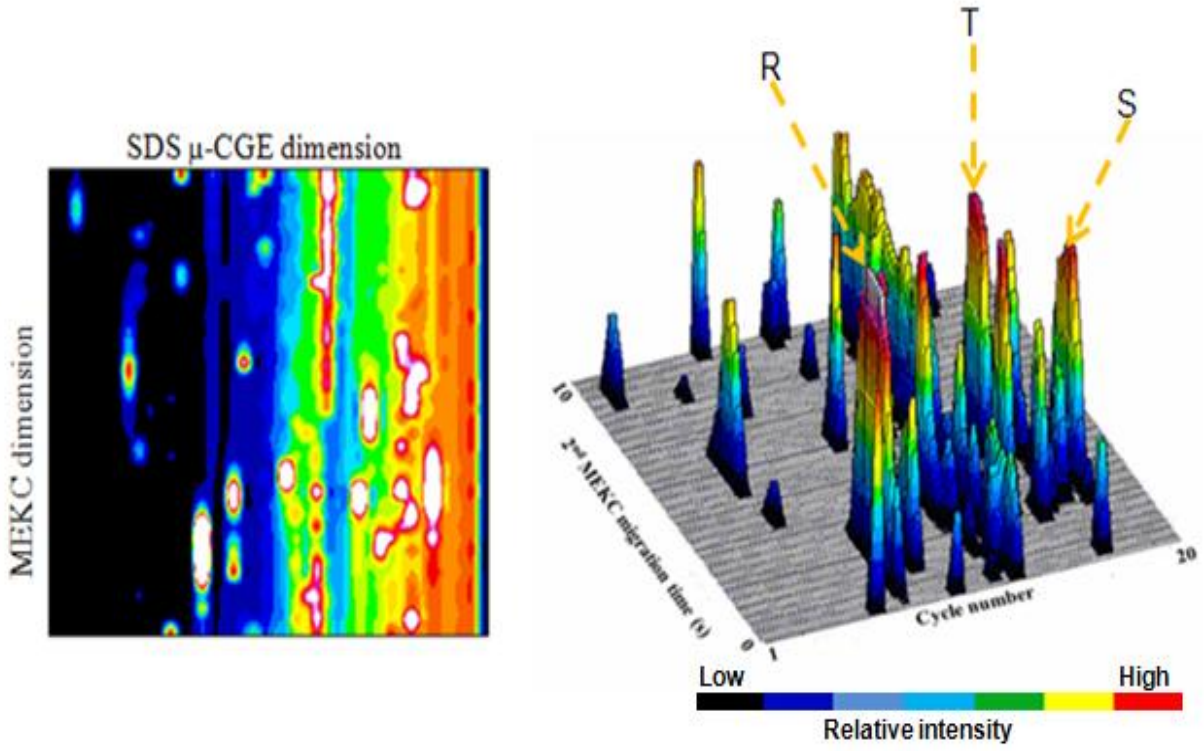

Figure 4.4 Left: 2-D contour image for the microchip 2-D SDS µ-CGE × MEKC separation of a protein mixture isolated from *E. coli*. The fluorescently-labeled *E. coli* protein sample was placed into reservoir A (see Figure 4.1) and electrokinetically injected into the separation channel at 200 V/cm. The run conditions were identical to those listed in Figure 4.3. Right: Corresponding 3-D landscape image for the microchip 2-D SDS µ-CGE × MEKC contour image shown on the left. The most intense peaks in the 2-D trace have been arbitrarily assigned letters R, S and T with T being the most intense peak followed by R and then S.

About 2,077 proteins of the *E. coli* protein sample contain at least one cysteine amino acid (see section 4.3.1), but we only were able to produce 103 spots using SDS µ-CGE × MEEKC (see Figure 4.3), which is well below the expected number of proteins associated with this proteome. We attribute this observation to several facts including: (i) the low expression levels of certain proteins in the proteome making them difficult to detect above baseline; (ii) the fact that strong RNA binding proteins may have been eliminated during the sample preparation protocol in an effort to remove nucleic acids [49]; (iii) the low occurrence of cysteine (0.19%) in some higher abundant ribosomal proteins [35] may have resulted in some proteins going undetected due to insufficient labeling and (iv)

the limited peak capacity to resolve every protein spot. A summary of the separation conditions and results of both microchip 2-D techniques are presented in Table 4.1.

4.3.7 Reproducibility of the 2-D Separations

Oil emulsions are known to generate high EOFs, especially in borate buffer [50], and the EOF ($2.95 \pm 0.95 \times 10^{-4}$ cm^2/Vs) in pristine PMMA chips can vary from chip-to-chip (~32% RSD) [51]. The variability in the EOF can result in variations in peak migration times. In order to reduce the EOF

Table 4.1. Summary of microchip 2-D separation results. The standard deviations were obtained for n = 3 experiments for each microchip 2-D method.

2-D Separation: SDS µ-CGE with	Number of spots generated	Plate Number (N)	2-D Peak Capacity	2-D Separation Time (s)	Production Rate (spots/min)
MEKC	43± 6	2.8×10^4	332 ± 17	220	91
MEEKC	103 ± 12	4.6×10^4	481 ± 18	220	131

the chip walls were dynamically coated by adding MHEC to the running buffer, which has been shown to be effective in suppressing the EOF in PMMA microchips [13]. To evaluate reproducibility, we measured the migration times for the three most intense peaks from three different chip separations. The calculated average migration times for these bands using the 2-D SDS µ-CGE × MEEKC separation were found to be 15 s (RSD 3.9%), 58 s (RSD 14.1%) and 112 s (RSD 7.5%) for protein peaks R, S, and T, respectively, with an average RSD value of 8.5%, which is comparable to previously reported values of 4.8% for SDS µ-CGE × MEKC [1] and 4.1% for microchip IEF × SDS CGE [52].

4.3.8 System Efficacy and Improvement in Peak Capacity

A peak capacity of ~500 was expected for a 20 mm effective length chip based on the total separation length and our previous results [13]. However, the 2-D SDS µ-CGE × MEEKC and the 2-D SDS µ-CGE × MEKC yielded peak capacities of 481 ±18 and 332 ±17, respectively, below the anticipated peak capacity based on the effective column length. Better peak capacity was achieved for

the SDS µ-CGE × MEEKC because of higher N value compared to the SDS µ-CGE × MEKC technique. $N = 4.6 \times 10^4$ for SDS µ-CGE × MEEKC (or $N/m = 2.3 \times 10^7$; $L_{eff} = 20$ mm) and $N = 2.8 \times 10^4$ for SDS µ-CGE × MEKC (or $N/m = 1.4 \times 10^7$; $L_{eff} = 20$ mm), compared to 6.2×10^5 (or $N/m = 5.6 \times 10^6$; $L_{eff} = 110$ mm) that was previously reported [13]. The gel used for this set of experiments was a linear polymer that forms a dynamic polymer network by entanglement, which serves as s sieving matrix during electrophoresis. To increase peak capacity while maintaining shorter separation channels, a crosslinked polymer instead of linear polymer could be used in the first SDS µ-CGE dimension. Solute diffusion is less in crosslinked polymers than in uncrosslinked polymers due to reduced convective phenomenon in the case of the former compared to the latter. This ultimately leads to less band broadening and hence higher plate number because of minimized longitudinal spreading since the diffusion of proteins within crosslinked gels would be lower compared to linear gels.

4.3.9 Proteins Presented in the 2-D Profiles

The *E. coli* has been the subject of several studies and as a result, a large amount of information on its proteome can be found in the literature. Ishihama and co-workers [33] have carried out a protein abundance profiling of the *E. coli* cytosol in which the authors assigned various characteristics including average length (number of amino acids) and hydrophobicity (in the Kyte-Doolittle scale) to high and low abundant proteins present in *E. coli* K12 MC4100. The Kyte-Doolittle scale is used to assign hydrophobic regions in proteins wherein more positive values are designated to be more hydrophobic.

Unlike the mammalian serum proteome where a single protein (albumin) is the most abundant protein accounting for ~55% of the total protein mass of serum [1], multiple proteins are highly abundant in the *E. coli* proteome. Up to 21% percent of the *E. coli* protein mass content are ribosomal in nature and consists of ~54 different proteins present in equal abundance (one copy per ribosome) plus two that are present as dimers making a total of 56 proteins [49]. Furthermore, highly abundant *E.*

coli proteins have been found to be shorter in length and less hydrophobic than low abundant proteins with average lengths and hydrophobicities of 309 amino acids/-0.25 (Kyte-Doolittle scale) and 386 amino acids/-0.20, respectively [33] (see section 4.2.3). It is our opinion that the intense peaks observed in the microchip 2-D profiles (see section 4.3.7) may contain high abundant ribosomal proteins in *E. coli* on the 2-D profiles since these proteins are highly expressed in *E. coli.*

During electrophoresis, proteins with shorter lengths are expected to migrate faster in the first dimension where the separation operates based on protein size differences. Less hydrophobic proteins are expected to interact less with the microemulsions because they would generally possess lower partition coefficients and would therefore spend more time in the aqueous phase where they would migrate according to their electrophoretic mobilities. Considering that high abundant proteins present in *E. coil* possess an average length of 309 amino acids [33], we calculated the migration time, in the first dimension, of a 309 amino acid using Equations 4.1 and 4.2 to be ~12 s. This means that on the average that high abundant proteins are expected to be sampled into the second dimension after migrating ~12 s in the first dimension.

Interestingly, the migration order of the most intense peaks in the SDS μ-CGE × MEKC trace (see Figure 4.4) was different from what was observed for SDS μ-CGE × MEEKC (see Figure 4.3). In the case of SDS μ-CGE × MEKC and relative to SDS μ-CGE × MEEKC, protein peak R migrated around 72 s, followed by protein peak T (112 s), and lastly by protein peak S, which migrated at 124 s. In other words, the order of migration changed from R, S, and T for SDS μ-CGE × MEEKC to R, T, and S for SDS μ-CGE × MEKC. This is not surprising because changes in migration order is commonly observed when analytes are separated in MEEKC compared to MEKC [19, 53]. It is possible that peaks R, S and T and any other peaks on the profiles for that matter are composed of multiple proteins which were not resolved due limited peak capacity. Accurate identification of peaks on the profile can be accurately obtained by MS, and as discussed in Chapter 1, MS analysis can be

coupled to a separation unit, such as the one presented here, but this is beyond the scope of this chapter.

4.4 Conclusions

We have developed a 2-D platform that provides relatively high spot production rates and reasonable peak capacities in spite of the fact that short separation lengths were employed (10 mm in each dimension of this 2-D system). An average peak capacity of 481 was obtained by coupling MEEKC to SDS μ-CGE requiring only a 220 s development time. The 2-D separation using MEEKC coupled to SDS μ-CGE had the advantage of generating a higher peak capacity compared to MEKC coupled to SDS μ-CGE. Generation of a higher peak capacity was attributed to better plate numbers afforded by the MEEKC phase. Furthermore, better resolution was obtained in the case of SDS μ-CGE × MEEKC compared to SDS μ-CGE × MEKC due to favorable selectivity and better partitioning of protein into oil droplets. However, in order to achieve ultra-fast separations, short column lengths with effective lengths of 10 mm were used for both dimensions. Many applications require ultra-fast analysis, such as in pharmaceutical formulations, in monitoring short-lived bio-chemical events and in performing high throughput studies. The peak capacity of this present system can be improved by using crosslinked polymer gels in the first SDS μ-CGE dimension instead of linear polymer gels while maintaining the short columns that is required for ultra-fast separations. Because of the difficulty in filling highly viscous crosslinked gels within the microchannels, photo-polymerization of crosslink gels in the first dimension of polymer chips appears to be a better alternative.

While fluorescently labeling the proteins by targeting only the thiol groups within the proteins provided an exquisite detection scheme, appending dyes onto protein bio-molecules can be laborious and time consuming. Also, impurities can be introduced into the sample during the labeling process, and the dyes constituted an additional cost to the analytical process. To mitigate some of the drawbacks associated with fluorescent labeling, we are developing a label-free detection scheme as an

alternative. To this end, we are fabricating 2-D separation devices with integrated on-chip electrodes both at the end of the first and second dimensions to enable us perform a heart-cutting transfer of protein plugs from the first (output) dimension into second dimension. Not only does this conductivity-based heart-cutting method allow us to perform a label-free protein analysis, it also gives us better control with the transfer of protein bands from the first dimension into the second - a fraction of a protein peak migrating at the end of the first dimension can be transferred into the second dimension in a controlled fashion using the electrode sensors at the end of the first dimension. This capability allows us to keep the sampling efficiency high. Furthermore, this new approach will effectively alleviate the issue of over sampling that plagues our current technique [1, 13], in which a single band from the first dimension was injected into the second band multiple times.

4.5 References

[1] Osiri, J. K., Shadpour, H., Park, S., Snowden, B., Chen, Z-Y., Soper, S. A., *Electrophoresis* 2008, *29*, 4984 - 4992

[2] Herr, A. E., Molho, J. I., Drouvalakis, K. A., Mikkelsen, J. C., *et al.*, *Anal. Chem.* 2003, *75*, 1180-1187.

[3] Li, Y., Buch, J. S., Rosenberger, F., DeVoe, D. L., Lee, C. S., *Anal. Chem.* 2004, *76*, 742-748.

[4] Chen, X. X., Wu, H. K., Mao, C. D., Whitesides, G. M., *Anal. Chem.* 2002, *74*, 1772-1778.

[5] Emrich, C. A., Medintz, I. L., Chu, W. K., Mathies, R. A., *Analytical Chemistry* 2007, *79*, 7360-7366.

[6] Yang, S., Liu, J. K., Lee, C. S., Devoe, D. L., *Lab on a Chip* 2009, *9*, 592-599.

[7] Monnig, C. A., Jorgenson, J. W., *Anal. Chem.* 1991, *63*, 802-807.

[8] Moore, A. W., Jorgenson, J. W., *Anal. Chem.* 1993, *65*, 3550-3560.

[9] Gottschlich, N., Jacobson, S. C., Culbertson, C. T., Ramsey, J. M., *Anal. Chem.* 2001, *73*, 2669-2674.

[10] Ramsey, J. D., Jacobson, S. C., Culbertson, C. T., Ramsey, J. M., *Anal. Chem.* 2003, *75*, 3758-3764.

[11] Rocklin, R. D., Ramsey, R. S., Ramsey, J. M., *Anal. Chem.* 2000, *72*, 5244-5249.

[12] Zhang, T., Fang, Q., Du, W. B., Fu, J. L., *Anal. Chem.* 2009, *81*, 3693-3698.

[13] Shadpour, H., Soper, S. A., *Anal. Chem.* 2006, *78*, 3519-3527.

[14] Watarai, H., *Chemistry Letters* 1991, 391-394.

[15] Hansen, S. H., *Electrophoresis* 2003, *24*, 3900-3907.

[16] Timerbaev, A. R., Vasylenko, O. O., Foteeva, L. S., Rudnev, A. V., *et al.*, *Journal of Separation Science* 2007, *30*, 399-406.

[17] Xie, J. P., Chen, X. F., Zhang, J. Y., Liu, J. Q., *et al.*, *Journal of Pharmaceutical and Biomedical Analysis* 2004, *36*, 1-8.

[18] Zhou, G. H., Luo, G. A., Zhang, X. D., *Journal of Chromatography A* 1999, *853*, 277-284.

[19] Vomastova, L., Miksik, I., Deyl, Z., *Journal of Chromatography, B: Biomedical Applications* 1996, *681*, 107-113.

[20] Boso, R. L., Bellini, M. S., Miksik, I., Deyl, Z., *Journal of Chromatography, A* 1995, *709*, 11-20.

[21] Li, G., Hu, Z., *Analyst (Cambridge, United Kingdom)* 1998, *123*, 1501-1505.

[22] Pedersen-Bjergaard, S., Gabel-Jensen, C., Honore Hansen, S., *Journal of Chromatography, A* 2000, *897*, 375-381.

[23] Mrestani, Y., El-Mokdad, N., Ruettinger, H. H., Neubert, R., *Electrophoresis* 1998, *19*, 2895-2899.

[24] Debusschere, L., Demesmay, C., Rocca, J. L., Lachatre, G., Lofti, H., *Journal of Chromatography, A* 1997, *779*, 227-233.

[25] Hilder, E. F., Klampfl, C. W., Buchberger, W., Haddad, P. R., *Journal of Chromatography, A* 2001, *922*, 293-302.

[26] Siren, H., Karttunen, A., *Journal of Chromatography, B: Analytical Technologies in the Biomedical and Life Sciences* 2003, *783*, 113-124.

[27] Poouthree, K., Soonthorntantikul, W., Leepipatpiboon, N., Petsom, A., Nhujak, T., *Electrophoresis* 2007, *28*, 3705-3711.

[28] Huie, C. W., *Electrophoresis* 2006, *27*, 60-75.

[29] Hupert, M., Guy, J., Llopis, S., Shadpour, H., *et al.*, *Microfluidics and Nanofluidics* 2006, *ASAP*.

[30] Shadpour, H., Musyimi, H., Chen, J., Soper, S. A., *Journal of Chromatography, A* 2006, *1111*, 238-251.

[31] Terabe, S., Matsubara, N., Ishihama, Y., Okada, Y., *Journal of Chromatography* 1992, *608*, 23-29.

[32] Ishihama, Y., Oda, Y., Uchikawa, K., Asakawa, N., *Analytical Chemistry* 1995, *67*, 1588-1595.

[33] Ishihama, Y., Schmidt, T., Rappsilber, J., Mann, M., *et al.*, *Bmc Genomics* 2008, *9*.

[34] O'Farrell, P. H., *Biol Chem* 1975, 4007-4021.

[35] Miseta, A., Csutora, P., *Molecular Biology and Evolution* 2000, *17*, 1232-1239.

[36] Martelli, P. L., Fariselli, P., Casadio, R; , *Proteomics* 2004, *4*, 1665 - 1671.

[37] Liang, P., Labedan, B., Riley, M., *Physiological Genomics* 2002, *9*, 15-26.

[38] Wan, H. B., Liu, J., Ang, K. C., Li, S. F. Y., *Talanta* 1998, *45*, 663-671.

[39] Lewus, R. K., Carta, G., *Industrial & Engineering Chemistry Research* 2001, *40*, 1548-1558.

[40] Raymond, S., Weintraub, L., *Science (Washington, DC, United States)* 1959, *130*, 711.

[41] Shapiro, A. L., Vinuela, E., Maizel, J. V., Jr., *Biochemical and Biophysical Research Communications* 1967, *28*, 815-820.

[42] Laemmli, U. K., *Nature (London, United Kingdom)* 1970, *227*, 680-685.

[43] Herr, A. E., Singh, A. K., *Analytical Chemistry* 2004, *76*, 4727-4733.

[44] Altria, K. D., *Journal of Chromatography, A* 1999, *844*, 371-386.

[45] Altria, K. D., Clark, B. J., Mahuzier, P. E., *Chromatographia* 2000, *52*, 758-768.

[46] Fu, X., Lu, J., Zhu, A., *Journal of Chromatography, A* 1996, *735*, 353-356.

[47] Miola, M. F., Snowden, M. J., Altria, K. D., *Journal of Pharmaceutical and Biomedical Analysis* 1998, *18*, 785-797.

[48] Varela, A. S., Macho, M. I. S., Gonzalez, A. G., *Colloid Polym. Sci.* 1995, *273*, 876-880.

[49] Arnold, R. J., Reilly, J. P., *Analytical Biochemistry* 1999, *269*, 105-112.

[50] Ryan, R., Donegan, S., Power, J., McEvoy, E., Altria, K., *Electrophoresis* 2009, *30*, 65-82.

[51] Llopis, S. L., Osiri, J., Soper, S. A., *Electrophoresis* 2007, *28*, 984-993.

[52] Liu, J. K., Yang, S., Lee, C. S., Devoe, D. L., *Electrophoresis* 2008, *29*, 2241-2250.

[53] Terabe, S., Matsubara, N., Ishihama, Y., Okada, Y., Elsevier Science Bv 1992, pp. 23-29.

5 Cyclic Olefin Copolymer Microfabricated Chip with Integrated SU-8 Electrodes

5.1 Introduction

Many biological applications require the biological analyte to be labeled with some sort of dye for fluorescence detection or visualization. In flow cytometry, cells are often labeled with fluorescent dyes attached to antibodies that target integral membrane proteins (antigens) found on particular cells for their visualization and/or detection as well. In proteomics and genomics, proteins and deoxyribonucleic acids (DNAs) are in most cases appended with labels, such as fluorescent dyes or electrophores, so that they can be monitored by fluorescence or electrochemistry, respectively, for their analysis due to the fact that in many cases, ultra-sensitive analysis is required and the intrinsic fluorescence or electrochemical properties of these targets is not adequate for high sensitivity detection. This was demonstrated in Chapter 2 for DNAs and Chapters 3 and 4 for proteins. While covalent labeling of targets provides exquisite detection limits and sensitivity, the use of labels has its demerits, namely, preparing and appending the labels onto the target biomolecules or cells, which can be laborious and time consuming, the inability to label targets at low concentrations, impurities that can be introduced into the sample during the labeling process, the labels can be expensive and can add bias to the analytical process due to the selective labeling of only a subset of the entire sample population.

To mitigate some of the drawbacks associated with labeling, conductivity detection has been considered as an alternative due to the fact that it is a universal detection protocol and can potentially detect any target. A sensitive label-free conductivity readout modality has been developed by several different research groups [1] to detect various analytes, such as inorganic anions and oxalate in atmospheric aerosol [2], salts such as NaCl and KCl [3], bio-molecules, including amino acids, proteins and DNA fragments [4], and cells, such as circulating tumor cells (CTC) from whole blood [5]. In the case of the biomolecular and cell applications, cylindrical platinum (Pt) wires were

integrated with a poly (methyl methacrylate), PMMA, microfluidic device. The diameters of the Pt wires were 127 μm and 75 μm for the detection of biomolecules and CTCs, whereas the electrode gaps were 20 μm and 50 μm, respectively. The authors reported a mass detection limit of 3.4 amol [4] for amino acids and demonstrated the conductivity system's capability to detect a single CTC [5] from a whole blood sample. The performance of this type of detection scheme is governed by equation 5.1;

$$G = (\lambda_+ + \lambda_-)\, C / 1000K \qquad (5.1)$$

where G is the conductivity signal in S (siemens), λ_+ and λ_- are the limiting ionic conductances of cations and anions in S cm^2 $equiv^{-1}$; C is the concentration in M, and K is the cell constant (K = L/A); where L is the distance between the electrode pair and A the area of the electrodes. A high conductance buffer would generate high background conductivity, therefore, a buffer with a very low conductivity is preferred as this would improve the analyte limit-of-detection (LOD). Also, smaller electrode pair spacings and larger electrode areas translate into better detection limits of the system according to Equation 5.1. An advantage of utilizing this detection scheme is the inherent fact that conductivity detectors are not mass sensitive, but concentration sensitive [6], therefore, electrodes can be scaled down in size making it amenable for the fabrication of miniaturized devices without sacrificing detection limits.

Pt wires possess rigid sizes and shapes, which cannot be easily manipulated. In fact, in previous reports using Pt wires as conductivity sensors, the electrodes were inserted into the device by hand making it problematic to fabricate high density arrays of conductivity sensors for multi-channel chips and also, it become problematic to reduce the electrode gap and electrode size to improve detection limits. This limitation places enormous challenges on the fabrication of devices with integrated electrodes as sensors. For example, in order to be adequately sensitive, it was demonstrated that electrode pair spacing and diameters should be comparable to the diameter of the cell of interest to be detected [5]. This suggests that in order to detect *E. coli* cells for example, which are ~2 μm long and

~0.5 μm in diameter, Pt wires and electrode spacing comparable to the dimension of the *E. coli* cells should be used. This, in practice is not feasible considering the size and brittleness of Pt electrodes [5].

In a recent report [7], side-wall vertical electrodes in which lateral and uniform electrical fields that generated magneto-hydrodynamic forces were used to control the movement of cells within microchannels, where non-uniform electric fields generated dielectrophoretic forces that were used to focus micro-beads. In that work, 30 to 40 μm high Au electrodes were electroplated onto a UV cross-linked SU-8 platform. While the authors demonstrated a number of applications of these microdevices including cell sorting, pumping, sensing, and separations, the device fabrication process involved several steps (at least eight) with the fabricated device comprising three (top, middle and bottom) layers of SU-8 material, which formed the enclosed microchannels [7]. Furthermore, using pure metals, such as Pt or Au for making disposable biochips for clinical applications where cross-contamination is an issue is not realistic due to the high cost of these noble metals.

Conductive polymer composites (CPCs) can be considered viable alternatives for making integrated electrodes compared to metal wires or electroplated metals because of their robustness and low-cost. CPCs are formulated with a photo-sensitive polymer matrix, making them appropriate for photo-patterning electrodes with controllable depths and exquisite spatial resolution. With this approach, fabricating electrodes that are only a few micrometers in height and/or gap is plausible and by using high energy radiation, such as X-rays, fabricating electrodes with high aspect ratios is attainable as well [8]. Moreover, lithography lends itself to a high throughput fabrication process of polymer-based electrodes, especially in high density arrays of sensors comprised of electrode pairs.

CPCs are different from conductive polymers (CP), such as polyaniline. While CPCs are a mixture of two phases – a conductive phase (usually some metal filler) and a nonconductive polymer phase, CPs are composed of only one phase – a polymer that is inherently conductive or a polymer that has been chemically modified to make it conductive. The conductivity of CPs results from the inherent

chemical state of the polymer, whereas polymers can be made into CPCs by infusing a conducting phase into the polymer matrix. Conventional polymers like polyethylenes are insulators because their valence electrons are in a sp^3 state unlike conjugated polymers where there is a decoupled electron in the p_z orbital, which is responsible for the electrical property observed in CPs. Ultimately, conductivity in these polymers is due to the motion of charge defects within the conjugated polymer framework. Conductivities of CPs can be altered by varying the substituent on the CP [9] or by doping [10]. In as much as CPs possess impressive electrical conductivities (up to ~10^3 S/cm for doped polyacetylene for example) [10] they are generally not photo-sensitive, therefore, they cannot be patterned into electrodes on-chip via lithography. CPCs, on the other hand, are a blend of a photo-sensitive insulating polymer, such as SU-8, and highly conductive fillers, such as silver nanoparticles, making them photo-sensitve and electrically conductive only when the load of the metal particles exceeds the percolation threshold. For silver nanoparticles in SU-8, the percolation threshold was 6% by volume Ag load, which corresponds to a conductivity measurement of approximately 10^2 S/m [13].

PMMA is a common polymer resist, especially used for X-ray lithography [11]. It is a positive tone resist, which means that the polymer backbone is broken upon exposure to X-ray radiation changing the polymer's molecular weight and making the exposed polymer more soluble in a particular solvent, whereas the non-exposed polymer is not soluble in that solvent. There are also negative tone resists, such as the epoxy-based SU-8 resist, which are seventy times more sensitive to X-ray radiation compared to PMMA and can thus be used to pattern ultra-high aspect ratio microstructures [11]. This also means that SU-8 can be processed faster than PMMA – an important aspect for the fabrication process considering that longer times are needed to generate high energy X-ray radiation from synchrotron facilities. SU-8 is photo-sensitive due to the addition of triaryl sulfonium salt and sulfonium hexflorate, which are used as photo-acid generators in a solution of epoxy-based molecules with solvents consisting of either gamma-butyloracton or cyclopentanone.

Different metals have been used as fillers in epoxy resins to develop new CPCs including Ni [12], Al [13], Cu [13], Zn [13], and Ag [14]. To make a photo-responsive CPC, fullerene filler has been formulated with a polyimide matrix [15]. Also, in a report by Jiguel *et al*., insulating photo-sensitive SU-8 was formulated with Ag nanoparticles to produce a photo-responsive Ag/SU-8 CPC [13]. The average agglomerate size of Ag particles is ~1.5 μm with individual Ag particles in the size range of nanometers. The authors demonstrated a UV (365 nm) cured depth of ~20 μm for a 6% volume Ag/SU-8 CPC and less than 10 μm for a 10% volume Ag load. The cure depth reduced markedly as the percent Ag load was increased. Conversely, there was a direct relationship between percent Ag load and the conductivity of the CPC [16] after the percolation threshold of 6% volume Ag in SU-8 was used. As the silver load was increased, there was a corresponding increase in the electrical conductivity. The conductivity increased from 10^2 S/m for a 6% volume Ag load to about 10^6 S/m for a 36% volume Ag load in SU-8 CPC [16]. The CPCs were crosslinked on a glass substrate by exposing the CPC from the bottom of the substrate (backside illumination) because glass has a high (100%) UV transmittance. The authors also stated that backside illumination was necessary for the CPC to adhere strongly to the glass substrate [16, 17]. The use of the glass substrate was convenient because it was compatible with the SU-8 developer that was used to develop the patterned structures.

CPCs formulated with Ag as a filler are attractive because Ag possesses a high conductivity ($>10^6$ S/m) and Ag nanoparticles have low absorption at an irradiation wavelength of 365 nm compared to other metals [16]. The 365 nm wavelength is typically used to crosslink the negative tone SU-8 resist. For example, 10% Ag nanoflakes have been mixed with negative tone polyimide to develop a CPC with an electrical conductivity of 10^4 S/cm [18]. Also, Ag powder dispersed in poly(dimethyl siloxane), PDMS, pre-polymer has been used as a photo-resist with the addition of a curing agent [19]. However, the reflectance of Ag particles can also affect the crosslinking of the CPC by preventing radiation from reaching through the entire composite layer. In most of the literature

discussed so far, UV radiation was used to crosslink the CPC, but soft X-ray radiation can also be employed to crosslink native SU-8 to generate ultra-high aspect ratio (up to 80) structures [8].

In this work, we evaluated different polymers as potential substrates for the molding of fluidic networks that were compatible with the developing stages for producing integrated CPC electrodes. We investigated the use of X-rays for patterning Ag/SU-8 on different polymer substrates. The use of a photo-sensitive CPC for fabricating electrodes on polymer chips for conductivity analysis will be demonstrated in this report. As a proof of concept, we measured the conductivity responses of the Ag SU-8 electrodes to different NaCl ionic strengths.

5.2 Methods and Materials

5.2.1 Apparatus

PMMA, Polycarbonate (PC) and three different grades of COC were evaluated as potential lab-on-a-chip polymers upon which Ag/SU-8 electrodes could be generated. PMMA and PC plates (4" x 4") were cut from 5 mm thick sheets purchased from Goodfellow Corp. (Oakdale, PA, USA) whereas 2" thick COC plates with similar dimensions were cut from COC sheets purchased from Topas Advanced Polymer, Inc. (Florence, KY, USA). COC grades 6013S-04, 5013S-04 and 8007X10 were investigated. According to the manufacturer, 8007X10 is a "pure" form of COC without any additives and has a glass transition temperature (Tg) of 78 ^{o}C while the 6013S-04 or the 5013S-04 grades have the same additive package except that the latter was made to have a lower molecular weight giving it a higher melt index than the former. However, COC 5013S-04 (Tg = 134 ^{o}C) is more brittle than 6013S-04 (Tg = 138 ^{o}C), although, the 5013S-04 grade has a slightly higher light transmittance (~0.5%). Note that all grades of COC are not compatible with non-polar organic and aromatic solvents, but will tolerate polar organic solvents.

Ag/SU-8 CPC resist was exposed to X-ray radiation using an X-ray beam line (XRLM1 beamline, Port 2A) at the Center for Advanced Microstructures and Devices (CAMD, Louisiana State

University, Baton Rouge, LA). The XRLM1 beamline was equipped with a DEX2 scanner (Jenoptik, Jena, Germany). To determine if UV radiation was sufficient to crosslink the CPCs, CPCs were exposed to UV light using a UV exposure station that was equipped with an aligner, a vacuum chuck to hold a 4" diameter substrate, a 1000 Watt Hg (Xe) lamp (220 – 450 nm) and a digital timer.

5.2.2 Samples and Reagents

Ten percent volume and 20% volume Ag/SU-8 composites were obtained from Gersteltec Sarl (Pully, Switzerland). The formulation and characterization of both composites resulted in electrical conductivities around 10^4 and 10^5 S/m after crosslinking [16]. SU-8 developer, propylene glycol mono-methyl ether acetate (PGMEA), was obtained from MicroChem (Newton, MA) and NaCl was purchased from Sigma-Aldrich (St. Louis, MO). All solutions were prepared in 18 MΩ nanopure water that was obtained from an ultra-pure water system (Millipore, Milford, MA).

5.2.3 X-ray Mask and Radiation

Synchrotron accelerators produce a high energy electron beam, whose path can be altered by a bending magnet associated with the XRLM1 beamline (see Figure 5.1). The bending magnet alters the motion of the electron beam causing them to lose kinetic energy and to generate light at many wavelengths due to this loss of kinetic energy. The emission is a continuous spectrum of wavelengths (infrared to hard X-rays). At the XRLM1 beamline, the electron emission spectrum was passed through a 100 μm thick Be filter followed by another Be filter that was 120 μm in thickness so that all wavelengths are absorbed except the X-rays. The electron energy was 1.3 GeV. The distance from the X-ray source to the sample (*i.e.,* mask and Ag/SU-8 on polymer) was poised at 10.35 m with a plausible horizontal exposure plane of 104 mm.

The pattern on the X-ray mask was transferred onto the resist because the X-ray mask was composed of a "blank", which is a material that functions as a high bandpass filter that allowed the

transmission of X-ray radiation and an absorber, which absorbed X-ray radiation thereby preventing the radiation from reaching the CPC. Since SU-8 is a negative tone resist, the unexposed portions were washed away during the developing stage. The "blank" was composed of a 150 µm thick graphite layer on top of which was a 45 µm gold absorber that was electroplated onto the graphite. Six identical fields were contained within the mask (4" diameter), which allowed testing six different radiation doses in one run during the X-ray dose optimization. A photograph of the X-ray mask is shown in Figure 5.1.

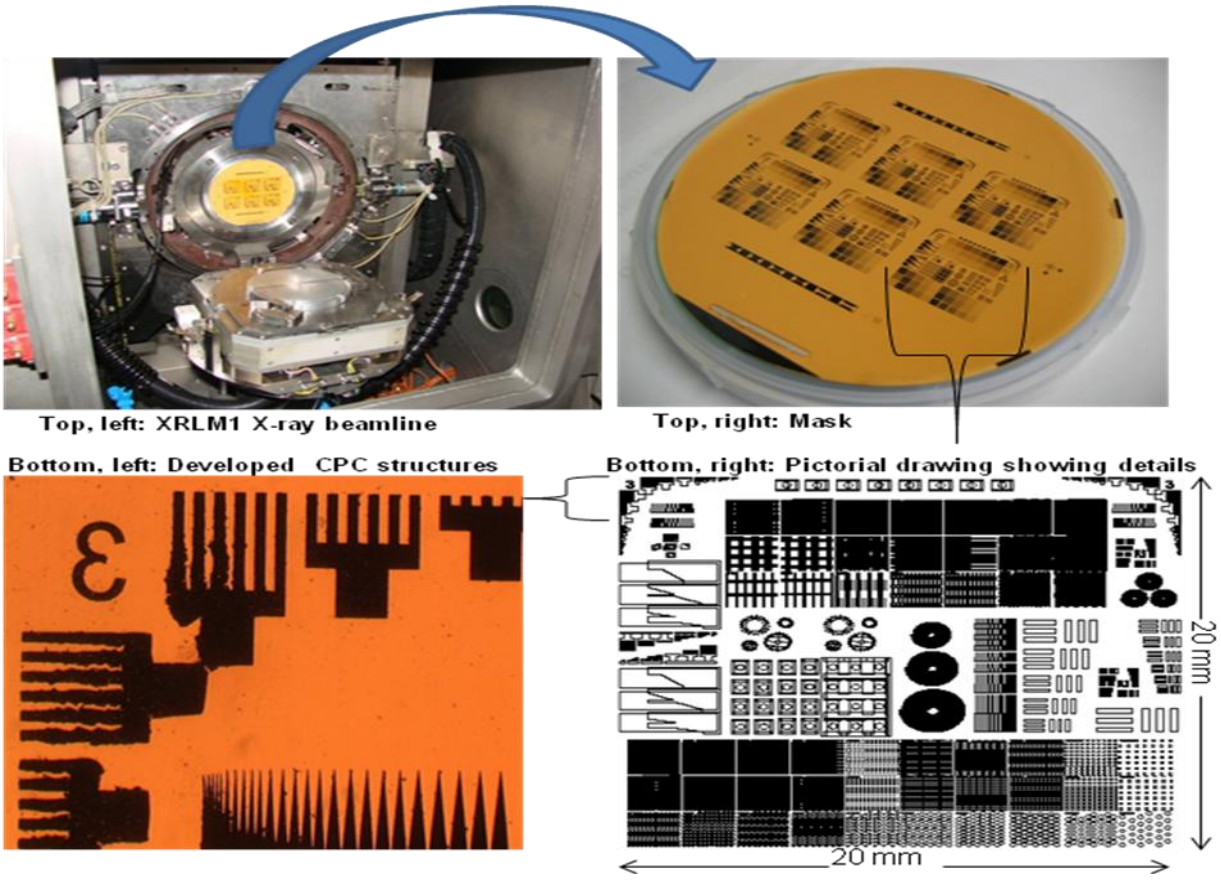

Figure 5.1 **Top, left**: Sample exposure end of the XRLM1 X-ray beamline located at CAMD, LSU, Baton Rouge. White spectrum was passed through two Be filters. The beamline electron energy was at 1.3 GeV. The distance from the radiation source to the sample (mask and Ag SU-8 on COC) was 10.35 m. **Top, right:** X-ray mask composed of 45 µm Au X-ray absorber (gold color) electroplated on 150 µm thick graphite (grey color). The mask has six identical fields on a 4" diameter circle (see text for detail). **Bottom, right:** A picture AUTO-CAD drawing revealing details of the structures on of the mask. **Bottom, left:** Developed Ag SU-8 structures showing an expanded view of the comb structures in the mask.

5.2.4 Fabricating Polymer-based Electrodes on a Polymer Substrate

Properties such as the glass transition temperature (Tg), resistance to SU-8 developer, and resistance to degradation upon exposure to X-ray radiation were considered in the polymer substrate containing the fluidic network selection process. To determine polymer resilience against the developer, pieces of PMMA, PC and two different COC grades (6013S-04 and 5013S-04) were immersed in the PGMEA developer for 5 min, 10 min, 30 min and 60 min followed by visual observation and inspection using a microscope. COC grade 8007X10 with a Tg of 78 ^{o}C was not tested as it already failed to meet the high temperature requirement of 120 ^{o}C needed for the CPC electrode processing downstream (see Section 5.3.1 for further explanation). The Ag/SU-8 CPC was spread onto the substrate by using a spatula instead of spin-coating to avoid redistribution and sedimentation of the Ag powder [16]. In order to obtain a 50 µm tall CPC, 50 µm thick shims were placed on the top of the two sides of the polymer substrate to facilitate the application of the desired thickness. A surface profiler was used to confirm the thickness of the applied CPC.

5.2.5 X-ray Exposure and Development of Composite

After applying the CPC on the substrate to the desired thickness, it was pre-baked overnight in a convection oven at 65 ^{o}C to evaporate the solvents within the SU-8 resin and then the temperature was increased to 95 ^{o}C for 5 h. This was followed by a direct (front side) X-ray illumination (0.4 nm – 0.8 nm) of the CPC through the gold mask at the XRLM1 beamline (see Figure 5.1). This exposure began to slowly crosslink the irradiated portions of the CPC. A post-bake at 95 ^{o}C for 10 min was necessary to complete the crosslinking process. The crosslinked CPC became inert and stable against degradation in the presence of the SU-8 developer. Crosslinked CPCs on the polymer substrate were immersed in the PGMEA developer for 1 h to remove the unexposed CPC resist and then rinsed with isopropyl alcohol (IPA). Developed CPC structures were heated to 120 ^{o}C for 90 min in a convection oven to enhance the conductivity property because conductivities around 10^{3} S/m and 10^{4} S/m

have been reported for a 10% volume Ag/SU-8 with and without heat treatment, respectively [16].

5.2.6 Chip Assembly and Conductivity Response

Microstructures were micromilled into a mold master made from brass, which was then used to replicate the fluidic structures onto the polymer substrates [20]. Figure 5.2 shows a flow chart depicting the process pathway that was followed to fabricate the chips with integrated Ag/SU-8 electrodes.

The fluidic network consisted of a simple channel with electrode guides as shown in Figure 5.3. Channel depth and width were both 50 µm. The total channel length was 6 cm and the electrode guide was located about 1 cm from the inlet reservoir. The electrode guides were 50 µm high and 450 µm wide. As a proof of concept, a microchip was fabricated in which the Ag/SU-8 CPC was first crosslinked within the electrode guides of the chip by flood exposing the CPC with X-ray radiation. X-ray radiation was selected at 60 J/cm^3 as this was found not to adversely affect or degrade the polymer substrate, therefore, not affecting downstream processing, such as cover slip annealing to the substrate.

A 50 µm milling bit was then used to mill a gap in the crosslinked CPCs within the fluidic channel followed by rinsing with nanopure water and thermal annealing with a polymer cover slip slightly below the polymer Tg. Then, a 15-cm long capillary with a 250 µm outside and 150 µm inner diameter was connected to the inlet reservoir of the microchip using epoxy glue. Solutions of different NaCl concentrations were pumped through the channel using a syringe pump and the conductivity was monitored using an in-house constructed conductivity system [5].

5.3 Results and Discussion

5.3.1 Selection of Polymer

It is common practice in lithography to spin coat, crosslink and develop polymer resists, such as SU-8, on glass substrates or silicon wafers because glass and silicon are robust materials that can withstand high temperatures and importantly, do not degrade in the presence of the developers. In

addition, glass substrates allow nearly 100% light transmission, which favors backside exposure of the resist [16]. However, there are numerous benefits associated with polymer microfluidic devices [20-26], especially in the area of biomolecular or cell analysis, and therefore, we set out to select a polymer substrate that was compatible with the process of lithography, and thus has a high transmission to the patterning radiation, has a high Tg and is compatible with the developers used for the CPC while meeting the requirements as a candidate for bioanalysis.

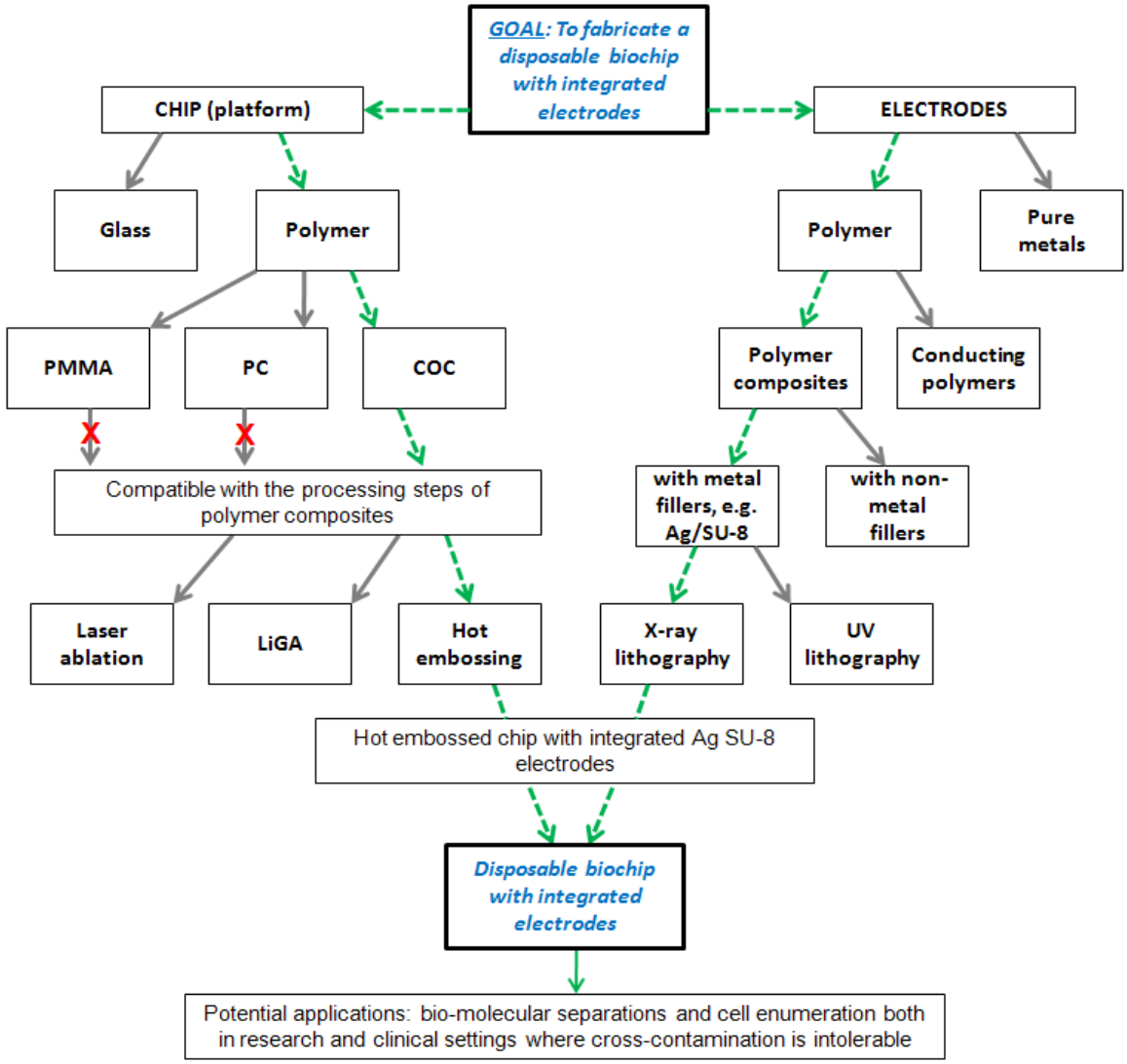

Figure 5.2 Flow chart depicting process pathways that were followed that resulted in the test biochip reported herein stemming from the goal of fabricating disposable biochips with integrated electrodes. Fluidic networks were stamped into the polymers using a mold insert and hot embossing. A formulation 10% Ag volume SU-8 CPC was integrated on the chip as electrodes as shown in Figure 5.3. The CPC was crosslinked on the chip using X-ray radiation.

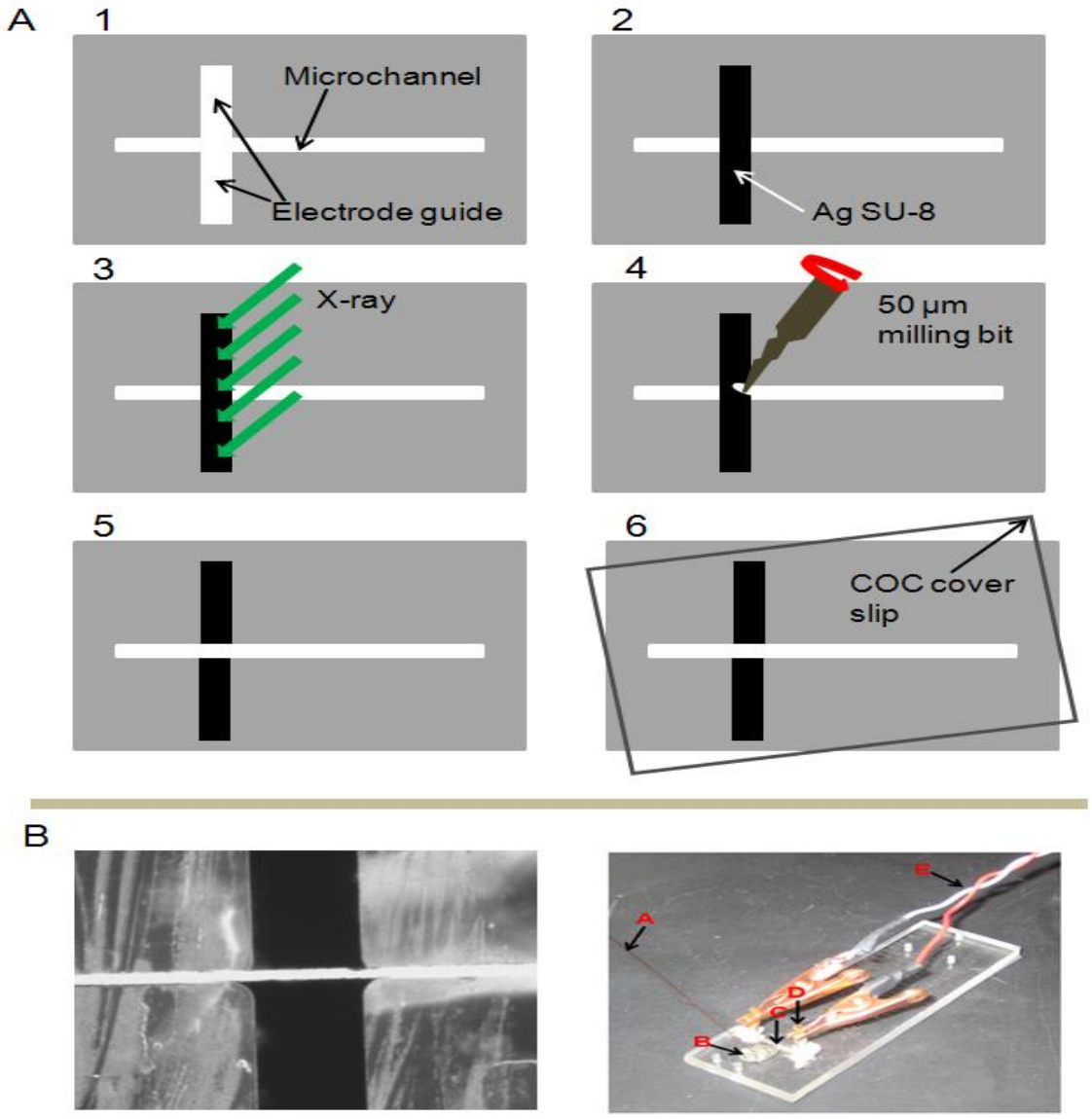

Figure 5.3 (A) Schematic of how Ag SU-8 CPC was embedded within the electrode guide within a COC chip demonstrating the concept of fabricating polymer-based electrodes on polymer substrates. (1.) COC chip with fluidic network and electrode guide. (2.) 10% Ag SU-8 CPC was applied within the electrode guides. (3.) The CPC was flood exposed to X-ray radiation at 60 J/cm^3. (4.) A 50 µm milling bit was used to mill off about 450 µm long (width of the electrode guide) or any crosslinked CPC within the fluidic channel so that (5.), which shows a fluidic channel with orthogonal electrodes resulted. (6.) After rinsing with nanopure water, a COC cover slip was thermally annealed to the substrate at around 132 - 134^{o}C. (B) Left: Actual image of 10% Ag vol. SU-8 CPC electrode embedded in a COC chip as illustrated in Figure 5.3A taken with a fluorescence microscope. Right: Photograph of COC chip with integrated CPC electrode. A 15-cm long capillary (A) was connected to the inlet reservoir of the microchip using epoxy glue (B). NaCl solutions were pumped through the capillary into the microchannel so that the traversed the electrodes (C) whose expanded view are shown in Figure 5.3B (left). Copper cylinders (D) were use to make contact between the µ-CPC electrodes and the macro world. Alligator clips terminating the ends of electrical wires (E) emanating from the conductivity detector system was used to make contact with the copper connectors.

PMMA has been adopted in both research labs and in clinical settings for biomolecular separations and cell analysis, and has proven to be an attractive polymer, in part, because several surface chemistries that allow for its modification have been established and it is highly machinable and moldable [27, 28]. PC, on the other hand, has a higher Tg (150 ^{o}C) compared to PMMA (Tg = 107 ^{o}C), a characteristic that favors our current application, and just like PMMA, surface modification chemistries for PC have also been well established [28]. Unfortunately, the integrity of both PMMA and PC polymers were compromised in the presence of the SU-8 developer as shown in Figure 5.4.

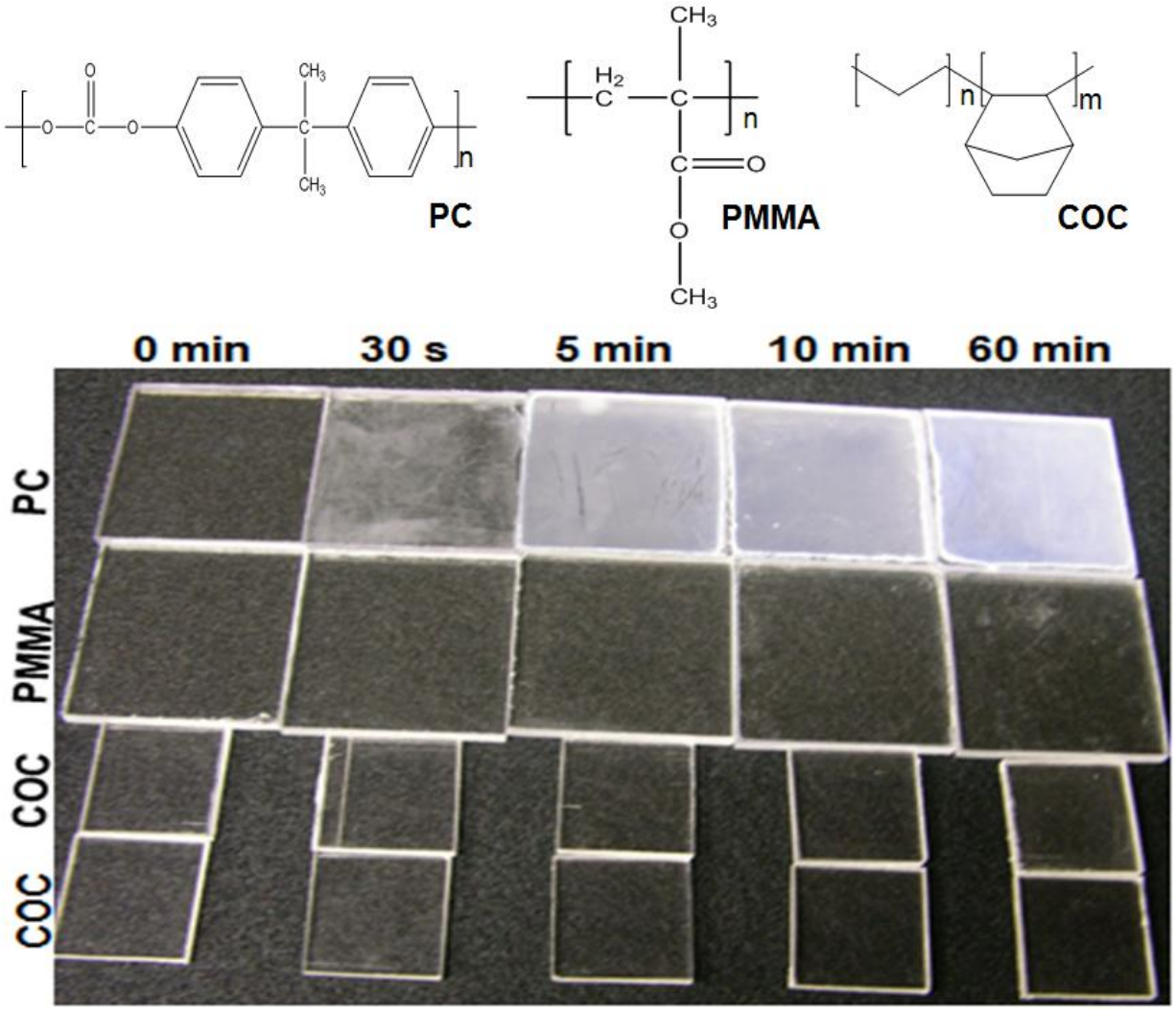

Figure 5.4 Photograph showing the compatibility with PGMEA developer solvent of the various polymers whose backbone structures are also shown. A photograph of each polymer was taken after immersing the polymer for 0 min, 30 s, 5 min, 10 min and 60 min in the solvent. Top and bottom COCs are the Topas grades 6013S-04 and 5013S-04, respectively.

COCs are a new set of copolymers whose components can be varied to tune their physicochemical properties. Topas^{R} COC is a product of ethylene (n) and norbornene (m) as shown in Figure 5.4. A small amount (0.1 - 0.4%) of tetrakis[methylene(3,5-di-tert-butyl-4hydroxyhydrocinnamate)]methane is often added as a stabilizer. COC 8007X10 does not contain any stabilizer and has nearly 100% light transmittance. In general, COCs possess qualities such as surface tunability, low autofluorescence, good adhesion to metal sensors, good UV transmittance, high chemical and temperature resilience and high impact strength. These qualities make them superior to PC or PMMA [29], therefore, they have been adopted for a variety of bioanalysis applications using microfluidics [30-35]. Because a heat treatment at 120 ^{o}C for 90 min was required to improve the conductivity of the CPC [16], we selected COC 5013S-04 (Tg = 134 ^{o}C) with a Tg that is higher than 120 ^{o}C. Furthermore, COC 5013S-04 and 6013S-04 were observed to be compatible with the PGMEA developer. Figure 5.4 shows the resiliency of selected polymers upon immersion in the PGMEA developer over a period of time. Based on the developer compatibility studies, COC was selected as the substrate for the Ag/SU-8 CPC electrodes.

5.3.2 Optimization of X-ray Dose

We were first interested in determining the X-ray dose required to crosslink SU-8 resist that contained no Ag particles. Ag/SU-8 CPCs were then exposed to 20 J/cm^3, 30 J/cm^3, 40 J/cm^3, 60 J/cm^3, 80 J/cm^3 and 100 J/cm^3 of X-ray radiation. For a 10% volume Ag/SU-8, we observed that 20 J/cm^3 was not sufficient to crosslink the entire CPC; some structures did not adhere to the COC surface, rather they lifted off the COC substrate during the developing stage (see Figure 5.5). Radiation at 20 J/cm^3 did not reach the bottom of the CPC from the front side for a 50 μm thick resist layer. When the CPCs were exposed to high dose ranges of 80 J/cm^3 and 100 J/cm^3, we observed that portions of unexposed CPC portions remained attached to the COC substrate even after a 1 h developing step.

We found the optimal range for crosslinking a 10% volume Ag/SU-8 was found to be 30 J/cm^3 to 60 J/cm^3 (see Figure 5.5) for a 1 h development time. SU-8 composites with higher Ag loads have been shown to possess greater electrical conductivity compared to a 10% volume Ag/SU-8 CPC [17]. For this reason, a 20% volume Ag/SU-8 was subjected to similar X-ray radiation and development processes. Similarly, lower radiation doses were found not to be sufficient to penetrate the CPC layer because the radiation was absorbed by the Ag particles (see Figure 5.6), whereas for higher doses, we observed that unexposed sections remained attached to the COC substrate even after a 2 h developing process.

5.3.3 Effects of Silver Particles on the Crosslinking of the CPC

In previous reports, Ag/SU-8 was crosslinked via UV lithography at 365 nm [16, 17]. At this wavelength, the reflectance of Ag is near zero. Despite the favorable reflectance of Ag at this wavelength, the authors could only achieve a crosslinked depth of 5 μm or less for a 10% Ag/SU-8 CPC. We found that UV radiation at 365 nm at doses of 900 mJ/cm^2, 1500 mJ/cm^2 and 3000 mJ/cm^2 did not provide sufficient energy to crosslink the entire depth of a 50 μm Ag/SU-8 material in the present case - the CPC structures lifted off the COC support during the developing process within 10 min in the developer. This corroborates with the fact that UV radiation did not penetrate deeper than ~5 μm into the CPC. Since UV radiation can crosslink up to a 1000 μm thick native SU-8 (i.e., epoxy matrix without any metal filler) [36, 37], we concluded that UV photons were greatly absorbed or scattered by Ag particles in the CPC, thereby limiting the achievable cure depth. X-ray radiation can also be absorbed by Ag particles. When this happens, the radiation penetrates the inner core of the atoms thus exciting bound electrons. Absorption by Ag atoms occurs when the X-ray photon energy matches the energy required to promote an electron from a lower state (bound electrons) to a higher state. The likelihood of Ag particles absorbing X-ray photons increases as the Ag load in the CPC increases.

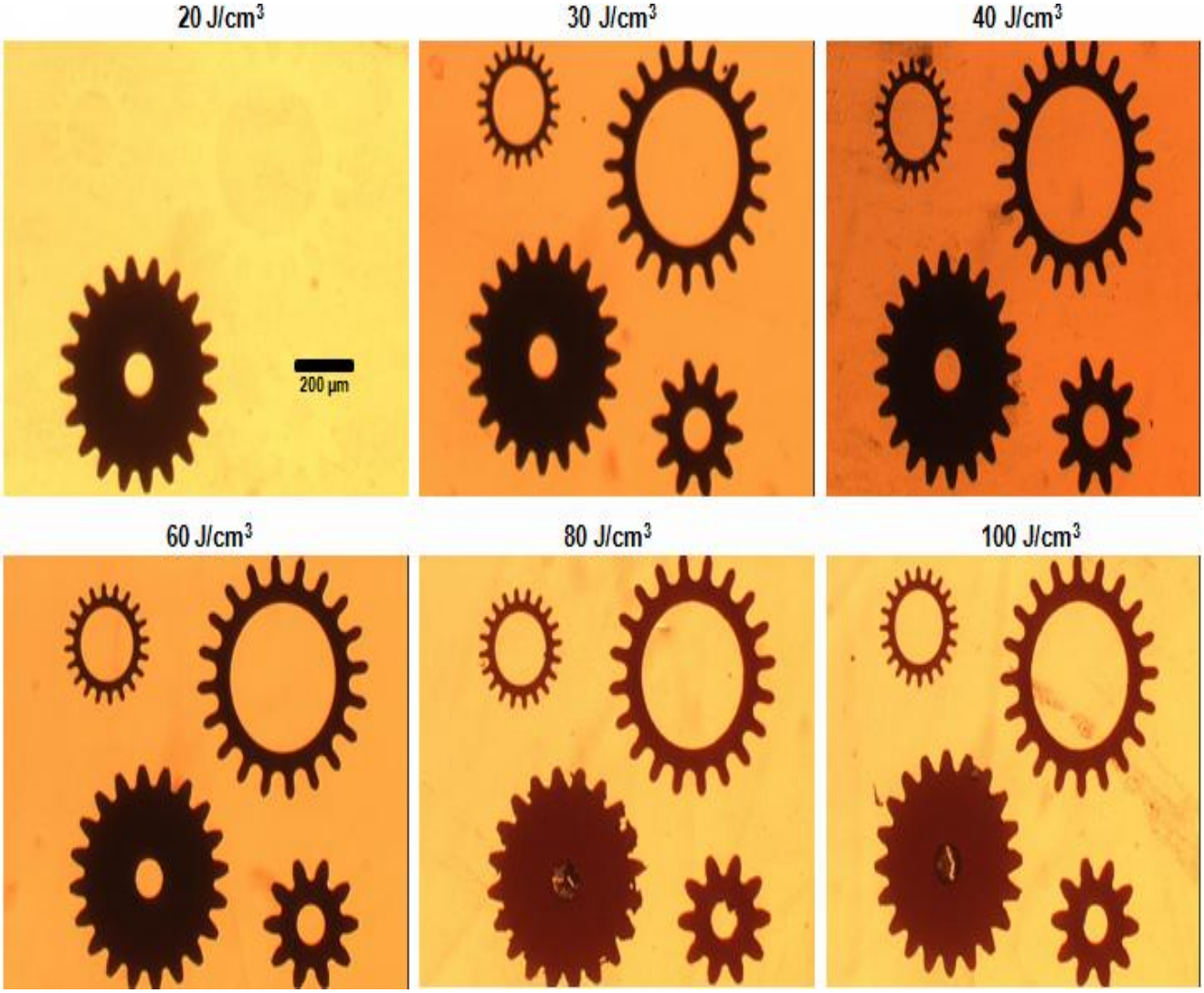

Figure 5.5 Gear structures developed from a 10% vol. Ag SU-8 CPC. Image shows the gear structures (50 µm tall) on different areas of a COC substrate after the developing process prior to which the CPC had received X-ray radiation doses of 20 J/cm^3, 30 J/cm^3, 40 J/cm^3, 60 J/cm^3, 80 J/cm^3 and 100 J/cm^3 on the different areas. X-ray radiation at 20 J/cm^3 was inadequate to crosslink the CPC. All images shown here were taken after a 1 h developing process. Additional 15 min was required to fully develop CPCs that received 80 J/cm^3 and 100 J/cm^3. An optimal range for crosslinking a 10% vol. Ag SU-8 was around 30 J/cm^3 and 60 J/cm^3 for a development time of 1 h.

Absorption of X-ray photons by the Ag particles in the CPC translates to less radiation to crosslink the SU-8 resist of the CPC, but if the energy is high enough, the radiation can penetrate through the Ag particles reaching the underlying SU-8 resist. Lower energies (higher wavelength) were highly absorbed by the Ag particles thereby preventing the SU-8 resist to be fully crosslinked resulting in a weak adherence between the CPC and the COC substrate (see Figures 5.5 and 5.6). Similar to the

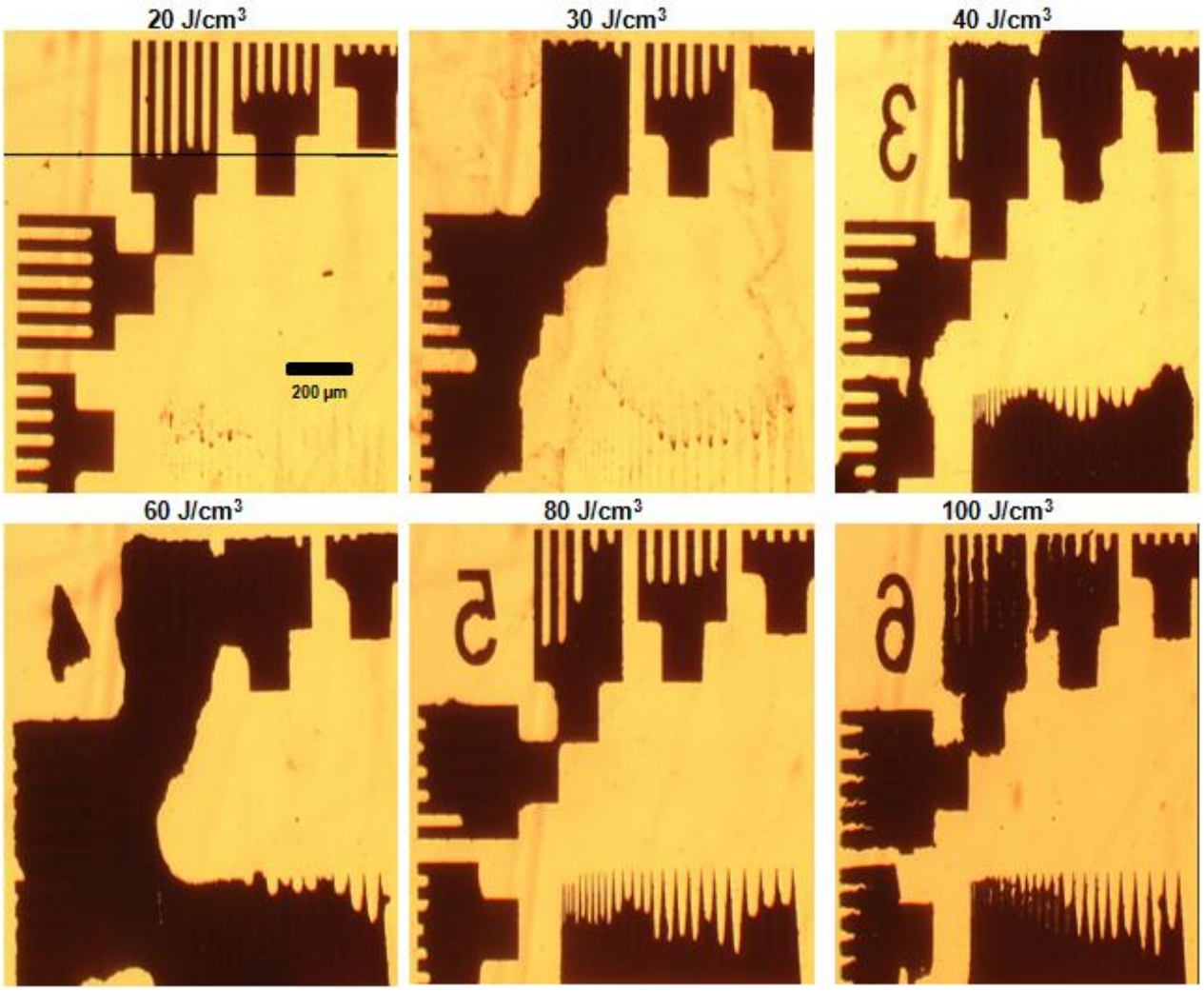

Figure 5.6 Comb structures developed from a 20% vol. Ag SU-8 CPC. Image shows the structures (50 µm tall) on different areas of a COC substrate after the developing process prior to which the CPC had received radiation doses of 20 J/cm^3, 30 J/cm^3, 40 J/cm^3, 60 J/cm^3, 80 J/cm^3 and 100 J/cm^3 on the different areas. X-ray radiation at 20 J/cm^3 and 30 J/cm^3 were inadequate to crosslink the CPC from the front side. Because of additional Ag particles compared to the 10% vol. CPC, some radiation were reflected to unexposed SU-8 causing some degree of crosslinking to occur in unexposed areas, which resulted in poor quality structures.

case of the 10% volume Ag/SU-8, 20 J/cm^3 was not sufficient to crosslink a 20% volume of the Ag/SU-8. We also found that 30 J/cm^3 was insufficient for crosslinking a 20% volume Ag/SU-8 because the additional Ag load absorbed the radiation (see Figure 5.6). However, we attribute the poor quality structures generated with 20% volume Ag/SU-8 for the dose at 40 J/cm^3 or higher due to the reflectance of Ag arising from additional Ag particles. We reasoned that additional Ag particles

reflected the radiation to unexposed SU-8 causing some degree of crosslinking to occur in those unexposed areas. Figure 5.7 is a scanning electron microscope (SEM) image of fully developed structures composed of a 10% volume Ag/SU-8 on a COC substrate. The image showed 50 μm tall comb structures that had been crosslinked using X-ray radiation at 60 J/cm^3 and developed in a PGMEA solvent for 1 h.

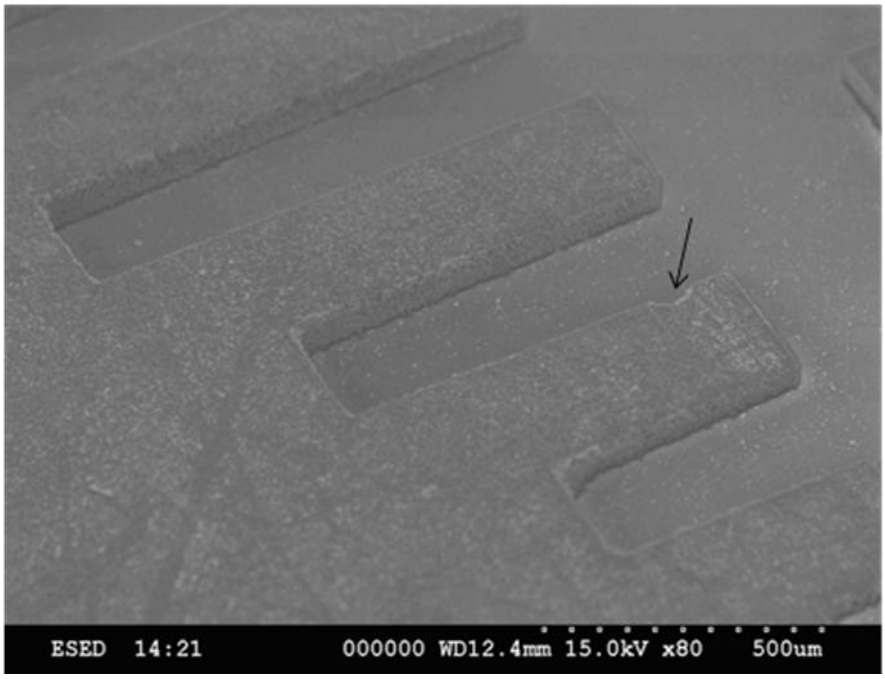

Figure 5.7 Scanning Electron Microscope (SEM) image of a segment of fully developed structures composed of a 10% vol. Ag SU-8 on a COC substrate. The image shows 50 μm tall comb structures. The CPC was crosslinked using X-ray radiation at 60 J/cm^3 and developed in a PGMEA solvent for 1 h. Arrow shows a dent that resulted during handling indicating that the free-standing CPC structures should be dealt with care.

5.3.4 Conductivity Response of SU-8 Electrodes

To demonstrate the feasibility of the fabricated device with the integrated on-chip Ag/SU-8 electrode described in section 5.2.6, we hydro-dynamically pumped different concentrations of NaCl solutions prepared in nanopure water (0.1 mM, 1 mM, 2.5 mM, 5 mM and 10 mM) through the chip (see Figure 5.3). We then monitored the conductivity responses and observed that different ionic strengths resulted in different conductivities as shown in a plot of NaCl concentration (mM) versus response in volts (V) in which a linear correlation was found to be 0.9934 (see Figure 5.8). The plot

shows that the voltage decreased linearly as the NaCl concentration in the solution was increased. Increased NaCl concentration increased the solutions conductivity, which means a decrease in the resistance within the detection area. Since a fixed AC current was supplied through the detection area by the conductivity system, the voltage drop across the detection area was found to reduce in accordance to ohm's law (V = IR; V = voltage, I = current and R = resistance). The on-chip Ag SU-8 electrodes were orthogonal to the fluidic channel as shown in Figure 5.3 and were connected to the conductivity detector system, which was essentially an AC current source. The wire connectors extending out of the detector system were terminated with alligator clips, which were used to connect Cu metals (~2 mm diameter, ~15 mm tall) that were in turn made contact with the CPC electrodes. The Cu metals were inserted in ~2 mm holes that were drilled through the CPC electrodes after the chip assembly process and were glued in place using conductive epoxy.

The detector system measured changes in the solution's conductivity across the detection area situation between the electrodes. In deed, the conductivity detector system performs two tasks, (i) it supplies AC current across the detection area and (ii) it measures current at the end of a bipolar pulse. The current is in turn converted into voltage by a voltage converter and that voltage corresponds to a conductance. The conductivity detector circuit was endowed with a synthetic inductor and a gyrator, which were in parallel to the double layer capacitance, C_d and stray (or parasitic) capacitance, C_s. This configuration eliminated the adverse effects of the C_s thereby improving the overall sensitivity of the detector system. The detector system provided an AC current of ±5 µA at ~ 40 kHz to avoid charge build up at the electrode surfaces due to C_d [4].

Given an electrode cross-sectional area (A) of 22,500 μm^2 (50 µm high x 450 µm wide) and a spacing (L) of 50 µm for the present work, we calculated the electrode cell constant, K (L/A) of 0.0022 μm^{-1}. McWhorter and Soper [38] in a similar detection scheme, employed Pt wire electrodes (360 µm diameter) that were integrated in capillary channels, reported a concentration limit of detection (LOD)

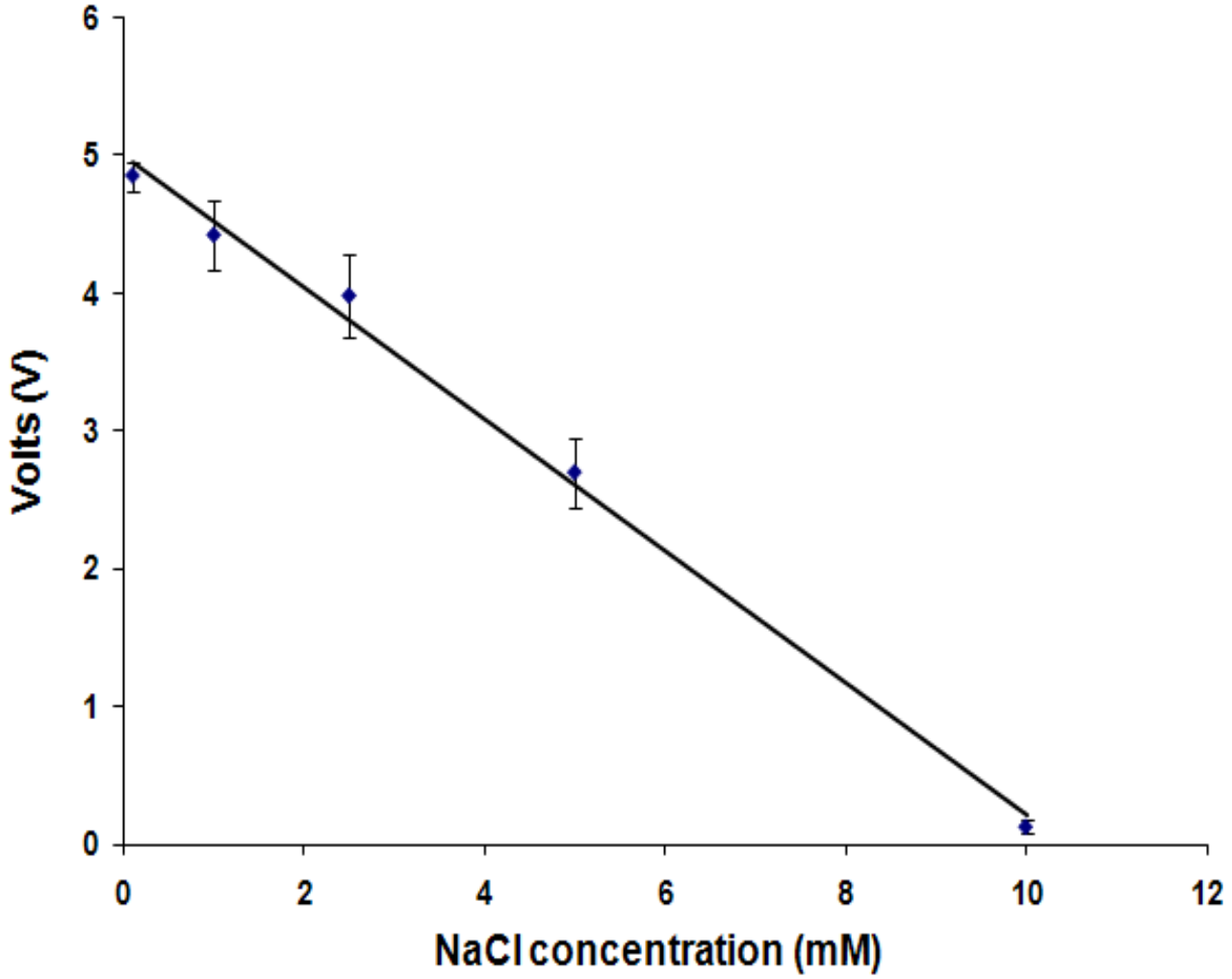

Figure 5.8 Plot of NaCl concentration (mM) against background conductivity responses (V). NaCl solutions prepared in nanopure water. Responses were obtained by continuously pumping the NaCl solutions through the fuidic channels so that the solutions traversed the CPC electrodes. The responses were recorded using a conductivity detector system, which provided an AC current of ±5 µA at ~ 40 kHz. Different NaCl concentrations on the X-axis (0.1 mM, 1mM, 2.5 mM, 5 mM and 10 mM) educe corresponding conductivities on the Y-axis. The Y-axis is in volts, which is inversely related to conductivity.

of 34.6 µg/L or 4.6 x 10^{-1} µM (K = 0.0006 μm^{-1}, electrode spacing = 60 µm) for KCl in a ddH_2O carrier solution. In the present case, the concentration LOD was found to be 0.134 mM using the average signal (4.89 V) plus three times the standard deviation (0.0214 V, n = 10) of a blank signal. We attribute the favorable LOD to lower K values reported here compared to the author's previous K value.

5.4 Conclusions

A new approach for fabricating on-chip electrodes was investigated and a microchip with the integrated electrode was tested. The electrode fabrication relied upon the photo-patterning of a CPC, such as a blend of Ag nanoparticles and negative-tone SU-8 photoresist using X-ray lithography. The electrodes were patterned on COC substrates, which were found to be compatible with the electrode fabrication process. A CPC with a 10% volume Ag load in SU-8 was used to fabricate the electrodes by crosslinking the CPC using an optimal X-ray dose of 60 J/cm^3 and developing the structures in a PGMEA developer for 1 h. Twenty percent volume Ag/SU-8 resulted in poor quality structures because additional Ag particles reflected the radiation to neighboring unexposed SU-8 essentially crosslinking some of the unexposed SU-8. For both 10% and 20% volume Ag load, structures were found not to adhere to the substrates because Ag particles absorbed the radiation. Radiation absorption of this sort prevented the CPC from crosslinking and typically occurred at lower doses. Front side (or direct) illumination was used for all radiation exposures. Using a conductivity detector system, conductivities of NaCl solutions with varying concentrations was monitored and a LOD of 1.34 x 10^{-1} mM for this scheme was calculated.

5.5 References

[1] Sonlinova, V., Kasicka, V., *J. Sep. Sci.* 2006, *29*, 1743-1762.

[2] Noblitt, S. D., Schwandner, F. M., Hering, S. V., Collett, J. L., Henry, C. S., *Journal of Chromatography A* 2009, *1216*, 1503-1510.

[3] Wu, Z. Y., Fang, F., Josserand, J., Girault, H. H., *Electrophoresis* 2007, *28*, 4612-4619.

[4] Galloway, M., Stryjewski, W., Henry, A., Ford, S. M., *et al.*, *Analytical Chemistry* 2002, *74*, 2407-2415.

[5] Adams, A. A., Okagbare, P. I., Feng, J., Hupert, M. L., *et al.*, *Journal of the American Chemical Society* 2008, *130*, 8633-8641.

[6] Guijt, R. M., Evenhuis, C. J., Macka, M., Haddad, P. R., *Electrophoresis* 2004, *25*, 4032-4057.

[7] Wang, L. S., Flanagan, L., Lee, A. P., *J. Microelectromech. Syst.* 2007, *16*, 454-461.

[8] Reznikova, E., Mohr, J., Boerner, M., Nazmov, V., Jakobs, P. J., *Microsystem Technologies-Micro-and Nanosystems-Information Storage and Processing Systems* 2008, *14*, 1683-1688.

[9] Waltman, R. J., Bargon, J., *Can. J. Chem.-Rev. Can. Chim.* 1986, *64*, 76-95.

[10] Hayes, W., *Contemp. Phys.* 1985, *26*, 421-441.

[11] del Campo, A., Arzt, E., *Chem. Rev.* 2008, *108*, 911-945.

[12] Strumpler, R., *J. Appl. Phys.* 1996, *80*, 6091-6096.

[13] Tsangaris, G. M., Kazilas, M. C., *Mater. Sci. Technol.* 2002, *18*, 226-230.

[14] Busmann, H. G., Gunther, B., Meyer, U., Pergamon-Elsevier Science Ltd 1999, pp. 531-534.

[15] Tajima, Y., Shigemitsu, Y., Arai, H., Takeuchi, E., Takeuchi, K., Elsevier Science Sa 2001, pp. 1167-1168.

[16] Jiguet, S., Bertsch, A., Hofmann, H., Renaud, P., *Advanced Engineering Materials* 2004, *6*, 719-724.

[17] Jiguet, S., Bertsch, A., Hofmann, H., Renaud, P., *Advanced Functional Materials* 2005, *15*, 1511-1516.

[18] Li, T. L., Hsu, S. L. C., *Journal of Polymer Science Part a-Polymer Chemistry* 2009, *47*, 1575-1583.

[19] Cong, H. L., Pan, T. R., *Advanced Functional Materials* 2008, *18*, 1912-1921.

[20] Hupert, M. L., Guy, W. J., Llopis, S. D., Shadpour, H., *et al.*, *Microfluidics and Nanofluidics* 2007, *3*, 1-11.

[21] Christopher, G. F., Anna, S. L., *Journal of Physics D-Applied Physics* 2007, *40*, R319-R336.

[22] Becker, H., Gartner, C., *Analytical and Bioanalytical Chemistry* 2008, *390*, 89-111.

[23] Teles, F. R. R., Fonseca, L. R., *Materials Science & Engineering C-Biomimetic and Supramolecular Systems* 2008, *28*, 1530-1543.

[24] Tsao, C. W., DeVoe, D. L., *Microfluidics and Nanofluidics* 2009, *6*, 1-16.

[25] Chung, T. D., Kim, H. C., *Electrophoresis* 2007, *28*, 4511-4520.

[26] Abgrall, P., Gue, A. M., *Journal of Micromechanics and Microengineering* 2007, *17*, R15-R49.

[27] Llopis, S. L., Osiri, J., Soper, S. A., *Electrophoresis* 2007, *28*, 984-993.

[28] Dolnik, V., *Electrophoresis* 2004, *25*, 3589-3601.

[29] Lamonte, R. R., McNally, D., *Plastics Engineering* 2000, *56*, 51-+.

[30] Pu, Q. S., Oyesanya, O., Thompson, B., Liu, S. T., Alvarez, J. C., *Langmuir* 2007, *23*, 1577-1583.

[31] Okagbare, P. I., Soper, S. A., *Analyst* 2009, *134*, 97-106.

[32] Mair, D. A., Geiger, E., Pisano, A. P., Frechet, J. M. J., Svec, F., *Lab Chip* 2006, *6*, 1346-1354.

[33] Kameoka, J., Craighead, H. G., Zhang, H. W., Henion, J., *Analytical Chemistry* 2001, *73*, 1935-1941.

[34] Gaudioso, J., Craighead, H. G., *Journal of Chromatography A* 2002, *971*, 249-253.

[35] Mela, P., van den Berg, A., Fintschenko, Y., Cummings, E. B., *et al.*, *Electrophoresis* 2005, *26*, 1792-1799.

[36] Shaw, J. M., Gelorme, J. D., LaBianca, N. C., Conley, W. E., Holmes, S. J., *Ibm Journal of Research and Development* 1997, *41*, 81-94.

[37] Gunde, M. K., Hauptman, N., Macek, M., Kunaver, M., *Applied Physics a-Materials Science & Processing* 2009, *95*, 673-680.

[38] McWhorter, S., Soper, S. A., *Journal of Chromatography A* 2000, *883*, 1-9.

6 Summary and On-going Developments

6.1 Summary

Many groups have attempted to integrate various proteomic processing steps onto a single chip to build autonomously-operating system, but the ultimate goal of integrating a multitude of proteomic analysis units into one system for complete and automated multifunctional operation has not been realized to-date. As discussed in Chapter 1, our approach is to design, build and evaluate the performance of an integrated proteomic analysis system that consists of the following processing devices; a cell lysis unit, protein extraction unit, 2-D separation unit, protein digestion unit, and peptide separation unit prior to online coupling of the integrated chip to a mass spectrometer. Amongst these units, multidimensional protein separation is regarded as the workhorse of many proteomic projects; therefore, careful attention must be paid toward the development and implementation of multidimensional microelectrophoresis platforms whether as an independent proteomic unit or as an integral part of a multifunctional system. To fully realize the potential of polymer microfluidic devices for routine separation applications, the reliability of the devices must be improved in terms of their walls' chemical composition. To this end, we developed a procedure to covalently anchor an LPA coating to the PMMA wall to stabilize and suppress the EOF of PMMA as well as reduce potential solute-wall interactions. However, we also found that dynamically coating PMMA surfaces with MHEC produced similar EOF values that were observed in covalently LPA-modified PMMA.

We demonstrated the ability to generate peak capacities around 2,600 (±149) within 30 min for a biological serum protein sample using a microchip separation platform, whose effective separation length was 11 cm. While this peak capacity is still far below the total number of protein components typically found in a serum proteome, isolating sub-populations of common protein types, such as glycosylated or phosphorylated protein types, could make this peak capacity tractable for exhaustive analysis of complex protein samples, like the serum proteome. In order to perform ultra-fast

separations, we utilized a 2-D platform that provided relatively high spot production rates and reasonable peak capacities in spite of the fact that short separation lengths (effective length = 2 cm) were employed (10 mm in each dimension of this 2-D system). An average peak capacity of 481 (±18) was obtained by coupling MEEKC to SDS μ-CGE requiring only a 220 s development time. This particular 2-D separation format has the advantage of generating a higher peak capacity over the more traditional MEKC coupled to SDS μ-CGE due to better plate numbers afforded by the MEEKC phase compared to MEKC. In addition, interfacing the 2-D separation platforms discussed in Chapters 3 or 4 to a mass spectrometer as well as integrating sample preparation steps to the chip platforms prior to the 2-D separation will provide an autonomous system for discovery or diagnostic-based proteomic projects. To avoid issues associated with dye labeling, such as the availability of thiol groups in proteins, 2-D chips can be integrated with on-chip electrodes for label free analyses via conductivity sensing.

With the ultimate goal of performing a label free proteomic analysis in mind, we investigated a new approach for fabricating on-chip electrodes to provide the ability to carefully control the inter-electrode gap and to build electrodes that matched the output channel dimensions to keep the sampling efficiency high. The electrode fabrication relied upon the photo-patterning of CPC, such as a blend of Ag nanoparticles and the negative-tone SU-8 photoresist using X-ray lithography. The electrodes were patterned on COC substrates, which were found to be compatible with electrode fabrication process. A CPC composed of a 10% volume Ag load in SU-8 polymer resist was used to fabricate the electrodes by crosslinking them using an X-ray dose of 60 J/cm^3 and developing the resulting structures in a PGMEA developer solvent for 1 h. The CPC was directly exposed to X-ray radiation from the front side (*i.e.*, direct illumination). On-chip electrodes that were fabricated using this X-ray technique were tested for their responsiveness to changes in background conductivities. A conductivity detector system was used to monitor background conductivities of NaCl buffers with varying salt

concentrations, and a LOD of 1.34 x 10^{-1} mM was determined for this set-up. This method appears, in comparison to other lab-on-a-chip techniques for fabricating electrodes, to be cost efficient, less laborious, and amenable for a high-throughput fabrication of multiple electrodes.

6.2 On-going Developments

6.2.1 Background

In Chapters 3 and 4, we dealt with the separation of proteins from biological serum samples and *E.* coli lysates, respectively. Because these proteins reside in more or less aqueous environments, proteins from these sources tend to be less hydrophobic and as such easier to solubilize in aqueous media prior to and/or during separation. But a class of proteins, membrane proteins, is terribly difficult to handle during analysis. These proteins are associated with the membrane of cells and are known to perform several functions including, cell boundary, signal transduction, ion and metabolite transport, cell adhesion, endocytosis, etc [1]. The clinical importance of membrane proteins is evidence in the fact that though they are low abundant, constituting about one-third of all cellular proteins [1], over two-thirds of all drugs are designed to modulate their activities [1, 2]. There are two types of membrane proteins: (1) Integral membrane proteins; and (2) peripheral membrane proteins. As their name suggests, integral membrane proteins are membrane proteins that are permanently attached to the cell membrane, either spanning through the cell lipid bilayer or permanently penetrating the bilayer at least from one side. Peripheral membrane proteins on the other hand, are loosely associated with the cell membrane. Integral membrane proteins are often targeted during the analysis of membrane proteins because their non-membrane spanning domains tend to be more hydrophilic and are often excluded along with cytosolic proteins during membrane protein extraction processes. Because integral membrane proteins are resident within the lipid cell membrane, they are composed of hydrophobic domains, which favor their occupancy in a highly hydrophobic environment. However, this extreme Hydrophobicity impedes their extraction, solubilization and separation, especially in aqueous

media, for example those required during isoelectric focusing.

As already alluded to in Chapters 3 and 4, 2-D isoelectric focusing-polyacrylamide gel electrophoresis (IEF-PAGE) technique [3] is inadequate for membrane protein analysis due to poor solubility of hydrophobic proteins in the IEF dimension. Thus, membrane proteins are considerably underrepresented in 2-D gel patterns [1]. Our approach toward 2-D protein separations is cognizant of the hydrophobic environmental needs of membrane proteins. With the first dimension of our novel separation platform employing SDS μ-CGE and the second dimension utilizing SDS micellar electrokinetic chromatography (MEKC) [3, 4], the issue of membrane protein solubility within the separation buffers is less of a concern compared to IEF buffers. Not only does SDS improve the compatibility of both dimensions, it also ensures that proteins remain denatured and solubilized throughout the entire separation process. As an alternative, microemulsion electrokinetic chromatography (MEEKC) could be used instead of MEKC [5] because microemulsions have been shown to possess greater solubilization capacity than micelles [5]. Sections 6.3.1 and 6.3.2 in this Chapter describe some of the on-going efforts in our labs to separate membrane proteins.

We are interested in developing a microchip-based differential expression electrophoresis platform of membrane proteins for protein biomarker discovery and for generating unique profiles for membrane proteins obtained from diseased cells compared to normal cells. To tackle the problem, we constructed a two-color LIF system that would enable us to monitor fluorescence from two protein samples (*i.e.*, diseased and normal), each labeled with dyes with different excitation and emission wavelengths to differentiate between the two. The two-color LIF system as well as some of the preliminary efforts that we have undertaken in this regard is discussed in section 6.3.1.

We have also been interested in performing microchip-based heart-cut 2-D separations of membrane proteins extracted from adipose stem cells. In this case, the readout modality would rely upon the change in background conductivity of the buffer due to the presence of separated membrane

protein bands; therefore, this approach does not require any fluorescence derivatization of proteins or post-staining with dyes unlike the projects described in Chapters 3 and 4 and this is elaborated upon in Section 6.3.1 of this Chapter. This project is especially attractive because electrode sensors are placed at the end of the first and second dimensions. As protein bands are detected from the first demission via an electrode sensor, the band can be quantitatively transferred into the second dimension for further MEKC or MEEKC separation. By doing this, we can drastically improve the transfer efficiency of the migrating protein plugs from the first into the second dimension unlike a "blinded" injection transfer protocol (described in Chapters 3 and 4), where only a small fraction of the protein peaks from the first dimension are transferred into the second dimension. In addition, using the "blinded" injection process described in Chapters 3 and 4 were plagued with over sampling issues, in which a single band from the first dimension was injected into the second band multiple times. The heart-cutting method that will be employed using conductivity detection at the end of the first and second dimensions will effectively alleviate this over sampling condition.

6.2.2 Microchip Differential Two-dimensional Membrane Protein Expression Profiling using a Two-color Laser Induced Fluorescence System

6.2.2.1 Materials and Methods

6.2.2.1.1 Chip Fabrication

PMMA was selected as the µ-CE substrate because of its suitable physiochemical properties for this application, such as minimal non-specific adsorption artifacts and low levels of autofluorescence to improve the detection limits for ultra-sensitive fluorescence detection [5]. A PMMA cover plate (0.125 mm) was thermally fusion bonded to the substrate by heating in a temperature programmable furnace to 107^{o}C, slightly above the Tg of PMMA. Figure 6.1 shows a topographical layout of the microchip used for this work. Channels were 100 µm deep and 25 µm wide. The 2-D chip platform and separation protocol used in this case was similar to the one described in Section 3.2.1 of Chapter 3.

6.2.2.1.2 Two-color LIF System, Power Supply and Data Analysis

To detect dye-labeled membrane proteins, we have constructed an in-house two-color LIF system. A schematic diagram of this detection system is shown in Figure 6.2. Programmed high-voltages could be applied to the solution reservoirs (A to F, see Figure 6.1) of the microchip with six independently-controlled high-voltage power supplies. The software for LIF data acquisition and control of the power supplies was created using LabVIEW (National Instruments, Austin, TX). Raw 2-D electropherograms could be converted to 2-D images and then to three-dimensional (3-D) landscape representations by dividing the LIF signals from successive runs for each MEKC or MEEKC cycle and plotting the electropherogram at the corresponding cycle on the SDS μ-CGE axis. This procedure can be performed using ImageJ software (National Institute of Health, Bethesda, MD).

The LIF system was configured in an epi-illumination format. Two excitation sources positioned orthogonal to each other consisted of a 532 nm laser diode (L1) positioned on the top (Module SLL-532-DT020-LM, OEM Laser Systems, Inc., East Lansing, MI) and a 633 nm laser diode, L2 (56DIB142/P1, Melles Griot, CO) positioned on the side. Both diodes were separately powered by a custom-built power supply with tunable output power. The lasers were filtered by the appropriate laser bandpass filters, F1 (CWL = 532 nm; part # XL08) and F2 (CWL = 633 nm; part # XL12) from Omega Optical, Brattleboro, VT, and directed onto a dichroic mirror (DF.1; XF2018; Omega Optical) so that L1 was reflected 45^{o} by DF.1 while L2 was allowed to transmit through DF.1 after which both wavelengths were passed through another dichroic mirror (DF.2; XF2055; Omega Optical) that reflected both excitation wavelengths into a microscope objective (40x, NA = 0.65; Nikon, Natick, MA) and into the fluidic channel. An X-Y-Z translational stage (Newport, Irvine, CA) was used to position the microdevice with respect to the laser beams. The resulting emissions were then collected through the same objective and routed through another dichroic mirror (DF.3; DMLP605; Thorlabs). Emission from L1 was reflected by DF.3 and filtered through a longpass filter (CWL = 550 nm;

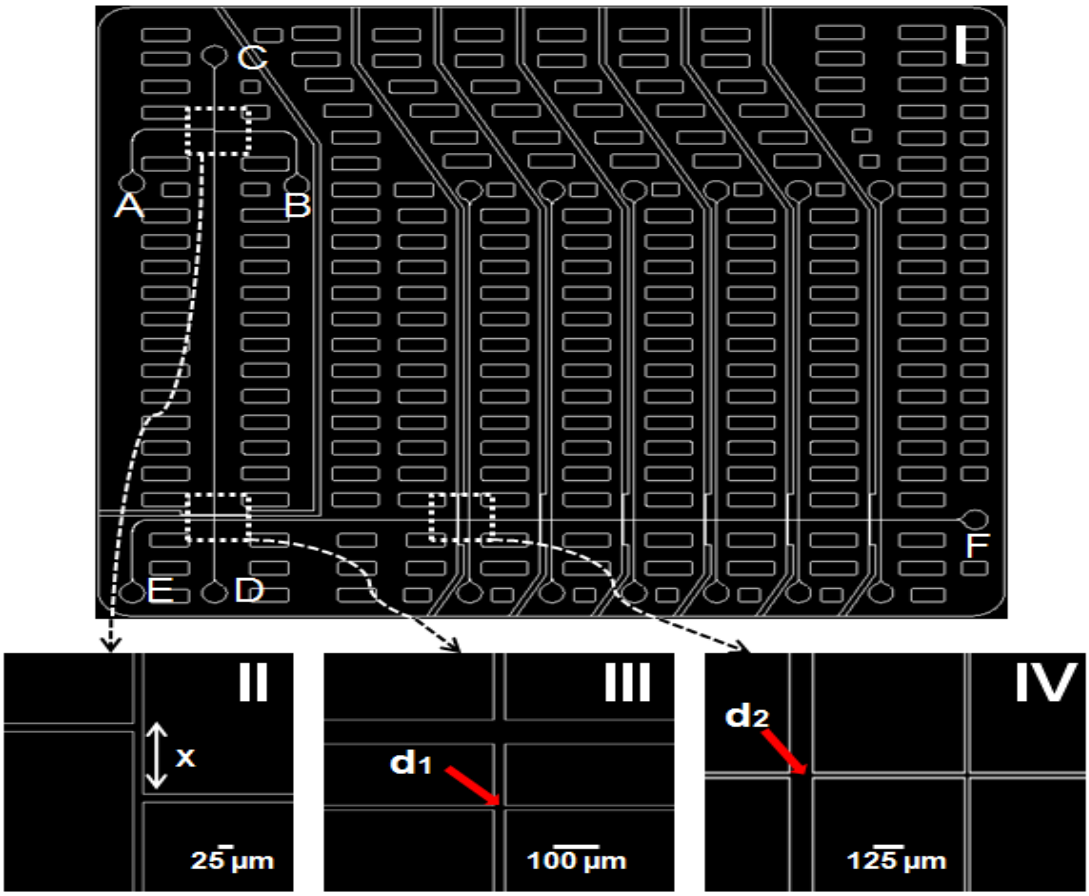

Figure 6.1 (I) Topography of the 2-D microchip, which was drawn using AutoCAD software. The channels were 100 µm deep and 25 µm wide in all cases. The 1st and 2nd dimension channels were 4 cm (filled with gel media) and 5.5 cm (filled with MEKC buffer), respectively, in terms of their total column lengths. The effective column lengths for the 1st and 2nd dimensions were 3 cm and 1.5 cm, respectively. (II) Inset showing an off-set injection cross for sample loading with X = 150 µm. (III) Inset showing the 1st dimension detection point (d_1) at the end of the 35.25 mm (i.e., 30.25 mm effective length) column. The vertical column is the 1st dimension channel spanning from C to D. Top horizontal channel is an electrode pair channel guide, whose application is discussed in Section 6.3.2 because the same chip would be used later for a 2-D separation with conductivity readout (see Section 6.3.2). Lower horizontal channel is a section of E-F intersecting with C-D. (IV) Inset showing the 2nd dimension detection point (d_2, at effective length = 15 mm). Horizontal column is a section of the 2nd dimension channel stemming from E to F. Left vertical channel is an electrode pair channel guide, whose application is also discussed in section 6.3.2.

3RD550LP; Omega Optical) and a bandpass filter (CWL = 570±10 nm; XB99 570BP10; Omega Optical) whereas emission from L2 transmitted through DF.3 and filtered through a longpass filter (CWL = 650 nm; part # 3RD650LP; Omega Optical) and a bandpass filter (CWL = 670 ±10 nm; XB114 670BP10; Omega Optical).

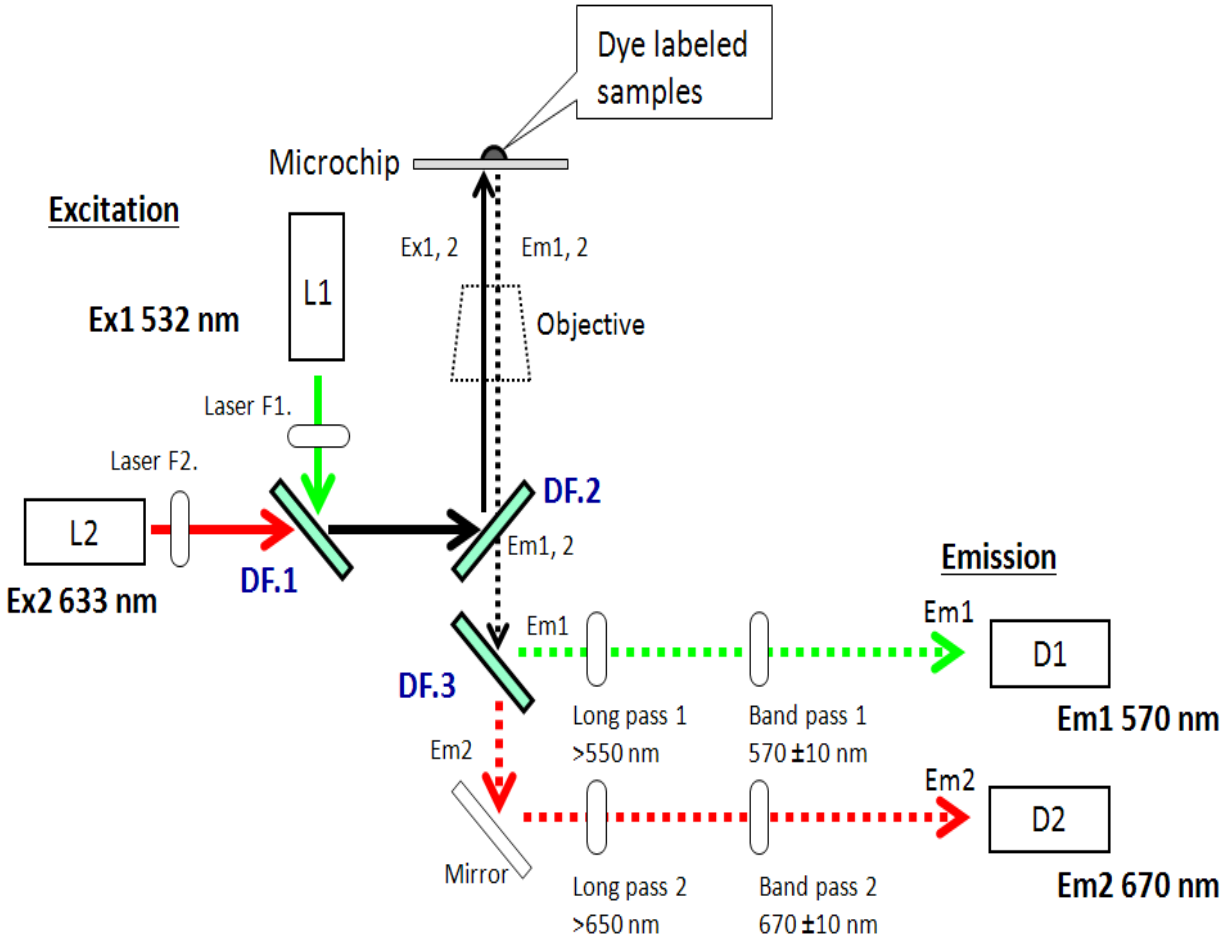

Figure 6.2 LIF system configured in an epi-illumination format. Two independent excitation sources consisted of a 532 nm (L1) solid-state YAG laser and a 633 nm (L2) diode laser. Laser radiation was filtered by bandpass filters, F1 and F2. The excitation sources were directed to an objective by first directing them through a dichroic mirror (DF.1), which reflected L1 and transmitted L2. The objective focused the lasers into the micro-separation channel. Resulting emissions were routed through the same objective and then through another dichroic mirror (DF.3), which directed emission from L1 through a set of filters and transmitted emission from L2 onto a mirror that in turn reflected the emission through another set of filters. The filtered fluorescence emissions were separately focused onto two independent single photon avalanche diodes. The LIF signal was acquired on a personal computer equipped with an I/O connector board (National Instruments model CB-68LP, Austin, TX) and a pulse converter (IBH model TB-01, Glasgow, UK). Data acquisition software was written in LabView.

Finally, the filtered fluorescence emission from L1 (Em1) and L2 (Em2) were focused onto two independent single photon avalanche diodes (SPADs; PicoQuant model SPCM 200B, Berlin, Germany). The LIF signals were acquired on a personal computer equipped with an I/O connector

board (National Instruments model CB-68LP, Austin, TX) and a pulse converter (IBH model TB-01, Glasgow, UK). Data acquisition software was written in LabView.

6.2.2.1.3 Extraction of Membrane Proteins from Human Cell Lines

Human breast (normal) epithelial cells (184A1; part # CRL-8798) and human breast adenocarcinoma (MCF7; part # HTB-22) were obtained from ATCC, Manassas, VA and were separately lysed following a protocol adapted from Pierce and using their Mem-PER Eukaryotic Membrane Protein Extraction Kit (part # 89826; Pierce, Rockford, IL). Briefly, ~2.8 x 10^6 cells of normal breast cells and ~5.6 x 10^6 cells of MCF7 cells were rinsed in 0.85 mL and 1.7 mL of 1x PBS buffer and centrifuged at 850 x g for 2 min. The supernatants were discarded and to the pellets, 5 µL (normal) and 10 µL (cancer) of protease inhibitor (part # 1860932; Thermo Scientific, Rockford, IL) plus 75 µL (normal) and 150 µL (cancer) of lysis buffer (Reagent A) were added, homogenized by pipetted and incubated for 10 min at room temperature with occasional vortexing. A solubilizing solution comprised of a mixture of Reagent C and B in the ratio of 2:1 were quickly added in the amounts of 225 µL (normal) and 450 µL (cancer) before the lysed cells were placed on ice. Reagent B is a proprietary detergent while reagent A is a dilution buffer. The tubes were centrifuged at 10,000 x g for 3 min at 4 ^oC after which the supernatant was transferred to new tubes and incubated for 30 min in a GC convection oven at 37^oC. The membrane fraction (bottom layer) of each sample was separated from the hydrophilic fraction (top phase) by centrifugation at 10,000 x g for 2 min at room temperature. The top layer, the hydrophilic phase, was quickly, but carefully removed using a pipette.

6.2.2.1.4 Membrane Protein Fluorescence Labeling

Because we used thiol reactive dyes to label the proteins, we first reduced the protein disulfide bonds to free thiols using TCEP. A 0.35 M TCEP stock solution was prepared by adding 12 mM Tris-HCl buffer (pH 7) to 100 mg TCEP to a total volume of 1 mL. Reduction of protein samples was done

by adding ~28.6 µL from the TCEP stock solution to each protein sample and making up each solution to 1 mL using the 12 mM Tris-HCl buffer so that a TCEP final concentration of 10 mM was used. The reaction was incubated in ice for 1 h with occasional vortexing. Conjugation of dye molecules to proteins was carried out by adding at a molar ratio of 1:10 (dye:protein), ~22 µL of DyLight 649 (Excitation/emission = 646/674 nm; product # 46615; Thermo Scientific) to the MCF7 membrane protein sample. The dye solution was prepared by dissolving 1 mg of the dye in 100 µL of DMF. A similar reaction was also carried out for the membrane proteins from the normal cells, except that DyLight 549 (Excitation/emission = 593/618 nm; product # 46607; Thermo Scientific) was used instead. Excess dyes were removed by dialyzing each protein sample using the Pierce Slide-A-Lyzer dialysis kit (part # 66380), whose membrane is made of cellulose with a 10 KDa cut off. Membrane protein concentrations were determined to be ~0.3 mg/mL and 0.013 mg/mL for MCF7 and normal cell line membrane proteins, respectively.

6.2.2.1.5 Microchip 2-D Electrophoretic Separations

Two-dimensional electrophoretic separations are performed with a microchip whose topography is shown in Figure 6.1. All channels are rinsed with a solution of 5 mg/mL of methyl hydroxyethyl cellulose (MHEC) dissolved in 1x PBS (pH = 7.2, Sigma-Aldrich, St. Louis, MO, USA). Prior to the µ-CE 2-D separation, the first dimension channel is filled with a seiving matrix consisting of a SDS 14-200 linear polyacrylamide gel (Beckman Coulter Inc., Fullerton, CA, USA) containing 0.05% w/v MHEC, while the second dimension channel is filled with the MEKC or MEEKC buffer (see Chapter 4). MCF7 membrane proteins are injected into the chip injection cross (i.e., X in II of Figure 6.1) and proteins in the plug (150 µm) separated along channel C-D in a 1-D membrane protein separation format (i.e., while monitoring fluorescence at d_1). Based on the 1-D electropherogram, we can carry out a 2-D separation of the membrane proteins following the strategy discussed in Chapter 3 in which co-migrating proteins reaching the end of the first dimension are “blindly” injected into the

second dimension for further separation. Profiles generated from the 2-D separation of the MCF7 membrane proteins can be compared to profiles generated from a 2-D separation of the membrane proteins isolated from the normal breast cell line. Furthermore, comparing these two unique profiles could lead to the identification of potential membrane protein biomarkers. A rigorous analysis can be made by separating the two protein samples in one run. This is possible because the two protein samples are labeled with dyes with different excitation wavelengths whose emissions are processed by two independent SPAD detectors (see Figure 6.2) and the display from the detectors appear on separate windows on the monitor as shown in Figure 6.3.

6.2.3 Heart-cut Two-dimensional Separation of Adult Stem Cell Membrane Proteins Using Polymer Microchip Integrated with Contact Conductivity Detection

6.2.3.1 Materials and Methods

6.2.3.1.1 Chip Fabrication

Because the readout modality for this particular separation project would rely upon the change in background conductivity, we proceeded to fabricate a PMMA chip with integrated platinum electrodes. The topography of the chip is the same as the one already described in Figure 6.1. Platinum electrodes (part # 357367-180MG; Sigma Aldrich), 100 μm in diameter, were cut into ~5 mm long pieces and manually placed in electrode guide channels (see Figure 6.1). An electrode pair is placed at the end of each dimension such that the spacing between the electrodes would be 25 μm (equal to the channel width).

The effective length, which is the distance from the injection cross to the electrode sensors in the first dimension, is 30 mm while the distance from the intersection of C-D and E-F is 15 mm. After ensuring that the electrodes are in the guides, a 125 μm thick cover slip can be thermally annealed onto the substrate with the embedded electrodes set at 107 ^{o}C in a GC oven. Cylindrical copper connectors can be used to make contact with the Pt electrodes so that electrical wires are emanating from the conductivity system (see Section 6.3.2.1.2) and terminated with alligator clips used to make contact

with the copper contacts.

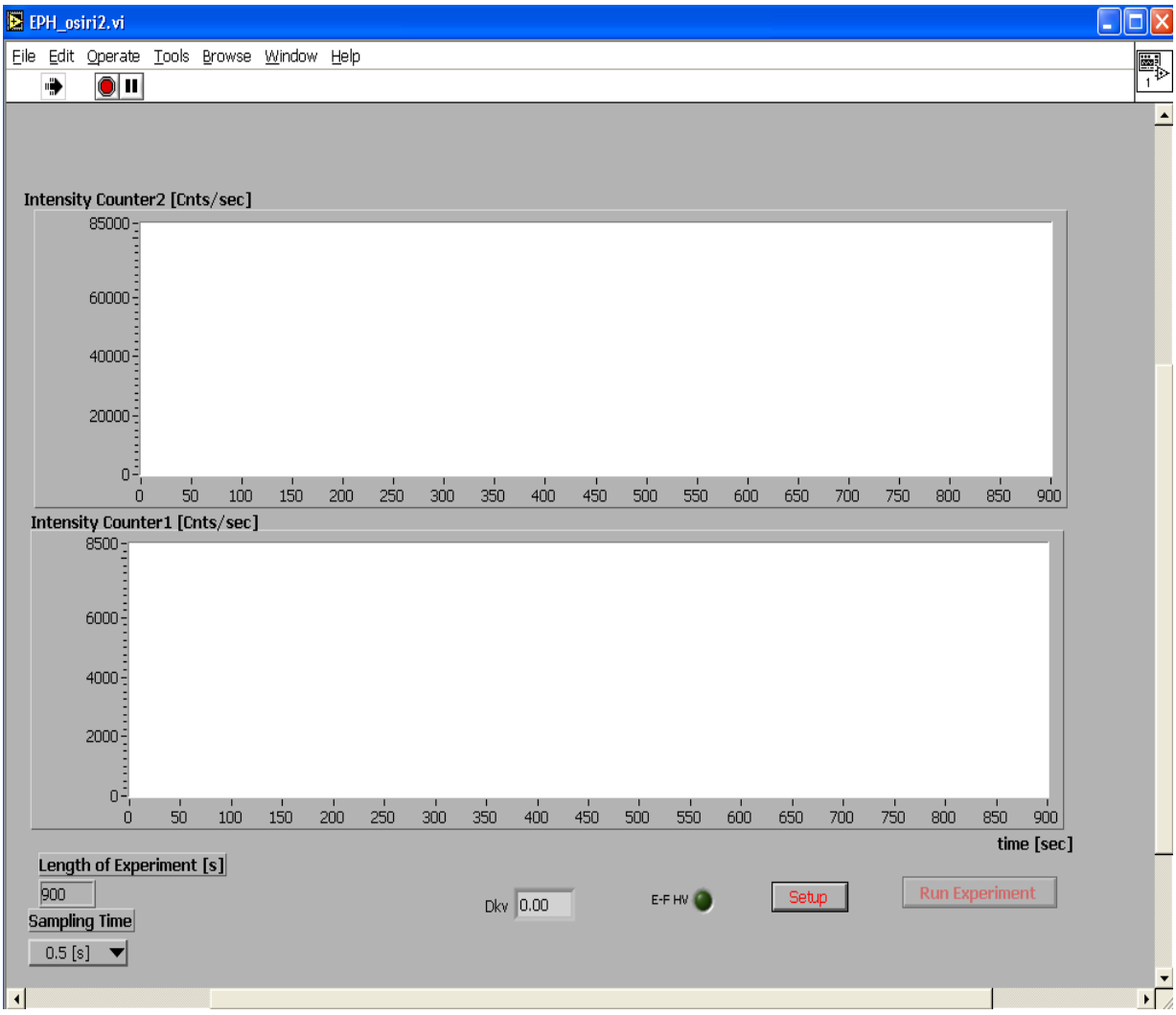

Figure 6.3 Window display for the two-color LIF detection system shown in Figure 6.2. Top display is associated with emission from DyLight 549 (Excitation/emission = 593/618 nm) while the bottom display is associated with emission from DyLight 649 (Excitation/emission = 646/674 nm).

6.2.3.1.2 Conductivity System and Electronics

The proposed conductivity system shown in Figure 6.4 is basically an AC current source. The detector system monitors changes in the solution's conductivity across the detection area between the electrodes. The conductivity detector circuit consists of a synthetic inductor and a gyrator, which are made in parallel to any double layer capacitance, C_d and stray (or parasitic) capacitance, C_s. This configuration eliminates any adverse effects of C_s thereby improving the overall sensitivity of the

detector system. The detector system supplies an AC current of ±5 µA at ~ 40 kHz to avoid charge build up at the electrode surfaces due to C_d [6].

Figure 6.4 Conductivity System Set-up. Monitors changes in the solution's conductivity across the detection area between the electrodes. The system supplies an AC current of ±5 µA at ~ 40 kHz to avoid charge build up at the electrode surfaces due to C_d. This system is capable of monitoring events at the first dimension (CHAN 1) and second dimension (CHAN 2).

The system is endowed with a sensitive detection circuit designed to be responsive to small conductivity changes within the buffer. Previous attempts at measuring these changes utilizing the bipolar conductivity technique [7] produced poor results, particularly when the channel width was increased to 50 µm. The commonly used bipolar conductivity method makes use of the fact that the time constant of C_d in Figure 6.5, is much larger than C_p. Thus, the parasitic capacitance is fully charged before the double layer, and therefore has little effect on the current sensed by the amplifier. This current is now dependent mostly on the conductivity, G_s of the solution. However, the sensitivity of this arrangement is limited and for a small change in conductivity on the order of 1%, the output of the amplifier with a bipolar voltage of ±500 mV will only be ±5 mV. Such small signals can easily be

obscured by background noise. This problem is compounded if the buffer's conductivity is so high that further increases in amplifier gain can result in saturation or at least, reduced dynamic range.

For these reasons, a different approach was taken. Referring to Figure 6.5, the following method was developed. First, to reduce the effect of parasitic capacitance, $C_{p,}$ due to wiring and electrode configuration, a synthetic inductor, L, of 132 mH was designed using a Gyrator circuit. Gyrators, for a given bandwidth, allow the creation of high quality factor (Q) inductors from RC components. The inductance generated was placed in parallel with the capacitance C_p, and the sine frequency varied to locate the resonance peak of the voltage across L and C_p. Once this resonance point is found (using the *freq* adjust knob), the voltage across the sample cell could be directly sensitive to changes in G_s. The equation for the impedance of the equivalent circuit consisting of the sample cell in parallel with the inductor is a third order polynomial. This makes the analytical determination of impedance difficult, but for a typical circuit values near resonance, the absolute value of the impedance; $| Z | \approx 1/G_s$. The sine wave generator produces a waveform that could be adjusted from 0 to ±1 V in amplitude and 25 – 50 kHz in frequency.

A target frequency of 40 kHz was chosen to minimize the impedance due to C_d and hold the inductance to a reasonable value. This signal was fed to a transconductance amplifier, $G_{1,}$ which converted the voltage sinusoid to a current. The gain of G_1 is 10 μA/volt. A current source was needed to drive the sample cell because a voltage source, with its low output impedance, would spoil the circuit's Q. For our experiments, the current was set to ±5 μA. The required resonance frequency could be approximated by the standard parallel resonance equation, $f = 1/2\pi (LCp)^{1/2}$. The voltage across the sample cell was fed to an Analog Devices AD630 synchronous modulator – demodulator that was configured as a phase sensitive detector. The AD630's reference input was driven from the phase delayed sine wave oscillator output. This phase adjustment was needed to compensate for phase lags in the detected sample voltage. This voltage is then fed to a low pass filter with a cutoff frequency of 180

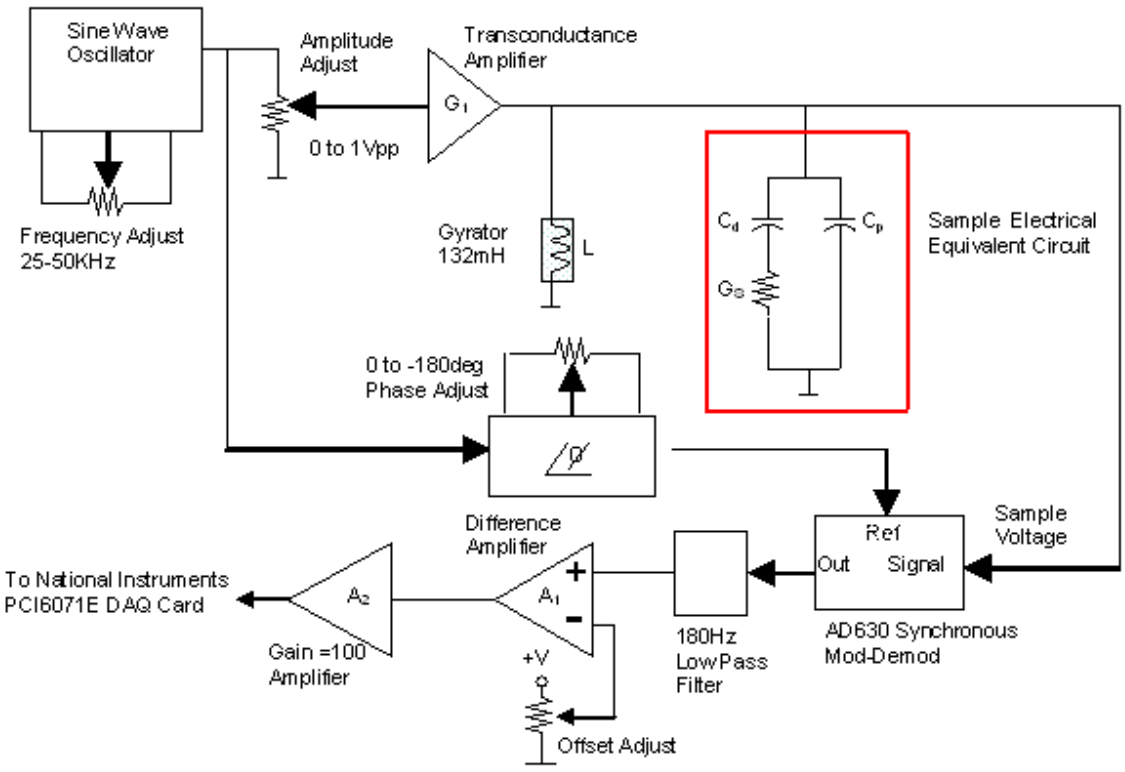

Figure 6.5. Schematic of the Conductivity Detection Electronics. Changes in background conductivity due to G_o is registered in the circuit as voltage change (sample voltage), which is filtered through a lowpass filter after comparing with the background reference. The signal is ultimately, amplified prior to user visualizing the signal on the computer monitor.

Hz. The filter produced an average DC signal that was sent to a differencing amplifier, A_1. The difference amp nulled the output to 0 V while measuring the buffer alone. Thus, the high gain amplifier, A_2, could amplify small changes in solution conductivity without saturating the voltage produced by the buffer itself. A National Instruments PCI6071E, 12 bit A/D acquisition card was used to convert the analog signal to 12 bit data.

6.2.3.1.3 Heart-cut 2-D Separation of Membrane Proteins

In a heart-cut transfer protocol securing a 1-D electropherogram of the membrane protein separation prior to a 2-D separation would not be necessary because the technique calls for material from the first dimension to be transferred into the second as they migrate towards the end of the first

dimension. In Chapters 3, 4 and 6 (Section 6.2.2), a 1-D separation was required primarily to determine when the first peak was expected at the end of the first dimension. In those separations, which employed "blinded" injection of material from the first dimension into the second dimension, one peak may be sampled multiple times into the second dimension, and the transfer efficiency can deteriorate as well. Also, prolonged development times are apparent with the blinded injection protocol. In our heart-cut protocol, electrode sensors are placed around the end of the first dimension and as a protein plug transverses the electrode sensors, the signal generated by the plug above baseline (or background buffer) would, after a preset time, initiate protein movement from the first dimension into the second dimension.

6.3 References

[1] Santoni, V., Molloy, M., Rabilloud, T., *Electrophoresis* 2000, *21*, 1054-1070.

[2] Braun, R. J., Kinkl, N., Beer, M., Ueffing, M., *Analytical and Bioanalytical Chemistry* 2007, *389*, 1033-1045.

[3] Osiri, J. K., Shadpour, H., Park, S., Snowden, B. C., *et al.*, *Electrophoresis* 2008, *29*, 4984-4992.

[4] Shadpour, H., Soper, S. A., *Analytical Chemistry* 2005, *ASAP*.

[5] Shadpour, H., Musyimi, H., Chen, J., Soper, S. A., *Journal of Chromatography, A* 2006, *1111*, 238-251.

[6] Galloway, M., Stryjewski, W., Henry, A., Ford, S. M., *et al.*, *Analytical Chemistry* 2002, *74*, 2407-2415.

[7] Johnson, D. E., Enke, C. G., *Analytical Chemistry* 1970, *42*, 329-&.

[8] McWhorter, S., Soper, S. A., *Journal of Chromatography A* 2000, *883*, 1-9.

Appendix A: Permissions

Dear Bettina Loycke,

Copyright Permission Request

I am the co-author (equal contributor) of the ELECTROPHORESIS article entitled, Surface modification of poly(methyl methacrylate) microfluidic devices for high-resolution separations of single-stranded DNA, by Llopis SL, Osiri J, Soper, SA and would like to obtain permission to incorporate it as part of my dissertation.

Thank you.

Sincerely,
John K. Osiri (Ph.D. Candidate)
Department of Chemistry
Louisiana State University
Baton Rouge, LA 70803
225 810 8520

Dear Customer

Thank you for your request.

We hereby grant permission for the requested use expected that due credit is given to the original source.
For material published before 2007 additionally: Please note that the author's permission is also required.

Ø Please note that we only grant rights for a printed version, but not the rights for an electronic/ online/ web/ microfiche publication, but you are free to create a link to the article in question which is posted on our website (http://www3.interscience.wiley.com)

If material appears within our work with credit to another source, authorisation from that source must be obtained.

Credit must include the following components:
- Books: Author(s)/ Editor(s) Name(s): Title of the Book. Page(s). Publication year. Copyright Wiley-VCH Verlag GmbH & Co. KGaA. Reproduced with permission.

- Journals: Author(s) Name(s): Title of the Article. Name of the Journal. Publication year. Volume. Page(s). Copyright Wiley-VCH Verlag GmbH & Co. KGaA. Reproduced with permission.

With kind regards

Bettina Loycke
****
Bettina Loycke

Copyright & Licensing Manager
Wiley-VCH Verlag GmbH & Co. KGaA
Boschstr. 12
69469 Weinheim
Germany
Phone: +49 (0) 62 01- 606 - 280
Fax: +49 (0) 62 01 - 606 - 332
Email: rights@wiley-vch.de
Dear Bettina Loycke,

Copyright Permission Request (II)

I am the first author of the ELECTROPHORESIS article entitled, Generating high peak capacity 2-D maps of complex proteomes using PMMA microchip electrophoresis, by Osiri JK, Shadpour H, Park S, Snowden BC, Chen ZY, Soper, SA and would like to obtain permission to incorporate it as part of my dissertation.

Thank you.

Sincerely,
John K. Osiri (Ph.D. Candidate)
Department of Chemistry
Louisiana State University
Baton Rouge, LA 70803
225 810 8520

Dear Customer

Thank you for your request.

We hereby grant permission for the requested use expected that due credit is given to the original source.
For material published before 2007 additionally: Please note that the author's permission is also required.

Ø Please note that we only grant rights for a printed version, but not the rights for an electronic/ online/ web/ microfiche publication, but you are free to create a link to the article in question which is posted on our website (http://www3.interscience.wiley.com)

If material appears within our work with credit to another source, authorisation from that source must be obtained.

Credit must include the following components:
- Books: Author(s)/ Editor(s) Name(s): Title of the Book. Page(s). Publication year. Copyright Wiley-VCH Verlag GmbH & Co. KGaA. Reproduced with permission.

- Journals: Author(s) Name(s): Title of the Article. Name of the Journal. Publication year. Volume. Page(s). Copyright Wiley-VCH Verlag GmbH & Co. KGaA. Reproduced with permission.

With kind regards

Bettina Loycke
****
Bettina Loycke
Copyright & Licensing Manager
Wiley-VCH Verlag GmbH & Co. KGaA
Boschstr. 12
69469 Weinheim
Germany
Phone: +49 (0) 62 01- 606 - 280
Fax: +49 (0) 62 01 - 606 - 332
Email: rights@wiley-vch.de

From: John Osiri [mailto:josiri1@tigers.lsu.edu]
Sent: Thursday, November 12, 2009 12:23 PM
To: Permissions - US
Subject: Copyright Permission Request (RAPID COMMUNICATIONS IN MASS SPECTROMETRY)

Copyright Permission Request

TO WHOM IT MAY CONCERN:

I am not an author of the Rapid Communications in Mass Spectrometry article entitled, Integration of immobilized trypsin bead beds for protein digestion within a microfluidic chip incorporating capillary electrophoresis separations and an electrospray mass spectrometry interface by Wang, C., Oleschuk, R., Ouchen, F., Li, J., et al., but I would like to obtain permission to incorporate a figure presented in the article (shown in the attachment) in my dissertation entitled, PLATFORMS AND PROTOCOLS FOR THE MULTIDIMENSIONAL MICROCHIP ELECTROPHORETIC ANALYSIS OF COMPLEX PROTEOMES.
Thanks,

John

From: Goldweber, Paulette - Hoboken On Behalf Of Permissions - US
Sent: 12 November 2009 20:54
To: Permission Requests - UK
Subject: FW: Copyright Permission Request (RAPID COMMUNICATIONS IN MASS SPECTROMETRY)

Dear John,

Thank you for your email request. Permission is granted for you to use the material below for your thesis/dissertation subject to the usual acknowledgements and on the understanding that you will reapply for permission if you wish to distribute or publish your thesis/dissertation commercially.

Best wishes,

Cassandra Fryer

Permissions Assistant
Wiley-Blackwell
9600 Garsington Road
Oxford OX4 2DQ
UK
Tel: +44 (0) 1865 476158Fax: +44 (0) 1865 471158
Email: cassandra.fryer@wiley.com
Paulette Goldweber| Associate Manager, Permissions| Global Rights - John Wiley & Sons, Inc.
Ph: 201-748-8765 | F: 201-748-6008| pgoldweb@wiley.com

Copyright Permission Request

TO WHOM IT MAY CONCERN:

I am not an author of the ANALYST article entitled, PDMS-based microfluidics for proteomic analysis by Dodge, A., Brunet, E., Chen, S., Goulpeau, J., et al., (Analyst, Cambridge, United Kingdom, 2006, 131, 1122-1128), but I would like to obtain permission to incorporate a figure presented in the article (shown in the attachment) in my dissertation entitled, PLATFORMS AND PROTOCOLS FOR THE MULTIDIMENSIONAL MICROCHIP ELECTROPHORETIC ANALYSIS OF COMPLEX PROTEOMES.
Thanks,
John

Dear Dr Osiri

The Royal Society of Chemistry hereby grants permission for the use of the material specified below in the work described and in all subsequent editions of the work for distribution throughout the world, in all media including electronic and microfilm. You may use the material in conjunction with computer-based electronic and information retrieval systems, grant permissions for photocopying, reproductions and reprints, translate the material and to publish the translation, and authorize document delivery and abstracting and indexing services. The Royal Society of Chemistry is a signatory to the STM Guidelines on Permissions (available on request).

Please note that if the material specified below or any part of it appears with credit or acknowledgement to a third party then you must also secure permission from that third party before reproducing that material. Please ensure that the published article carries a credit to The Royal Society of Chemistry in the following format:

[Original citation] – Reproduced by permission of The Royal Society of Chemistry

and that any electronic version of the work includes a hyperlink to the article on the Royal Society of Chemistry website. The recommended form for the hyperlink is http://dx.doi.org/10.1039/DOI suffix, for example in the link http://dx.doi.org/10.1039/b110420a the DOI suffix is ‘b110420a’. To find the relevant DOI suffix for the RSC paper in question, go to the Journals section of the website and locate your paper in the list of papers for the volume and issue of your specific journal. You will find the DOI suffix quoted there.

Regards
Gill Cockhead
Contracts & Copyright Executive
Gill Cockhead (Mrs), Contracts & Copyright Executive
Royal Society of Chemistry, Thomas Graham House
Science Park, Milton Road, Cambridge CB4 0WF, UK
Tel +44 (0) 1223 432134, Fax +44 (0) 1223 423623
http://www.rsc.org

Dear John

RE: Journal of the Royal Society Interface 2008, 5, S123-S130) by Sedgwick, H., Caron, F., Monaghan, P. B., Kolch, W., Cooper, J. M.,

The Royal Society is pleased to grant permission for use of the above material, subject to the following conditions:
1. Full acknowledgement is given to the original source, with full details of the author(s), title, figure/page numbers, year of publication and the publisher.
2. The permission of the author(s) or the author's estate is obtained where practical.
3. The material is to be used only as described in your email and this permission is granted for one-time use only.

Yours sincerely

Jennifer Kren
Editorial Administrator

Dear John,

Thank you for your explanation.

Permission is granted to reproduce the following figure

Development of a fully integrated microfluidic system for sensing infectious viral disease

ELECTROPHORESIS

Volume 29, Issue 14, Date: No. 14 July 2008, Pages: 2960-2969

Yun Suk Huh, Tae Jung Park, Eun Zoo Lee, Won Hi Hong, Sang Yup Integrated microfluidic system for on-chip analysis of biomolecules. (A) Schematic representation of the fully integrated microfluic system showing the sample mixing zone for disruption of cells, the sample purification zone with SPE, and the gold microcircle patterned analysis zone for detection infectious pathogens. Reservoirs in the mixing chamber were labeled as SI, EB, and LS for sample inlet, elution buffer, and lysis solution, respectively. Detection reservoirs were labled as RS, CS, and WP for reaction sample, control sample, and waste port, respectively. (B) Chemical structure of Teflon AF 1600 used for the hydrophobic film valve (V2). (C) The AAm functionalized SPE was packed by in situ polymerization. (D) Gold microarray for the detection of infectious viral disease. (E) Photograph of the integrated system

coupled with a magnetic stirrer. The cylinder-type micropillar for packing SPE is for removing debris (V3). Device dimension are 10.0 (width) x 18.0 (length) x 5 (height) mm. (Reproduced from Electrophoresis, 29, 2008, 2960-2969).

- We hereby grant permission for the requested use expected that due credit is given to the original source.
- For material published before 2007 additionally: Please note that the (co-)author's permission is also required.

If material appears within our work with credit to another source, authorisation from that source must be obtained.

Credit must include the following components:

- Books: Author(s)/ Editor(s) Name(s): Title of the Book. Page(s). Publication year. Copyright Wiley-VCH Verlag GmbH & Co. KGaA. Reproduced with permission.
- Journals: Author(s) Name(s): Title of the Article. Name of the Journal. Publication year. Volume. Page(s). Copyright Wiley-VCH Verlag GmbH & Co. KGaA. Reproduced with permission.

With kind regards

Bettina Loycke
****
Bettina Loycke
Senior Rights Manager
Wiley-VCH Verlag GmbH & Co. KGaA
Boschstr. 12
69469 Weinheim
Germany

Phone: +49 (0) 62 01- 606 - 280
Fax: +49 (0) 62 01 - 606 - 332
Email: rights@wiley-vch.de

From: John Osiri [mailto:josiri1@tigers.lsu.edu]
Sent: Thursday, November 12, 2009 12:23 PM
To: Permissions - US
Subject: Copyright Permission Request (RAPID COMMUNICATIONS IN MASS SPECTROMETRY)

Copyright Permission Request
TO WHOM IT MAY CONCERN:

I am not an author of the Rapid Communications in Mass Spectrometry article entitled, Integration of immobilized trypsin bead beds for protein digestion within a microfluidic chip incorporating capillary electrophoresis separations and an electrospray mass spectrometry interface by Wang, C., Oleschuk, R., Ouchen, F., Li, J., et al., but I would like to obtain permission to incorporate a figure presented in the article (shown in the attachment) in my dissertation entitled, PLATFORMS AND PROTOCOLS

FOR THE MULTIDIMENSIONAL MICROCHIP ELECTROPHORETIC ANALYSIS OF COMPLEX PROTEOMES.
Thanks,

John

--
Prince Dr. John K. Osiri, Ph.D.
Choppin 204, Microfluidic and Biomolecular Laboratories
Lousiana State University (LSU),
Baton Rouge, LA, 70803, USA
(225) 810-8520 (Cell)
(225) 274-7709 (Office)
(225) 274-3458 (Fax)

Mailing Address:
P. O. Box 17424
Baton Rouge, LA, 70893

Dear John,

Thank you for your email request. Permission is granted for you to use the material below for your thesis/dissertation subject to the usual acknowledgements and on the understanding that you will reapply for permission if you wish to distribute or publish your thesis/dissertation commercially.

Best wishes,
Cassandra Fryer

Permissions Assistant
Wiley-Blackwell
9600 Garsington Road
Oxford OX4 2DQ
UK
Tel: +44 (0) 1865 476158Fax: +44 (0) 1865 471158

ELSEVIER LICENSE
TERMS AND CONDITIONS

Nov 13, 2009

This is a License Agreement between John K. Osiri ("You") and Elsevier ("Elsevier") provided by Copyright Clearance Center ("CCC"). The license consists of your order details, the terms and conditions provided by Elsevier, and the payment terms and conditions.

All payments must be made in full to CCC. For payment instructions, please see information listed at the bottom of this form.

Supplier	Elsevier Limited The Boulevard,Langford Lane Kidlington,Oxford,OX5 1GB,UK
Registered Company Number	1982084
Customer name	John K. Osiri
Customer address	Choppin 204 Baton Rouge, LA 70803
License Number	2306180601026
License date	Nov 11, 2009
Licensed content publisher	Elsevier
Licensed content publication	Journal of Chromatography A
Licensed content title	Integrated microfabricated systems including a purification module and an on-chip nano electrospray ionization interface for biological analysis
Licensed content author	Julien Carlier, Steve Arscott, Vincent Thomy, Jean-Christophe Camart, Cécile Cren-Olivé and Séverine Le Gac
Licensed content date	15 April 2005
Volume number	
Issue number	
Pages	0
Type of Use	Thesis / Dissertation

Portion	Figures/table/illustration/abstracts
Portion Quantity	2
Format	Both print and electronic
You are an author of the Elsevier article	No
Are you translating?	No
Order Reference Number	
Expected publication date	Nov 2009
Elsevier VAT number	GB 494 6272 12
Permissions price	0.00 USD

ELSEVIER LICENSE
TERMS AND CONDITIONS

Nov 13, 2009

This is a License Agreement between John K. Osiri ("You") and Elsevier ("Elsevier") provided by Copyright Clearance Center ("CCC"). The license consists of your order details, the terms and conditions provided by Elsevier, and the payment terms and conditions.

All payments must be made in full to CCC. For payment instructions, please see information listed at the bottom of this form.

Supplier	Elsevier Limited The Boulevard,Langford Lane Kidlington,Oxford,OX5 1GB,UK
Registered Company Number	1982084
Customer name	John K. Osiri
Customer address	Choppin 204 Baton Rouge, LA 70803
License Number	2306191160185
License date	Nov 11, 2009
Licensed content publisher	Elsevier
Licensed content publication	Analytica Chimica Acta
Licensed content title	Protein digestion and phosphopeptide enrichment on a glass microchip

Licensed content author	Guihua Eileen Yue, Michael G. Roper, Catherine Balchunas, Abigail Pulsipher, Joshua J. Coon, Jeffery Shabanowitz, Donald F. Hunt, James P. Landers and Jerome P. Ferrance
Licensed content date	30 March 2006
Volume number	564
Issue number	1
Pages	7
Type of Use	Thesis / Dissertation
Portion	Figures/table/illustration/abstracts
Portion Quantity	1
Format	Both print and electronic
You are an author of the Elsevier article	No
Are you translating?	No
Order Reference Number	
Expected publication date	Nov 2009
Elsevier VAT number	GB 494 6272 12
Permissions price	0.00 USD
Value added tax 0.0%	0.00 USD
Total	0.00 USD

ELSEVIER LICENSE
TERMS AND CONDITIONS

Nov 13, 2009

This is a License Agreement between John K. Osiri ("You") and Elsevier ("Elsevier") provided by Copyright Clearance Center ("CCC"). The license consists of your order details, the terms and conditions provided by Elsevier, and the payment terms and conditions.

All payments must be made in full to CCC. For payment instructions, please see information listed at the bottom of this form.

Supplier	Elsevier Limited The Boulevard,Langford Lane Kidlington,Oxford,OX5

	1GB,UK
Registered Company Number	1982084
Customer name	John K. Osiri
Customer address	Choppin 204 Baton Rouge, LA 70803
License Number	2306210410550
License date	Nov 11, 2009
Licensed content publisher	Elsevier
Licensed content publication	Journal of Chromatography B: Biomedical Sciences and Applications
Licensed content title	Integrated microchip-device for the digestion, separation and postcolumn labeling of proteins and peptides
Licensed content author	Norbert Gottschlich, Christopher T. Culbertson, Timothy E. McKnight, Stephen C. Jacobson and J. Michael Ramsey
Licensed content date	4 August 2000
Volume number	
Issue number	
Pages	0
Type of Use	Thesis / Dissertation
Portion	Figures/table/illustration/abstracts
Portion Quantity	1
Format	Both print and electronic
You are an author of the Elsevier article	No
Are you translating?	No
Order Reference Number	
Expected publication date	Nov 2009
Elsevier VAT number	GB 494 6272 12
Permissions price	0.00 USD

ELSEVIER LICENSE
TERMS AND CONDITIONS

Nov 13, 2009

This is a License Agreement between John K. Osiri ("You") and Elsevier ("Elsevier") provided by Copyright Clearance Center ("CCC"). The license consists of your order details, the terms and conditions provided by Elsevier, and the payment terms and conditions.

All payments must be made in full to CCC. For payment instructions, please see information listed at the bottom of this form.

Supplier	Elsevier Limited The Boulevard,Langford Lane Kidlington,Oxford,OX5 1GB,UK
Registered Company Number	1982084
Customer name	John K. Osiri
Customer address	Choppin 204 Baton Rouge, LA 70803
License Number	2306191307950
License date	Nov 11, 2009
Licensed content publisher	Elsevier
Licensed content publication	Analytica Chimica Acta
Licensed content title	Protein digestion and phosphopeptide enrichment on a glass microchip
Licensed content author	Guihua Eileen Yue, Michael G. Roper, Catherine Balchunas, Abigail Pulsipher, Joshua J. Coon, Jeffery Shabanowitz, Donald F. Hunt, James P. Landers and Jerome P. Ferrance
Licensed content date	30 March 2006
Volume number	564
Issue number	1
Pages	7
Type of Use	Thesis / Dissertation
Portion	Figures/table/illustration/abstracts
Portion Quantity	1

Format	Both print and electronic
You are an author of the Elsevier article	No
Are you translating?	No
Order Reference Number	
Expected publication date	Nov 2009
Elsevier VAT number	GB 494 6272 12
Permissions price	0.00 USD

AMERICAN CHEMICAL SOCIETY LICENSE TERMS AND CONDITIONS

Nov 13, 2009

This is a License Agreement between John K. Osiri ("You") and American Chemical Society ("American Chemical Society") provided by Copyright Clearance Center ("CCC"). The license consists of your order details, the terms and conditions provided by American Chemical Society, and the payment terms and conditions.

All payments must be made in full to CCC. For payment instructions, please see information listed at the bottom of this form.

License Number	2306151090825
License Date	Nov 11, 2009
Licensed content publisher	American Chemical Society
Licensed content publication	Analytical Chemistry
Licensed content title	Autonomous Microfluidic Sample Preparation System for Protein Profile-Based Detection of Aerosolized Bacterial Cells and Spores
Licensed content author	Jeanne C. Stachowiak et al.
Licensed content date	Aug 1, 2007
Volume number	79
Issue number	15
Type of Use	Thesis/Dissertation
Requestor type	Not specified
Format	Print and Electronic
Portion	Table/Figure/Chart
Number of	1

Table/Figure/Charts	
Author of this ACS article	No
Order reference number	
Title of the thesis / dissertation	PLATFORMS AND PROTOCOLS FOR THE MULTIDIMENSIONAL MICROCHIP ELECTROPHORETIC ANALYSIS OF COMPLEX PROTEOMES
Expected completion date	Nov 2009
Estimated size(pages)	180
Billing Type	Invoice
Billing Address	Choppin 204 Louisiana State University Baton Rouge, LA 70803 United States
Customer reference info	
Total	0.00 USD

AMERICAN CHEMICAL SOCIETY LICENSE TERMS AND CONDITIONS

Nov 13, 2009

This is a License Agreement between John K. Osiri ("You") and American Chemical Society ("American Chemical Society") provided by Copyright Clearance Center ("CCC"). The license consists of your order details, the terms and conditions provided by American Chemical Society, and the payment terms and conditions.

All payments must be made in full to CCC. For payment instructions, please see information listed at the bottom of this form.

License Number	2306151380215
License Date	Nov 11, 2009
Licensed content publisher	American Chemical Society
Licensed content publication	Analytical Chemistry
Licensed content title	Fully Integrated Microfluidic Platform Enabling Automated Phosphoprofiling of Macrophage Response
Licensed content author	Nimisha Srivastava et al.
Licensed content date	May 1, 2009

Volume number	81
Issue number	9
Type of Use	Thesis/Dissertation
Requestor type	Not specified
Format	Print and Electronic
Portion	Table/Figure/Chart
Number of Table/Figure/Charts	1
Author of this ACS article	No
Order reference number	
Title of the thesis / dissertation	PLATFORMS AND PROTOCOLS FOR THE MULTIDIMENSIONAL MICROCHIP ELECTROPHORETIC ANALYSIS OF COMPLEX PROTEOMES
Expected completion date	Nov 2009
Estimated size(pages)	180
Billing Type	Invoice
Billing Address	Choppin 204 Louisiana State University Baton Rouge, LA 70803 United States
Customer reference info	
Total	0.0 USD

AMERICAN CHEMICAL SOCIETY LICENSE TERMS AND CONDITIONS

Nov 13, 2009

This is a License Agreement between John K. Osiri ("You") and American Chemical Society ("American Chemical Society") provided by Copyright Clearance Center ("CCC"). The license consists of your order details, the terms and conditions provided by American Chemical Society, and the payment terms and conditions.

All payments must be made in full to CCC. For payment instructions, please see information listed at the bottom of this form.

License Number	2306151480653

License Date	Nov 11, 2009
Licensed content publisher	American Chemical Society
Licensed content publication	Analytical Chemistry
Licensed content title	Integrated Microfluidic System Enabling Protein Digestion, Peptide Separation, and Protein Identification
Licensed content author	Jun Gao et al.
Licensed content date	Jun 1, 2001
Volume number	73
Issue number	11
Type of Use	Thesis/Dissertation
Requestor type	Not specified
Format	Print and Electronic
Portion	Table/Figure/Chart
Number of Table/Figure/Charts	1
Author of this ACS article	No
Order reference number	
Title of the thesis / dissertation	PLATFORMS AND PROTOCOLS FOR THE MULTIDIMENSIONAL MICROCHIP ELECTROPHORETIC ANALYSIS OF COMPLEX PROTEOMES
Expected completion date	Nov 2009
Estimated size(pages)	180
Billing Type	Invoice
Billing Address	Choppin 204 Louisiana State University Baton Rouge, LA 70803 United States
Customer reference info	
Total	0.00 USD

AMERICAN CHEMICAL SOCIETY LICENSE TERMS AND CONDITIONS

Nov 13, 2009

This is a License Agreement between John K. Osiri ("You") and American Chemical Society ("American Chemical Society") provided by Copyright Clearance Center ("CCC"). The license consists of your order details, the terms and conditions provided by American Chemical Society, and the payment terms and conditions.

All payments must be made in full to CCC. For payment instructions, please see information listed at the bottom of this form.

License Number	2306160053200
License Date	Nov 11, 2009
Licensed content publisher	American Chemical Society
Licensed content publication	Analytical Chemistry
Licensed content title	Integrated Microfluidic Device for Mass Spectrometry-Based Proteomics and Its Application to Biomarker Discovery Programs
Licensed content author	Marie-Helene Fortier et al.
Licensed content date	Mar 1, 2005
Volume number	77
Issue number	6
Type of Use	Thesis/Dissertation
Requestor type	Not specified
Format	Print and Electronic
Portion	Table/Figure/Chart
Number of Table/Figure/Charts	1
Author of this ACS article	No
Order reference number	
Title of the thesis / dissertation	PLATFORMS AND PROTOCOLS FOR THE MULTIDIMENSIONAL MICROCHIP ELECTROPHORETIC ANALYSIS OF COMPLEX PROTEOMES
Expected completion date	Nov 2009
Estimated size(pages)	180
Billing Type	Invoice
Billing Address	Choppin 204 Louisiana State University

	Baton Rouge, LA 70803
	United States
Customer reference info	
Total	0.00 USD

AMERICAN CHEMICAL SOCIETY LICENSE TERMS AND CONDITIONS

Nov 13, 2009

This is a License Agreement between John K. Osiri ("You") and American Chemical Society ("American Chemical Society") provided by Copyright Clearance Center ("CCC"). The license consists of your order details, the terms and conditions provided by American Chemical Society, and the payment terms and conditions.

All payments must be made in full to CCC. For payment instructions, please see information listed at the bottom of this form.

License Number	2306160146809
License Date	Nov 11, 2009
Licensed content publisher	American Chemical Society
Licensed content publication	Analytical Chemistry
Licensed content title	Poly(dimethylsiloxane)-Based Microchip for Two-Dimensional Solid-Phase Extraction-Capillary Electrophoresis with an Integrated Electrospray Emitter Tip
Licensed content author	Andreas P. Dahlin et al.
Licensed content date	Aug 1, 2005
Volume number	77
Issue number	16
Type of Use	Thesis/Dissertation
Requestor type	Not specified
Format	Print and Electronic
Portion	Table/Figure/Chart
Number of Table/Figure/Charts	1
Author of this ACS article	No

Order reference number	
Title of the thesis / dissertation	PLATFORMS AND PROTOCOLS FOR THE MULTIDIMENSIONAL MICROCHIP ELECTROPHORETIC ANALYSIS OF COMPLEX PROTEOMES
Expected completion date	Nov 2009
Estimated size(pages)	180
Billing Type	Invoice
Billing Address	Choppin 204 Louisiana State University Baton Rouge, LA 70803 United States
Customer reference info	
Total	0.00 USD

AMERICAN CHEMICAL SOCIETY LICENSE TERMS AND CONDITIONS

Nov 13, 2009

This is a License Agreement between John K. Osiri ("You") and American Chemical Society ("American Chemical Society") provided by Copyright Clearance Center ("CCC"). The license consists of your order details, the terms and conditions provided by American Chemical Society, and the payment terms and conditions.

All payments must be made in full to CCC. For payment instructions, please see information listed at the bottom of this form.

License Number	2306160228153
License Date	Nov 11, 2009
Licensed content publisher	American Chemical Society
Licensed content publication	Analytical Chemistry
Licensed content title	Dual-Function Microanalytical Device by In Situ Photolithographic Grafting of Porous Polymer Monolith: Integrating Solid-Phase Extraction and Enzymatic Digestion for Peptide Mass Mapping
Licensed content author	Dominic S. Peterson et al.
Licensed content date	Oct 1, 2003

Volume number	75
Issue number	20
Type of Use	Thesis/Dissertation
Requestor type	Not specified
Format	Print and Electronic
Portion	Table/Figure/Chart
Number of Table/Figure/Charts	1
Author of this ACS article	No
Order reference number	
Title of the thesis / dissertation	PLATFORMS AND PROTOCOLS FOR THE MULTIDIMENSIONAL MICROCHIP ELECTROPHORETIC ANALYSIS OF COMPLEX PROTEOMES
Expected completion date	Nov 2009
Estimated size(pages)	180
Billing Type	Invoice
Billing Address	Choppin 204 Louisiana State University Baton Rouge, LA 70803 United States
Customer reference info	
Total	0.00 USD

This is a License Agreement between John K. Osiri ("You") and American Chemical Society ("American Chemical Society") provided by Copyright Clearance Center ("CCC"). The license consists of your order details, the terms and conditions provided by American Chemical Society, and the payment terms and conditions.

All payments must be made in full to CCC. For payment instructions, please see information listed at the bottom of this form.

License Number	2306160351028
License Date	Nov 11, 2009
Licensed content publisher	American Chemical Society
Licensed content publication	Analytical Chemistry
Licensed content title	Preconcentration of Proteins on Microfluidic Devices Using Porous Silica Membranes

Licensed content author	Robert S. Foote et al.
Licensed content date	Jan 1, 2005
Volume number	77
Issue number	1
Type of Use	Thesis/Dissertation
Requestor type	Not specified
Format	Print and Electronic
Portion	Table/Figure/Chart
Number of Table/Figure/Charts	1
Author of this ACS article	No
Order reference number	
Title of the thesis / dissertation	PLATFORMS AND PROTOCOLS FOR THE MULTIDIMENSIONAL MICROCHIP ELECTROPHORETIC ANALYSIS OF COMPLEX PROTEOMES
Expected completion date	Nov 2009
Estimated size(pages)	180
Billing Type	Invoice
Billing Address	Choppin 204 Louisiana State University Baton Rouge, LA 70803 United States
Customer reference info	
Total	0.0 USD

AMERICAN CHEMICAL SOCIETY LICENSE TERMS AND CONDITIONS

Nov 13, 2009

This is a License Agreement between John K. Osiri ("You") and American Chemical Society ("American Chemical Society") provided by Copyright Clearance Center ("CCC"). The license consists of your order details, the terms and conditions provided by American Chemical Society, and the payment terms and conditions.

All payments must be made in full to CCC. For payment instructions, please see information listed at the bottom of this form.

License Number	2306160444028
License Date	Nov 11, 2009
Licensed content publisher	American Chemical Society
Licensed content publication	Journal of Proteome Research
Licensed content title	The Proteomic Reactor: A Microfluidic Device for Processing Minute Amounts of Protein Prior to Mass Spectrometry Analysis
Licensed content author	Martin Ethier et al.
Licensed content date	Oct 1, 2006
Volume number	5
Issue number	10
Type of Use	Thesis/Dissertation
Requestor type	Not specified
Format	Print and Electronic
Portion	Table/Figure/Chart
Number of Table/Figure/Charts	1
Author of this ACS article	No
Order reference number	
Title of the thesis / dissertation	PLATFORMS AND PROTOCOLS FOR THE MULTIDIMENSIONAL MICROCHIP ELECTROPHORETIC ANALYSIS OF COMPLEX PROTEOMES
Expected completion date	Nov 2009
Estimated size(pages)	180
Billing Type	Invoice
Billing Address	Choppin 204 Louisiana State University Baton Rouge, LA 70803 United States
Customer reference info	
Total	0.00 USD

Vita

John Kalu Osiri was born in Cotonou, Republic of Benin, to John K. Osiri, Sr., and Ngozi Osiri. He began his elementary education at the Nigerian International School, Cotonou, and finished at St. Bridget's Primary School, Aba, Abia State, Nigeria, after taking the secondary school entrance exam in 1990 in Primary 4. He attended St. Augustine's Anglican Seminary (SAAS) Secondary School in Nbawsi, Abia State, from 1991 through 1996. He was selected to be Science Laboratory Prefect in 1994 at SAAS. After his secondary education, he was admitted into the Petroleum Training Institute (PTI) in Warri, Delta State, Nigeria, in 1997. At PTI he was elected Assistant Secretary General of the Student Union Government in 1998, and earned a two-year National Diploma in Petroleum Marketing and Business Studies in 1999. In 2001, he accepted admission to study chemistry at Grambling State University (GSU), Louisiana, U.S.A.

At Grambling, John returned to the sciences and earned a bachelor of science in chemistry with Honors in the spring of 2005. During his time at GSU, he was elected Vice President of the Student Government Association and President of the International Student Organization in 2004, and he participated in numerous organizations. He is also a member of the Alpha Phi Alpha, Fraternity, Inc.

Following graduation from GSU, he enrolled at Louisiana State University, Baton Rouge, in the summer of 2005 where he was mentored in the Soper Research Group by Professor Steven A. Soper. He has co-authored over ten publications (including manuscripts) and has presented his scientific research findings at national and international conferences. His dissertation is entitled, "Platforms and Protocols for the Multidimensional Microchip Electrophoretic Analysis of Complex Proteomes." The degree of Doctor of Philosophy will be conferred at the May 2010 commencement ceremony.